ABSTRACT

Title of Document:	FUNCTIONAL POLYMERS FOR BIOSENSING APPLICATIONS
	Omar B Ayyub, Ph.D., 2014
Directed By:	Professor Peter Kofinas, Fischell Department of Bioengineering

The work presented in this dissertation involves two separate systems. The first system was the investigation of photonic crystals as a chemical and biosensing platform. The second investigation was the fabrication of a point-of-care blood ammonia sensor.

The photonic crystal fabricated was composed of the block copolymer polystyrene-b-poly(2-vinylpyridine)(PS-b-P2VP), which when cast into films, self-assembles into a multilayer structure. The P2VP block of the multilayer structure can be quaternized, causing it swell in aqueous media, providing the necessary spacing for it to operate as a 1D photonic crystal for visible wavelengths of light. The reflected wavelength or color of the photonic crystal is dictated by its spacing. Boronic acid functionalities were covalently attached to the P2VP block, which imparts the ability to bind to sugar molecules. When boronic acids bind sugars, such as fructose, the acid ionizes and becomes negatively charged, causing the P2VP block to swell, and changing the reflected color of the photonic crystal. In the following studies the covalent attachment of boronic acid to PS-b-P2VP was characterized. The resulting photonic crystal was then evaluated as a sensitive fructose sensor with a detection limit of $500\mu M$.

A novel method for the covalent attachment of primary amines to the P2VP block was also investigated. In Chapter 4, the utilization of trimethylsilyl amine protecting groups,

allowed for the chemical modification of P2VP with primary amines without compromising the microphase separated nanostructure of the PS-b-P2VP. The primary amine functionality was characterized and shown to be reactive with cross-linking agents such as glutaraldehyde.

A point-of-care blood ammonia sensor was engineered utilizing a specific, colorimetric ammonia reaction, termed the indophenol reaction, in conjunction with a cation exchange membrane(CEM). The membrane allowed for the rapid extraction of ammonium ions from whole blood. The extracted ammonia solution was then used with the indophenol reaction, which generates a blue color in the presence of ammonia. The sensor could extract ammonia in 20 minutes and had a detection range of 25-500μM in whole human blood with a COD of 0.9573.

FUNCTIONAL POLYMERS FOR BIOSENSING APPLICATIONS

By

Omar B Ayyub

Dissertation submitted to the Faculty of the Graduate School of the
University of Maryland, College Park in partial fulfillment
of the requirements for the degree of
Doctor of Philosphy
2014

Advisory Committee:
Professor Peter Kofinas, Chair
Professor William Bentley
Professor Robert Briber
Assistant Professor Steven Jay
Associate Professor Ian White

Preface

The scope of the following dissertation focuses primarily on the investigation of point-of-care (PoC) sensors. A PoC sensor is a sensing platform that can operate outside of the laboratory setting. Excellent examples of PoC sensors that the reader may be familiar with are blood glucometers and pregnancy tests. These provide the end-user the ability to detect certain analytes such as blood glucose or hCG in urine at home, with minimal training. PoC sensors have applications outside of at-home use. In environments with low resources, PoC sensors can provide health care professionals with the means to test for different diseases, such as in rural hospitals testing for hepatitis. PoC sensors have applications outside of healthcare as well. They are useful in the monitoring of agricultural products or in bioprocessing facilities by giving feedback on the formation of certain products. PoC sensors can also be designed to sense chemical or bioterrorism threats such as nerve gases, with ability to alert the user to the presence of a dangerous toxin.

In consideration of the many low resource scenarios in which sensors and diagnostics are needed, one would expect a certain set of design requirements for a PoC sensors. Specificity and selectivity are of course major requirements as the platform should accurately and reliably detect the analyte of interest. To reduce the training required to operate them, ideally, a PoC sensor should perform with little to no preprocessing of the sample. Additionally, the response given should easy to discern or qualitative, with little or no room for interpretation of the result. Since many uses for PoC sensors are in low resource environments, stability is also a major factor. The system should be shelf-ready, preferably with no need for refrigeration, but simply sits on a shelf at room temperature

until use. Finally, traditional sensing techniques found in laboratories are very expensive requiring complex equipment and sample preparation. A PoC sensor should only require cheap and low or no power, preferably hand-held, equipment. If designed properly, with these set of parameters, PoC sensors can essentially provide any low resource environment with a mobile 'laboratory' that will determine analyte concentration or alert users the presence of certain toxins or pathogens at a low cost.

The need for PoC sensors is the overarching motivation of the work presented in the dissertation. Two systems were investigated, one somewhat more specific than the other. The first of which was investigating materials referred to as photonic crystals as a color changing sensor platform. These photonic crystals could act a colorimetric litmus tests, in which one could quickly expose it to a sample and examine the color to determine if the analyte if present and at what concentration. The second investigated system is a PoC blood ammonia sensor. A blood ammonia sensor that can operate outside of laboratory setting would provide a great deal of disease management for individuals with hyperammonemia, or elevated blood ammonia, a fatal condition.

Dedication

I would like to dedicate this to my parents, Deena and Bilal. I love you and owe you everything.

Acknowledgements

The work presented in this dissertation could not have been done alone. I would of course like to acknowledge my wonderful advisor, Dr. Peter Kofinas. He was the most dedicated mentor a student could have asked for. I would also like to acknowledge my committee, Dr. Ian White, Dr. Robert Briber, Dr. William Bentley, and Dr. Steven Jay, for always being open to provide me with the support and critical commentary necessary for the following work to be completed. I would like to acknowledge Dr. Marshall Summar and Dr. Kristina Cusmano-Ozog for their critical commentary on the ammonia sensor project. Dr. Phillip DeShong was also an excellent help in giving me chemistry and research advice.

I would also like to thank Drs Dan Janiak, Josh Silverstein, Ta-I Yang and Xin Zhang for always being there to teach me experimental techniques or provide critical commentary on the work I was doing. I would like to acknowledge Mr. Adam Behrens for his contributions to the ammonia sensing project. I would also like to acknowledge Mr. Mert Vural and Wonseok Hwang for their assistance in experimental techniques and critical commentary. I also owe a great deal to the wonderful undergraduate I have worked with including Michael Ibrahim, Brian Heligman and Mary Natoli. The presented work would not have been possible without them.

Table of Contents

Table of Figures

1.0. Photonic Crystals Sensors

1.1 Photonic Crystals and Structural Color

Traditional dyes are colored through the absorption of certain wavelengths of light. The wavelengths that are not absorbed but reflected are perceived as the color of the dye or material. Sometimes, nature takes advantage of another mechanism to produce brilliant pigments, known as structural color. Structural color arises from photonic bandgaps created by periodic nanostructures of dieletric materials. Similarly to electronic bandgaps, they prevent the transmission of certain energies of electromagnetic radiation. This phenomenon can be seen in many colorful birds, insects and even plants. These nanostructured photonic bandgap materials are commonly referred to as photonic crystals*(1)*.
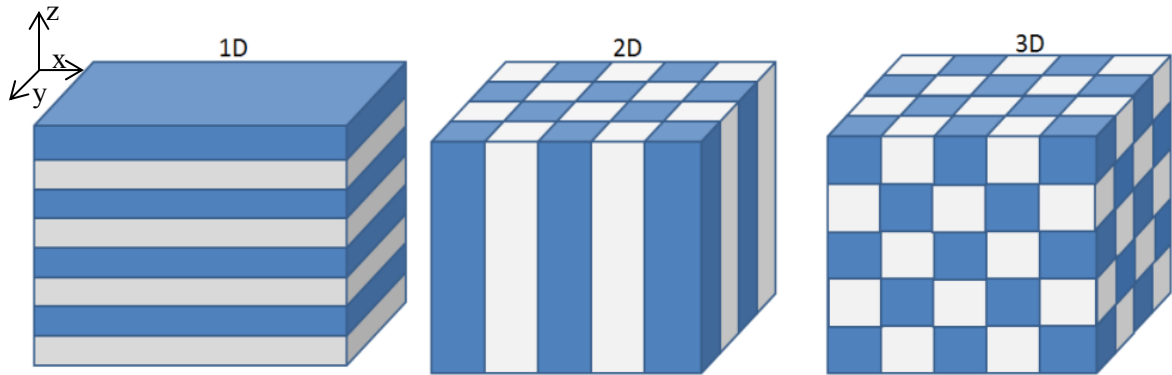
Figure 1.1: The periodicity of dielectric materials can be one, two and three dimensions. In the 1D case, there is only a periodicity in the z direction. In a 2D crystal, the periodicity exists in the x and y directions. In the 3D crystal the periodicity is in the x,y and z directons.

The periodic structure of a photonic crystal can be 1, 2 and 3-dimensional as depicted in Figure 1.1. Photonic crystals have found applications as waveguides, mirrors, optical

filters and more recently as chemical and biological sensors*(2)*. This chapter seeks to describe the physical phenomenon, fabrication techniques, and how photonic crystals can be exploited as a colorimetric sensor.

1.2 Geometric Description

The concept of a one-dimensional photonic band gap was first described by Lord Rayleigh in 1887. This geometric description is still relevant, despite electromagnetic depictions existing. Light passing through a periodic structure, such as in x-ray diffraction, is described by Bragg's law which states:

$$m\lambda = 2\ d\ \cos\theta \tag{1.1}$$

where m is the order of diffraction, λ is the wavelength of light, d is the distance between periodicities, and θ is the angle of the light. When these periodicities are dielectrics with differing indices of refraction, Snell's law, equation 1.2, can be used in conjunction with Bragg's law to produce a description of a photonic crystal seen in equation 1.3, where n_{eff} is the average index of refraction.

$$\frac{\sin\theta_1}{\sin\theta_2} = \frac{n_2}{n_1} \tag{1.2}$$

$$m\lambda = 2d(n_{eff}^2 - \sin^2\theta)^{1/2} \tag{1.3}$$

The alternating dielectrics can be composed of silicon, silica, polymer, water and even air. In this dissertation, photonic crystals that reflect visible wavelengths of light were investigated, allowing for an easily discernable response.

1.3 Fabrications

1.3.1 Inorganic Fabrication

Producing the nano and microscale order required for a photonic crystal is difficult. Inorganic fabrication techniques were initially investigated to facilitate this process due to their precision. 1D multilayer photonic crystals have been produced from Ag/MgF_2 using thermal evaporation techniques[3], Silica/TiO_2 using the sol-gel technique[4, 5], and Silica/Silicon by vapor chemical deposition[6, 7]. 2D photonic crystals have been fabricated from gallium arsenide by use of metal-organic vapor phase epitaxy and electron-beam lithography[8, 9], silica through electron-beam lithography[10] and silicon via lithography and alkaline etching[11]. Each of these systems fabricated a 2-dimensional triangular lattice of cylindrical pores. Inorganic fabrications techniques are highly effective, consistent and produce photonic bandgaps that are close to theoretical perfection. In terms of fabrication, their biggest shortcoming is the laborious nature of synthesis. Additionally, as will be discussed in later sections, they are not ideal candidates for biosensing platforms.

1.3.2 Organic Fabrication

Organic fabrications of photonic crystals are generally easier to synthesize than their inorganic counterparts. A polymeric one-dimensional photonic crystal was initially investigated by Thomas' group[12, 13]. They investigated the use of self-assembled block copolymers to produce the periodicities required to synthesize a photonic bandgap. A block copolymer is a macromolecule composed of sequences or blocks of chemically distinct repeat units. The covalent bond between constituent blocks allows for microphase separation into spherical, cylindrical, bi-continuous, and lamellar morphologies. The morphology and domain sizes of these self-assembled periodic nanostructures can generally be controlled by adjusting the length of each block and the total molecular

mass*(14)*. Figure 1.2 demonstrates the different morphologies obtained at different mass fractions of one block versus another.

Spherical	Cylindrical	Bi-continuous	Lamellar
0 to 0.17	0.17 to 0.34	0.34 to 0.37	0.37 to 0.5
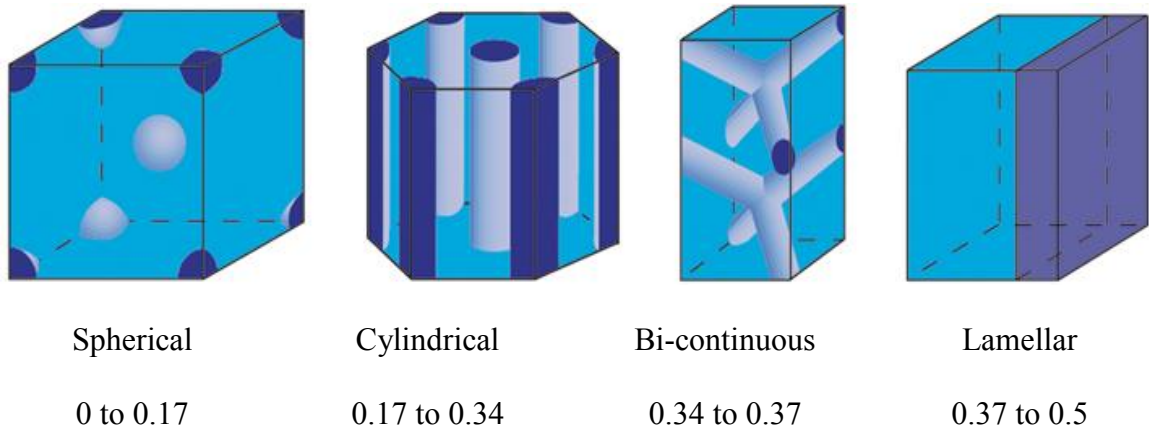
Figure 1.2 When block copolymers are cast into films they will self-assemble into different nanostructures. The nanostructure is dictated by the relative mass fraction each block. As the ratio approaches 0.37 the system will assemble into a spherical, cylindrical, bi-continuous or lamellar morphology*(15)*.

It is fairly apparent how microphase separation can be utilized to produce a photonic crystal. Thomas specifically examined BCPs that microphase separated into lamellar morphology to be used as a multilayer 1D photonic crystal. In one such system polystyrene-b-poly(2-vinylpyridine) (PS-b-P2VP) films were synthesized*(12)*. When the P2VP block was quaternized, the introduced positive charge allowed the block to swell in aqueous media, introducing a refractive index different between PS and water and the proper spacing to reflect visible wavelength of light as seen in Figure 1.3.
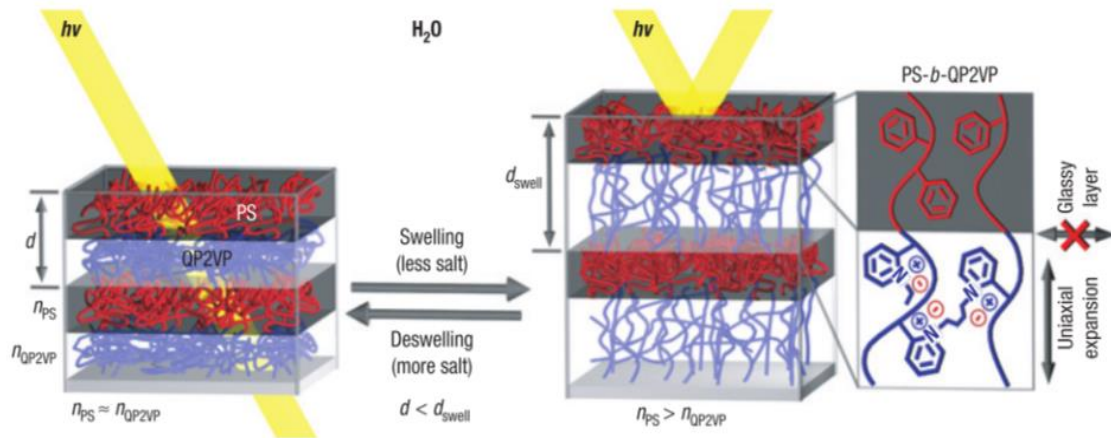
Figure 1.3: In the PS-b-P2VP system reported by the Thomas group, quaternizing the P2VP block allowed it to swell in aqueous media. The swelling event introduced a large enough spacing to reflect visible wavelengths of light. The reflected wavelength could then be turned using salt concentrations.*(12)*

Block copolymer 1D photonic crystals were also heavily investigated by Grubbs*(16)*. In this system, block copolymers with reduced chain entanglements would self-assemble into a multilayer brush structure upon deposition on a substrate. By altering the molecular weight of each block, the reflected peak wavelength could be tuned.

Another approach to fabricate organic photonic crystals came from Asher's group*(17)*. This approach utilized colloidal nanoparticles to produce a 3D photonic crystal. Asher synthesized highly negatively charged polystyrene nanoparticles, that when placed in aqueous solutions, would self-assemble into a 3D crystal colloidal array. It is believed that this system exists as a body centered cubic crystal. At high enough nanoparticle concentrations the system would act as a photonic bandgap for visible wavelengths of light. This colloidal crystal array(CCA) can be locked into a polymer network or

hydrogel, keeping the spacing static, and allowing the spacing and thus the color to be dictated by the hydrogel as seen in Figure 1.4.
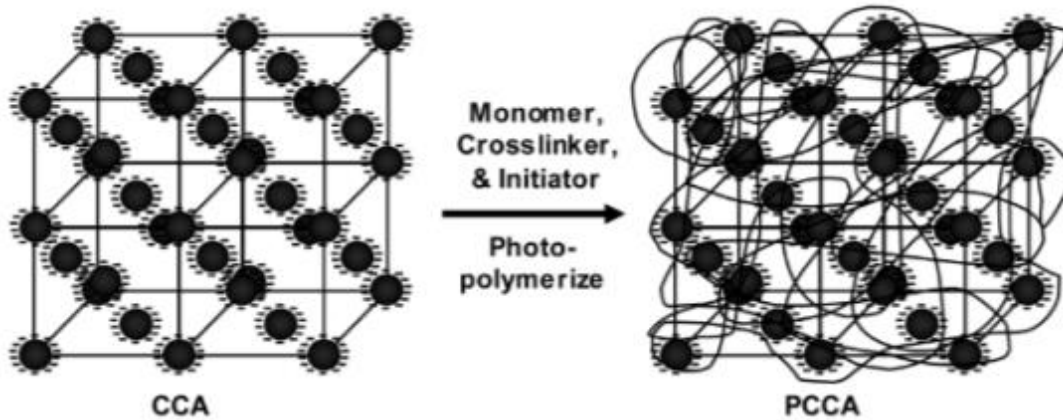
Figure 1.4: Highly charged nanoparticles will assemble into a crystal colloidal array provided that the ionic strength of the media is low. This system can be produced in the presence of hydrogel precursors which are polymerized to form a polymerized crystal colloidal array. This effectively locks the nanoparticles in place, and forces their spacing to be dictated by hydrogel swelling events.*(18)*

The colloidal crystal array has become an increasingly common technique due to its facile fabrication. The Weitz group developed a technique to produce colloidal crystal arrays in core-shell hydrogel microparticles as opposed to bulk hydrogels*(19, 20)*. This system was further developed by Manoharan to produce pigments of any visible color*(21)*. By using osmosis-driven condensation, the color of the microparticle CCAs was tuned to any specification and then UV-cured to lock the system in place.

The inkjet printing of CCA based hydrogels have allowed for the incorporation of photonic crystals into microfluidic channels*(22)*. This facilitates the production of multiplexed sensors. Shen et al loaded highly charged silica particles into an inkjet printer dispersed in volatile solvents. Once printed, the solvents would be allowed to evaporate

6

until the desired concentration and color of the silica particle suspension was achieved. The major advantage of the CCA system is that it can be used in any aqueous polymer network, increasing the types of sensing events that can be utilized.

1.4 Sensors

1.4.1 Invoking a Response in Photonic Crystal Sensors

The colorimetric nature of photonic crystals has generated an entire field surrounding their use as chemical and biological sensors[2]. In the context of a sensor, photonic crystals can produce an output through a change in reflected wavelength. It can be surmised from equation 1.3 that to invoke a shift in reflected wavelength the refractive index or the spacing of the dielectric materials must change. Theoretically, shifts in refractive index cause fairly minimal changes in reflected wavelength. Refractive indices of materials can vary from ~1-4, allowing for a maximum change in reflected wavelength of 4.6λ. Realistically, materials with a refractive index higher than ~1.6 also absorb or reflect visible wavelengths of light, such as silicon. Additionally, invoking a change in refractive index as a chemical or biological sensing event is difficult and in the best scenarios will produce a 0.1-0.2 shift in refractive index, as will be discussed later.

Triggering a change in spacing of a photonic crystal can cause a very large shift in reflected wavelength and is easily accomplished in the organic systems discussed in section 1.3.2. Each system reviewed utilized a polymer network swollen in aqueous media. Any change in the swelling properties of these networks would change the spacing of the periodicities and accordingly the reflected wavelength.

The swelling of a polymer network is described by Flory's model of a swollen ionic network[23]. In the case of a non-ionic network the major factors influencing the

swelling are the free energy of mixing, F_m, and the elastic restoring force, F_{el}. They are

described by the following equations respectively:

$$\pi_m = N \left(\frac{\partial \Delta F_m}{\partial n_1} \right)_{T,P} = -RT \left(ln \left(1 - \frac{V_o}{V_m} \right) + \frac{V_o}{V_m} + \chi \left(\frac{V_o}{V_m} \right)^3 \right)$$

(1.4)

$$\pi_{el} = N \left(\frac{\partial \Delta F_{el}}{\partial a_s} \right)_{T,P} = RT \left(V_1 \left(\frac{v_e}{V_o} \right) \left(\left(\frac{V_o}{V_m} \right)^{1/3} - \frac{2V_o}{fV_m} \right) \right)$$

(1.5)

where N is Avogadro's number, V_o is the volume of the network when initially cross-

linked, V_m is the volume of the network at swelling equilibrium, V_1 is the molar volume

of water, v_e is the number of cross-links, χ is the Flory-Huggins interaction parameter and

f is the cross-link functionality. These two equations can then be equated to the Donnan

potential seen below:

$$\pi_i = RT(C_+ + C_- - C_+^* - C_-^*)$$

(1.6)

where C_+ is the mobile cations in the polymer network, C_- are the mobile anions in the

polymer network, C_+^* represents the mobile cations in the bulk solution and C_-^*

represents the mobile anions outside the polymer network. If composed of ionic

polymers, the network will contain immobile charges prompting a higher concentration

of mobile ions in the network. This will create a Donnan potential causing an increase in

osmotic pressure. When equated with the pressures developed from the free energy of

mixing and the elastic restoring force, a relationship between changes in osmotic pressure

and changes in volume can be developed assuming the system is at equilibrium. From

equations 1.4-1.6, the most readily available methods to invoke a major

swelling/deswelling event are changes in χ, the number of cross-links or the number of immobile ions in the polymer network.

1.4.2 Infrared and Low Shift Sensors

A number of reported photonic crystal based sensors rely on changes in refractive index rather than spacing. These systems are almost exclusively based on porous silicon, also referred to as rugate mirrors or filters. The shift in reflected wavelength generally relies on materials adsorbing to the inside of the pores of silicon, changing the refractive index. In one example, it was demonstrated that the porous silicon could be used to template photonic crystals out of hydrophobic polymers and was utilized for the sensing of ethanol vapors*(24)*. This system only interacted with infrared light, however. The use of biological capture moieties such as antibodies has also been incorporated into the pores of porous silicon*(25, 26)*. These systems also reflected infrared light and the reported shifts in wavelength of the response were only several nanometers. Another approach to the rugate filter as photonic crystal sensor is the response to protease activity. Two different methods have been reported by Orosco et al and Kilian et al*(27, 28)*.

In the system developed by Ososco et al, porous silicon was coated with a thin layer of casein, leaving the pores filled with air. Once the protease pepsin was applied, the protein layer was digested allowing the influx of water, changing the refractive index and thus the color. This system has a 1.8pmol detection limit and a 30nm range in responses. The group published a follow up, which examined a system which contained two sets of pores, in which the second smaller set pores could only be infiltrated by the digested peptide, as seen in Figure 1.5*(29)*. While effective, this approach would have major issues in any system containing 'dirty' samples.

First layer
Second layer

+ Protease

+ Substrate

Porous silicon
double layer
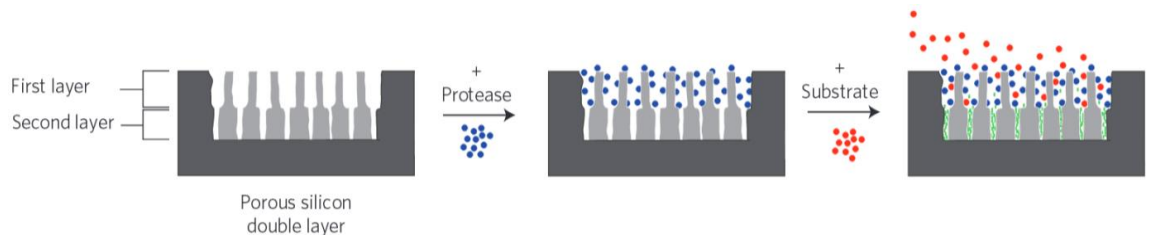
Figure 1.5: Orosco et al investigated dual porous silicon photonic crystal. The larger pores are lined with a protease. When the protein substrate is introduced it is cleaved in smaller peptide which have the correct size to infiltrate the smaller pores causing a change in refractive index and thus reflected wavelength.*(29)*

Kilian et al investigated a different approach; in which the porous silicon was back filled with peptide based silanizations. When introduced to the protease subtilisin, the mass of peptide within the pores would degrade, causing a change in refractive index and a shift in reflected wavelength. In this case, the detect limit was 7.4pmol; but the shift from concentrations as high as 3.7μM was only 6nm. This system was utilized in what was termed 'Smart Tissue Culture'*(30)*. The porous silicon was back-filled with gelatin, which is degraded by matrix metallo-proteinases produced by human monocyte-derived macropages. This system could detect the presence of certain cells, but again only produced a response of 15nm in the highest concentrations of the targeted enzyme.

Rugate filters have demonstrated that photonic crystals are a potential biosensing platform. The biggest pitfall of these systems is their low response of only several nanometers. These types of responses can certainly be measured using complex spectrometers with integrating spheres or elipsometers that can measure reflectivity, but they cannot be resolved by the human eye. One of the biggest advantages of photonic crystals sensors is they have the potential for qualitative read outs without the need for

10

any extraneous equipment or power. While these inorganic techniques are considered "label-free", the still require the sample fabrication steps of other techniques such as fluorescence. The photonic crystal must be fabricated and attached to the capture moiety, much in the same way in fluorescence. The advantage of these non-visible or low shift systems is that no additional steps are required as compared to fluorescence techniques; the sample of interest is simply applied to the material. They also have the distinct advantage of high precision as compared to visible, organic based photonic crystals, making them suited for low concentration detection.

1.4.3 Highly Visible Sensors

Literature surrounding organic photonic crystal sensors generally report large, visible changes in color as opposed to their inorganic counterparts. These approaches all rely on changes in spacing rather refractive index. Organic photonic crystal sensors all rely on polymer networks or hydrogels, in which swelling/deswelling of the hydrogel is mediated by changes in Donnan potential or crosslink density.

The previously discussed BCP system, quaternized PS-b-P2VP films, was investigated by the Thomas group as potential chemical and voltage sensors. By quaternizing the P2VP block with bromoethane and dibromobutane, they produced pH responsive films with hysteresis. The control of the hysteresis allowed for 'shape memory' of the optical events[31]. The voltage sensing system relied on unmodified films of PS-b-P2VP. When potentials ranging from 1-5V were applied, it would cause the P2VP block to become charged, inducing a Donnan potential and causing the system to swell. As more voltage was applied, the films would continue to swell and redshift[13].

The crystal colloidal array has generated a very large body of literature for its use as a photonic crystal sensor. The system was first described by Asher for its use as a lead sensor*(17, 32)*. It was further demonstrated that when the CCA was locked in an acrylamide hydrogel it could respond as a pH and ionic strength sensor*(33)*. When large concentrations of NaCl, for example, are introduced, the mobile ions diffuse into the hydrogel to associate with any immobile ionic species within the hydrogel. This causes a change in osmotic pressure and thus a swelling event and redshift in color. Similarly, when exposed to increasing alkaline solutions, more groups within the hydrogel ionize, further driving a higher osmotic pressure and therefore more swelling of the network. Similar systems have been reported, in which the CCA is removed after hydrogel network formation. This generates what is termed as an inverse-opal photonic crystal. This system has also been shown to have similar properties as a pH sensor*(34)*. Polyacrylamide/CCA photonic crystals have also been exploited as humidity sensors, where increasing humidity results in swelling of the hydrogel matrix and a redshift in color*(35)*.

One of the first selective chemical sensors utilizing the polymerized CCA (PCCA) came from Asher's group. Boronic acid functionalities were introduced to the backbone of an acrylamide based hydrogel to impart glucose sensing capabilities to the photonic crystal hydrogel*(18, 36–39)*. Boronic acids reversibly bind to diols such as glucose. The binding event lowers the pKa of the boronic acid, meaning that upon introduction of glucose, a larger percentage of boronic acid will form the boronate anion. This again introduces immobile charges within the hydrogel matrix, generating a Donnan potential and causing the network to swell. Another approach involved the incorporation of both boronic acid

and crown ether functionalities. In this case, multiple boronic acid units could bind one glucose molecule, a complex which was stabilized by the presence of the crown ethers*(36)*. The wavelength shifts in each of these reported glucose sensors were as high as 300nm, which is a very large visual change, spanning the entire visual spectrum.
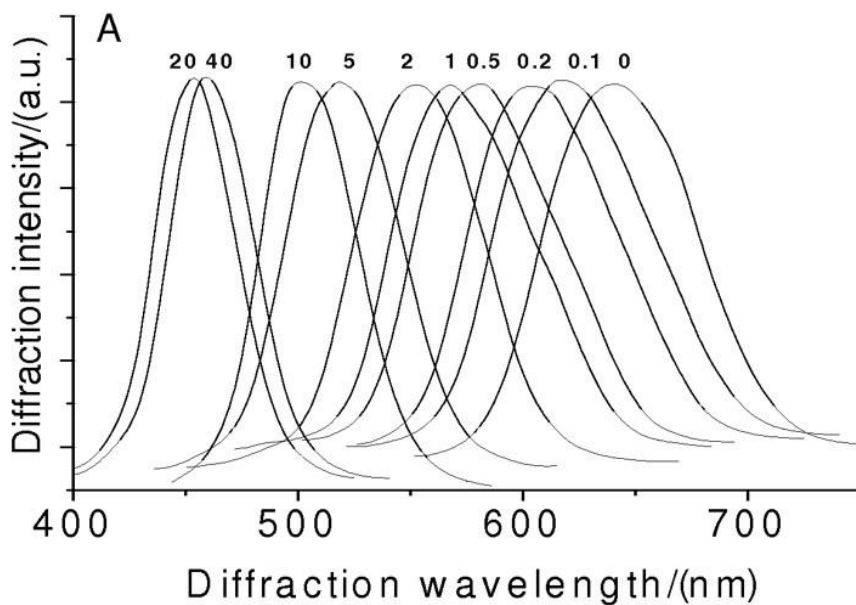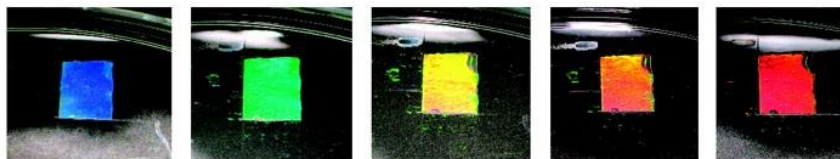
Figure 1.6 The boronic acid PCCA photonic crystal reported by Asher's group would respond with visible changes in color to concentrations of glucose ranging from 0 to 40mM.*(37)*

Other selective chemical sensors have been reported utilizing the PCCA approach. Instead of introducing binding moieites into the polymer network structure, enzymes are entrapped in the matrix of the hydrogel. In this case enzymatic products produce a swelling and colorimetric change. In two such systems*(40, 41)*, an organophosphate

13

sensor was fabricated utilizing either organophosphorous hydrolase(OPH) or acetylcholinesterase. In the case of acetylcholinesterase, organophosphates bind to the enzyme, disabling it. This mechanism phosphorylates the enzyme, introducing an immobile negative charge within the PCCA. The OPH based photonic crystal sensor instead responds to the protons produced by the hydrolysis of organphosphates by the OPH.

Synthetic binding moieties have also been used in conjunction with PCCA based photonic crystals. Aptamer based sensors for the colorimetric, selective detection of heavy metal ions have been reported*(42)*. The polymer network is cross-linked with aptamers specific to mercury and lead. Upon recognition, the aptamers bind, forming hairpin-based complexes which cause the hydrogel to shrink, blueshifting the peak reflected wavelength. Another approach to producing synthetic binding moiety based photonic crystals is the use of molecularly imprinted polymers(MIPs). MIPs are polymers synthesized in the presence of a template molecule. When the template is removed it leaves a site which has a complementary shape and functionality to the original molecule. These imprinted sites then have a specific and selective binding affinity to the molecule of interest. In one such system developed by Hu et al*(43)*, MIPs containing a CCA of silica particles were molecularly-imprinted with theophylline. When theophylline was reintroduced, the binding event caused the hydrogel to swell. The resulting photonic crystal had a reported detection limit of 0.1 fM, but its maximum response was only 20nm shift in reflected wavelength. Similar MIP based photonic crystals have been reported for the detection of a variety of amino acids*(44)*. This system

had responses as high as 80nm redshifts, unfortunately these MIP based technologies do not have the selectivity seen in enzymatic, antibody or aptamer based sensors.

1.5 Outlook on Photonic Crystal Sensors

Photonic crystals provide an interesting sensing platform because they can respond analytes of interest with an easy to discern, color change. If they are properly design, no other equipment is required to ascertain if a color change has occurred in response to a sensing event. Photonic crystals can also respond with different colors depending on the concentration of the analyte of interest. In this sense they can be designed as quantitative litmus tests that do not require training, similar to a pH strip in operation. Other colorimetric sensing systems such as gold nanoparticles are very effective at conveying sensing events but must be used in conjunction with a microfluidic or paper-based chromatography. Alternatively photonic crystals can act as passive autonomous sensors, as it is a singular material that is responding colorimetrically to the sensing event. It has been demonstrated that photonic crystals can be fabricated as paints*(21)*, sprays*(16)* and even as printer inks*(22)* which opens them up to a variety of manufacturing techniques and platforms. Ultimately, photonic crystals should be investigated as passive color changing sensors that can be placed in a medium and monitored visually until the sensing event occurs. For these reasons, infrared and low response shift photonic crystal sensors do not have a lot of purpose as the do require extraneous equipment. In scenarios where a powered sensor is utilized, other more sensitive techniques are preferable such as fluorescence, amperometric measurements or surface enhanced Raman.

2.0 Color Changing Block Copolymer Films for Chemical Sensing of Simple Sugars

2.1. Abstract

We investigated the use of functionalized photonic block copolymer films for the detection of glucose. Polystyrene-b-poly(2-vinyl pyridine) (PS-b-P2VP) block copolymers were chemically functionalized with 2-(bromomethyl)phenylboronic acid and cast into films that reflect a visible color when exposed to aqueous media. The 2-(bromomethyl)phenylboronic acid functionality can reversibly bind to glucose. When exposed to high concentrations of glucose the polymer responded with a red shift in color. Low concentration exposure of glucose caused the polymer films to blue shift in color. The BCP films also exhibited a selective response to fructose, mannose or galactose, giving a different response depending on which sugar is present. The color of the polymer was tuned to blue, green, yellow or orange by varying the film's crosslink density. The color change can be visually observed without the use of equipment such as a spectrometer. It should be noted that the following chapter has been published in Biosensors and Bioelectronics, doi: 10.1016/j.bios.2011.07.043

2.2. Introduction

Chemical sensors have been developed from a wide array of materials that can change color upon exposure to a target molecule. These sensor systems are generally based on photonic crystals that have been modified to recognize the target molecule. The photonic crystal contains periodic nanostructures with differing indices of refraction that interact with visible light. The material can be functionalized to recognize or bind to specific chemical targets. Recognition of the target will alter the spacing of the periodic nanostructure thereby changing the way it interacts with visible light. The advantage of

such systems lies in producing a discernable change in color. This concept has been applied in the fabrication of colloidal hydrogel systems, porous silicon systems as well as through the use of lithography techniques on other substrates. Asher *et al* demonstrated the use of a photonic crystal polymerized colloidal hydrogel system.*(45, 46)* Such material could act as a sensor for glucose but required the complex process of synthesizing monodisperse, highly charged polystyrene particles. Porous silicon*(24, 26)* and nanoprint lithography *(25)* have also been reported as photonic crystal chemical sensing platforms. These systems can be problematic in producing a discernable response without analytical measurements. Therefore, a sensor that can be easily fabricated and yield an instantaneous, visibly discernable response is needed.

One of the material systems investigated for its use as photonic crystals is self-assembled microphase separated layers in block copolymer films*(12, 47, 48)*. Block copolymers (BCPs) consist of two or more chemically distinct sequences of monomer repeat units linked together through a covalent bond. Upon evaporation from a solvent, BCPs will microphase separate into solid films displaying a number of different morphologies (e.g hexagonal, cubic, gyroid, lamellar) depending on the relative volume fraction of each block*(14)*. BCPs in which both blocks are of equal molecular weight generally exhibit the lamellar morphology. Self-assembly into a lamellar morphology is significant in producing a BCP photonic crystal. If there is enough contrast in refractive index between the two blocks in the lamellar structure then certain wavelengths of light will be reflected by the material. This phenomenon is dictated by:

$\lambda_1 = 2(n_1 d_1 + n_2 d_2)$

(2.1)

where λ_1 is the reflected wavelength, n_i is the refractive index of layer i and d_i is the thickness of layer i.

In this study, the diblock copolymer polystyrene-b-poly(2-vinylpyridine) (PS-b-P2VP) , which microphase separates into a lamellar periodic stack, was explored for its use as a chemical sensor to detect and respond to glucose with a change in color. The 2-vinyl pyridine (P2VP) block was quaternized with 2-(bromomethyl)phenylboronic acid, which placed a positive charge on the pyridine ring of the block. This charge allows the BCP film to swell in aqueous media. The swelling changes the thickness of the block allowing it to interact with wavelengths of visible light. Kang *et al (12)* has reported lamellar PS-b-P2VP films quaternized with bromoethane, which places a positive charge in the P2VP block, and attaches an ethyl group to the nitrogen atom. In our work, the quaternizing agent used contributes a boronic acid residue, giving the BCP the ability to bind to sugars such as glucose. We hypothesized that binding would induce a change in the distance between the lamellae causing a change in the wavelength light reflected by the polymer, thus allowing the BCP to act as a glucose sensor.

Boronic acids have been of great interest in chemical sensing due to their ability to covalently bind to sugar molecules such as glucose *(49–51)*. Although sensing glucose has applications in diabetic medicine our decision to explore glucose sensing using the boronic acid functionalized BCP system, was designed to serve as a model system to test the concept that block copolymer based photonic crystals can be fabricated to act as chemical sensors for small molecule detection. In the work described in this manuscript, the polymer film was tested for successful attachment of the boronic acid, retention of the

lamellar morphology post-functionalization, and sensitivity and specificity to simple sugar binding.
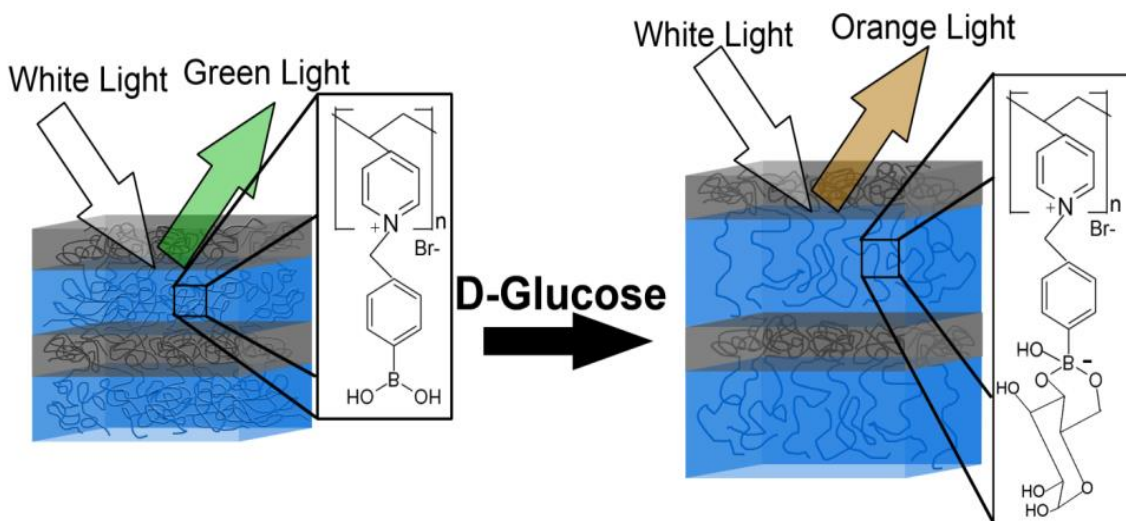
Figure 2.1: Schematic depicting the BCP film color change. Initially the BCP film is in deionized water. The positive charge on the pyridine allows the P2VP block to swell in the water. This gives the BCP film sufficient thickness to reflect visible light, in this case green light. When D-glucose is introduced it binds to the phenylboronic acid functionality which lowers the pKa of the boronic acid forming the negatively charged boronate complex. The additional negative charge swells the BCP film causing it to reflect light in the wavelength of orange.

A schematic of the BCP film sensor can be seen in Figure 2.1. Initially the BCP film is fabricated to exhibit a periodic lamellar stack. The P2VP block of the block copolymer is functionalized with phenylboronic acid placing a positive charge on the pyridine ring, which allows the P2VP block to swell in aqueous media until its thickness is large enough to interact with visible light, in this case reflecting green light. The phenylboronic

acid can bind sugars and will do so when exposed to a glucose solution. As shown in Scheme 1 the boronic acid binds to the 1,3 diol functionality. It has been reported that this is the kinetically favored binding site on glucose as well as the 1,2 cis diol*(52)*. This binding event lowers the *pKa* of the phenylboronic acid causing it to form the negatively charged boronate complex. The negative charge triggers additional swelling of the BCP film changing it color from green to orange. We have shown that after functionalization the BCP film can respond to a glucose solution and shows a selective response when exposed to different sugars such as fructose, mannose or galactose.

2.3. Methods

2.3.1. Fabrication of Photonic BCP films

The procedure for fabrication of the PS-b-P2VP films was adapted from Kang et al*(12)*. The PS-b-P2VP block copolymers were purchased from Polymer Source (Montreal, Canada). The molecular weight of each block of the copolymer was 133,000 g/mole. A 5% weight/volume stock solution of PS-b-P2VP was prepared in propylene glycol monomethyl ether acetate (PGMEA). The films were prepared by spin-casting 300µl of the PS-b-P2VP solution onto 1''x1'' glass slides at 350rpm for two minutes. The glass slides were purchased from Ted Pella (Redding, CA), and were functionalized with 3-(aminopropyl)triethoxysilane. The spin-cast block copolymer films were subsequently annealed in chloroform vapor at room temperature for 24 hours to allow them to self-assemble into a lamellar structure.

2.3.2. Functionalization and Tuning of Photonic Properties

The P2VP block of the spincast films was quaternized with 2-(bromomethyl)phenylboronic acid. The quaternization reaction places a phenylboronic

acid functional group in the P2VP block, allowing the polymer to bind sugars such as glucose. The quaternization reaction was carried out by immersing the spincast, annealed block copolymer films in a solution of 40mg of 2-(bromomethyl)phenylboronic acid in 40mL of acetonitrile and allowing it to reflux for 5 hours. The quaternized polymers were then removed from the solution and dried in a 50°C oven for 1 hour. To tune the optical properties of BCP film a crosslinking agent, 1,4-dibromo-2-butanol, was introduced into the acetonitrile solution. Different molar ratios of 2-(bromomethyl)phenylboronic acid to 1,4-dibromo-2-butanol were tested at 0.05mmol as the total monomer amount. The same protocol was used to investigate the effect of different degrees of crosslinking on the color of the BCP films.

2.3.3. Characterization

Fourier transform infrared spectroscopy (FTIR) was utilized to determine whether the boronic acid functionality was successfully attached. The functionalized polymer film was removed from the glass slide by immersion in a 5%v/v aqueous solution of hydrofluoric acid. The freestanding polymer film was dried for 24 hours in a 50°C oven. An FTIR spectrum was obtained of the functionalized polymer film using a Thermo Nicolet FT-Raman, Model 670. To determine whether the lamellar morphology was maintained after functionalization, images of the polymer were taken using transmission electron microscopy (TEM). The sample was prepared by embedding a section of the functionalized polymer film in Spurr's resin purchased from Ted Pella. The embedded polymer film was then dry microtomed and stained through exposure to solid iodine for 1 hour. The images were taken using a JEM-2100F 200kV transmission electron microscope.

2.3.4. Sugar detection

Once the films were functionalized with 2-(bromomethyl)phenylboronic acid, they were exposed to various concentrations of D-glucose to observe if the films would respond with a color change. Aqueous solutions of 50, 40, 30, 10, 5 and 1mg/ml of D-glucose were prepared. The films were soaked in 20mL of DI water and a coverslip was placed on top of the polymer film on the glass slide to retain the water in the film as it was transferred to the UV-Visible spectrometer. The water-swollen control sample was then placed in a Perkin Elmer Lambda25 UV-Visible spectrometer and the visible spectrum was measured. Each film was then soaked in one of the prepared glucose concentrations and the visible spectrum was again measured and compared to the film soaked in pure water. To test for selectivity between glucose and other sugars, films were prepared and exposed to 50mg/ml solutions of glucose, fructose, galactose and mannose and their visible spectra measured.

2.4. Results and Discussion

2.4.1. Characterization

In order for the BCP film to diffract light towards the observer, the lamellar morphology must be oriented parallel to the glass substrate. The 3-(aminopropyl)triethoxysilane functionalization on the glass substrate interacts with the P2VP block of the BCP by influencing the morphology to be parallel to the substrate. The BCP film is then annealed by exposing it to cholorform vapor, mobilizing the polymer chains and allowing them to form the parallel lamellae. This annealing process is very specific, requiring precise conditions to be successful. Environmental factors such as room humidity and evaporation rate of the annealing solvent can cause the BCP film to have poor

morphology or break the interactions between the BCP and the substrate. It was found that low humidity, approximately 20%, and relatively slowed evaporation rate of the choloform dramatically improved morphology. After completion of the annealing process the BCP film is chemically functionalized by attaching 2-(bromomethyl)phenylboronic acid to the P2VP block. This chemical modification requires that the BCP film be exposed to acetonitrile at an elevated temperature. Such harsh conditions could potentially damage the BCP film or disrupt its delicate lamellar morphology. If the lamellar morphology is disrupted by the chemical modification, then the photonic properties of the BCP film will be diminished. TEM was utilized to determine whether the lamellar morphology was maintained after functionalization with the 2-(bromomethyl)phenylboronic acid. Figure 2.2 presents the electron micrograph of the cross section of both an unmodified BCP film and of a BCP film functionalized with 2-(bromomethylphenylboronic acid). As seen in Figure 2.2 the lamellar morphology needed for the film's optical properties is maintained after functionalization of the P2VP block. In the unmodified film of Figure 2.2A, the layer thickness of the P2VP block and PS block are similar in size as the molecular weight of each block is comparable. The iodine-stained block is the P2VP. After chemical functionalization, as seen in Figure 2.2B, the lamellar morphology is maintained however; there is an apparent increased thickness of the darker iodine stained P2VP block versus the lighter PS block due to the increased mass added to the P2VP block from the 2-(bromomethyl)phenylboronic acid.
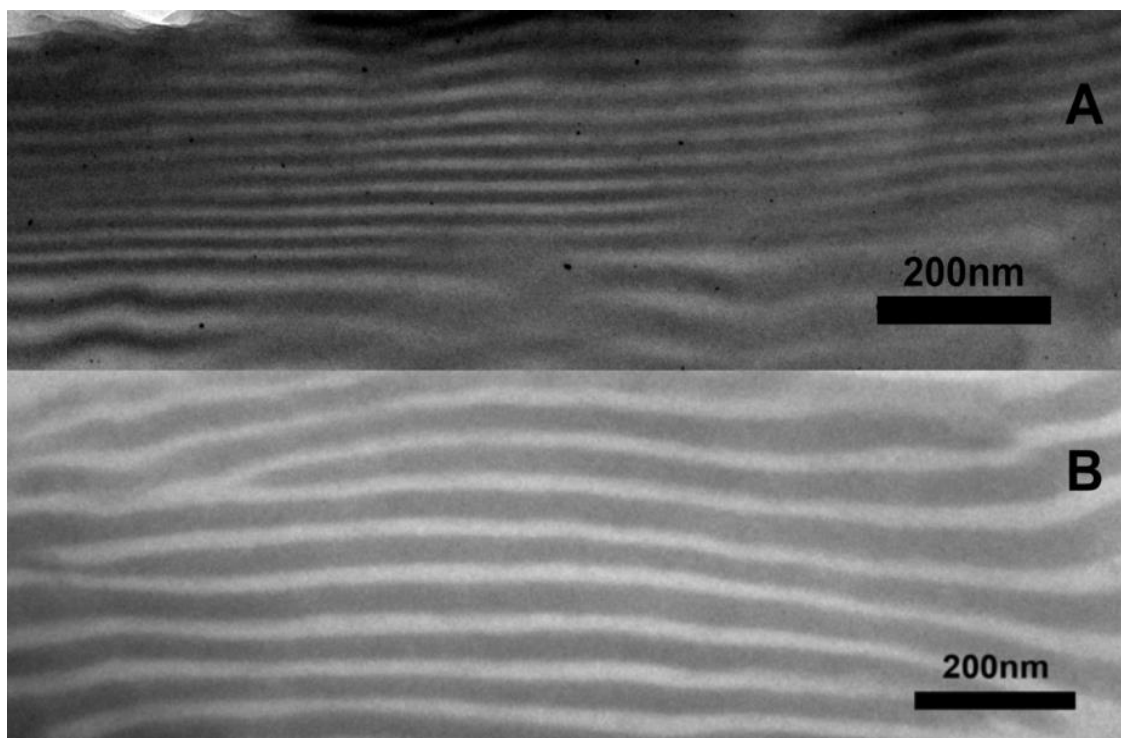
Figure 2.2 A) TEM of annealed, unmodified PS-b-P2VP film. B) TEM of PS-b-P2VP film functionalized with 2-bromomethylphenylboronic acid exhibiting a lamellar morphology. The darker iodine stained P2VP block appears thicker due to the increased mass of the P2VP block from the functionalization as compared to the cross section seen in the unmodified film, A.

Verification that the PS-b-P2VP films were functionalized was obtained by analyzing the chemical structure with FTIR. The pyridine group of the P2VP block substitutes the bromine in the 2-(bromomethyl)phenylboronic acid which covalently bonds the boronic acid functionalization to the pyridine. The boronic acid functionalization places a positive charge on the nitrogen atom in the pyridine ring of the P2VP block as the pyridine groups are converted to pyridinium. This conversion from pyridine to pyridinium can be observed using FTIR. The FTIR spectrum of a modified and unmodified film was taken.

A peak appeared at 1627cm^{-1} in the modified film indicating the conversion of pyridine to pyrindinium, or the placement of a formal positive charge on the nitrogen atom of the pyridine ring. This functionalization serves two important purposes. The first of which is to place a formal positive charge on the P2VP block of the BCP film allowing it to swell in water. This swells the P2VP block to a large enough thickness, which allows it to interact with visible light as dictated by Bragg's law. The second purpose of the functionalization is to introduce boronic acid to the BCP film. Boronic acid binds to sugar molecules allowing the BCP film to recognize and respond to simple sugars with a change in color. This substitution reaction was relatively easy to perform requiring exposure of the BCP film to a solution of 2-(bromomethyl)phenylboronic acid in acetonitrile while refluxing for 5 hours. This methodology could potentially open up other avenues for different chemical functionalizations each with their own sensing application.

2.4.2. Tuning the Polymer Film Photonic Properties

Demonstrating control over the optical properties or color of the BCP film is vital for producing a reliable chemical sensor. To tune the color of the functionalized BCP film, varying degrees of crosslinking were introduced into the P2VP block. The crosslinker used was 1,4-dibromo-2-butanol in conjunction with the boronic acid functionalization. The BCP was exposed to various molar ratios of 1,4-dibromo-2-butanol (crosslinker) to 2-(bromomethyl)phenylboronic acid (quaternizer). Increasing or decreasing the mole fraction of the crosslinker, allows the collapsing or swelling the polymer film in water, which tunes the color of the BCP.
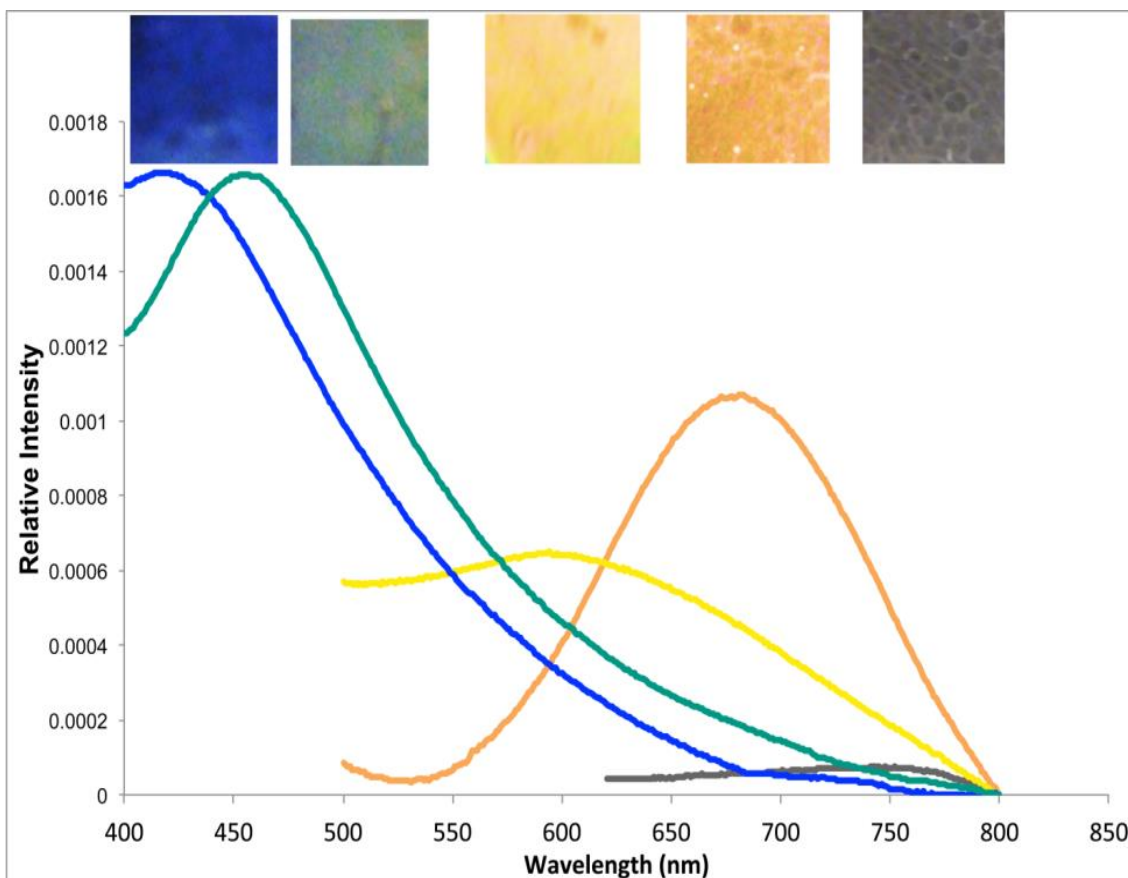
Figure 2.3 The BCP film color can be tuned to blue, green, yellow, orange or transparent(infrared) colors depending on the degree of crosslinking. Increasing the crosslink density inhibits swelling which blueshifts the color of the polymer film. As seen each BCP film displays a different color and visible spectra depending on the molar ratio of crosslinker to quatenizer.

The BCP films can be fabricated to exhibit different colors by controlling the swelling of the polymer film through variations in crosslink density. The BCP films have successfully been tuned to blue, green, yellow, orange or infrared colors. Figure 2.3 shows each of the colored BCP films and their corresponding visible spectra. As seen the BCP film's color is intense and easy to recognize by eye. There is no need for extraneous equipment to distinguish one color from another. This allows the simple fabrication

26

sensor to be utilized by individuals who would not need specific training to determine if the BCP film has responded to a specific analyte.

2.4.3. Response to Glucose

Boronic acid can bind to 1,2 and 1,3 cis diols, a chemical functionality commonly found in sugar molecules. The binding of a sugar to the boronic acid lowers its pKa. The pKa change increases the number of boronic acid residues that form the boronate complex, which is negatively charged. Such negative charge then causes the BCP film to swell, thereby changing its color. The PS-b-P2VP films functionalized with 2-(bromomethyl)phenylboronic acid were exposed to a range of concentrations of aqueous D-glucose solutions. The tested polymer films were initially green in pure deionized water due to the functionalization placing a positive charge on the P2VP block. The green films exposed to the 50mg/ml glucose solution instantly swelled and became orange in color. This shift in color is visible to the eye and can detected without the use of equipment such as spectrometer. This color change and UV-Visible spectrum can be seen in Figure 2.4.
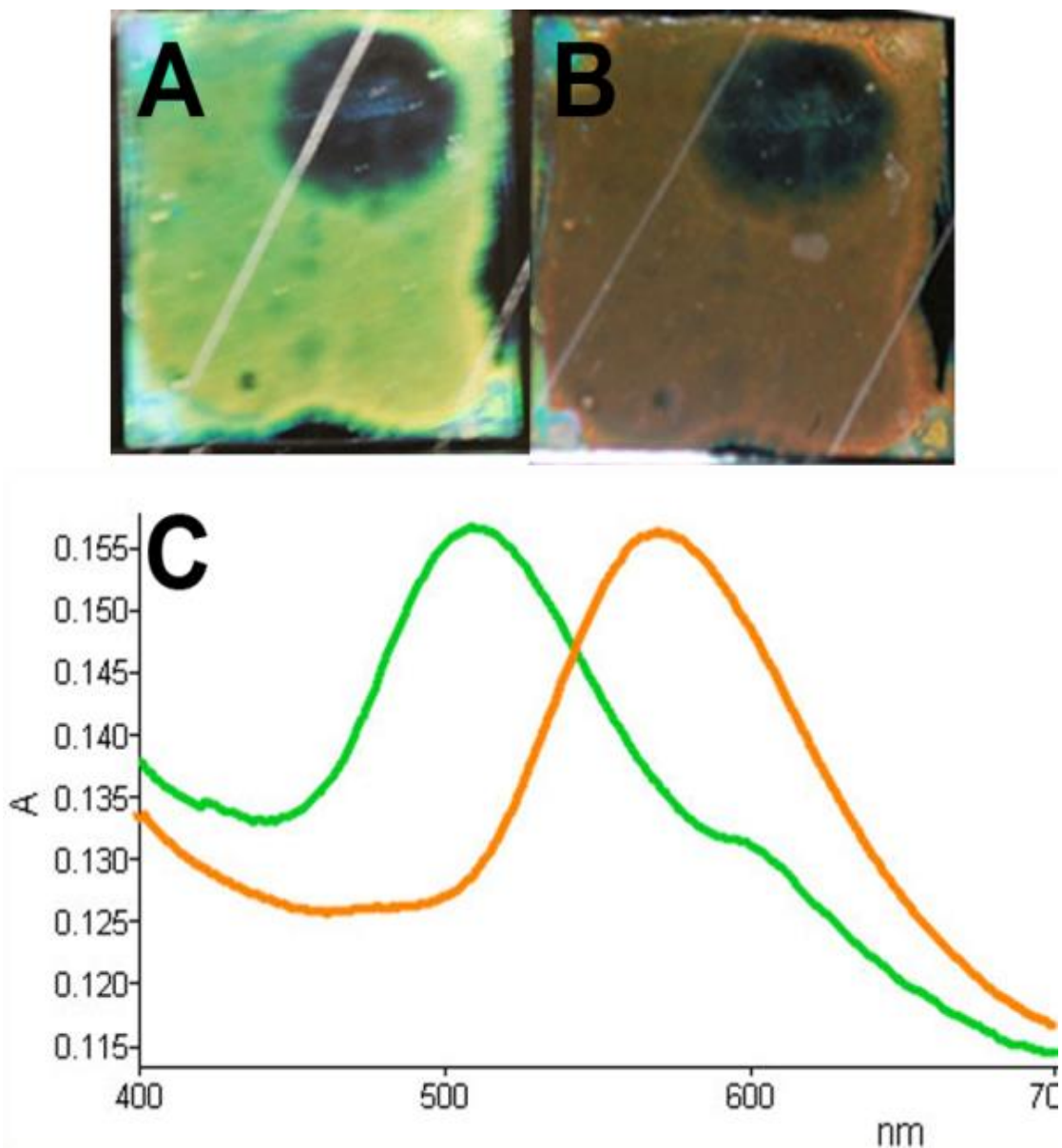
Figure 2.4(A) When exposed to pure water the film swelled due to the positive charge placed on the P2VP block from the functionalization. (B) Once immersed in a glucose solution the functionalized polymer film swelled further due to the boronic acid groups binding glucose. When bound to glucose, a negative charge exists on the boron atom of the boronic acid moiety causing the film to further swell and become orange in color. (C) The UV-Visible spectrum of the functionalized film in both water and glucose solution. In water the film swells to reflect a peak wavelength of 510 nm corresponding to the

color green. In the glucose solution, the film swells and reflects a peak wavelength of 590 nm corresponding to orange.

UV-Vis spectroscopy was used to quantify the films' exposure to a range of aqueous concentrations of glucose (0-50 mg/ml). It was predicted that the spectrum peak should redshift after exposure to glucose due to the binding and incorporation of the glucose molecule causing swelling. When exposed to concentrations of 50mg/ml and 40mg/ml glucose, the films shifted from green to orange or yellow, respectively as seen in Figure 2.5. This indicates that they became swollen as expected. However, exposure to lower concentrations of glucose had a very different effect.
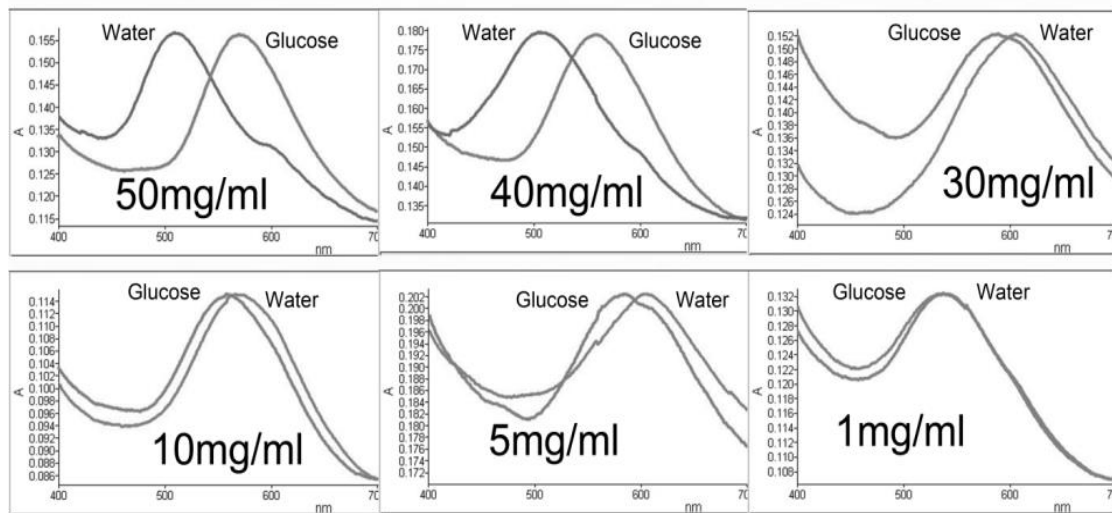
Figure 2.5 The shift in peak wavelength of each BCP sample immersed in various concentrations of glucose solution of (a) 50mg/ml (b) 40mg/ml (c) 30mg/ml (d) 10mg/ml (e) 5mg/ml and (f) 1mg/ml. 50 and 40mg/ml solutions caused an increase, or redshift, in wavelength indicating that the polymer film had swelled. However, a decrease, or blueshift, was observed in the BCP samples exposed to 30, 10, and 5 mg/ml solutions, indicating that the film collapsed.

As seen in Figure 2.5, after exposure to concentrations of 30, 10 and 5mg/ml glucose, the films blueshifted, indicating that the polymer film had collapsed when exposed to these concentrations of glucose solution. Interestingly, this counterintuitive observation of swelling at high concentrations and collapsing at lower concentrations has been reported in similar boronic acid based detection systems*(45, 46)*. Asher *et al* demonstrated a similar bi-modal response in a polymerized crystalline colloidal hydrogel system. Their group reported that when their hydrogel was exposed to high concentrations of glucose each boronic acid functionality bound to one glucose molecule, placing a negative charge on the boron atom, which caused the film to swell and redshift in color. Exposure to lower concentrations caused two boronic acid functionalities to bind to one glucose molecule. This effectively creates crosslinking in their hydrogel system, causing it to collapse and blueshift in color. Based on our results illustrated in Figure 2.5 it is reasonable to assume that a similar phenomenon is occurring in the functionalized block copolymer system. The effect of pH on phenylboronic acid's ability to bind sugars such as glucose has been demonstrated. It has been shown that higher pH increases the Keq of the glucose binding reaction while lower pH decreases the Keq of binding glucose.*(53)* Other photonic crystal chemical sensors have also shown successful response to a target analyte, particularly those fabricated from porous silicon *(24, 26)* or nanoprint lithography*(25)*. The observed response in these systems, however, is small, non-visible, and thus cannot be measured without the aid of supplementary equipment.

2.4.4. Selectivity

The phenylboronic acid functionality introduced to the P2VP block of the BCP can covalently bind to any diol-containing sugar such as glucose, fructose, mannose and

galactose. The K_{eq} of boronic acid binding to each one of these sugars varies depending on the sugar. This suggests that the boronic acid functionalized film should have a selective response to each simple sugar. To observe this effect, a BCP film functionalized and crosslinked to yield a blue color in water was exposed to 50mg/ml solution of either glucose, fructose, mannose or galactose. After 30 minutes of exposure the BCP film's visible spectra was measured using UV-Vis spectroscopy. The peak difference in wavelength was then calculated as the difference between the peak wavelength of the film in water and in the sugar solution.
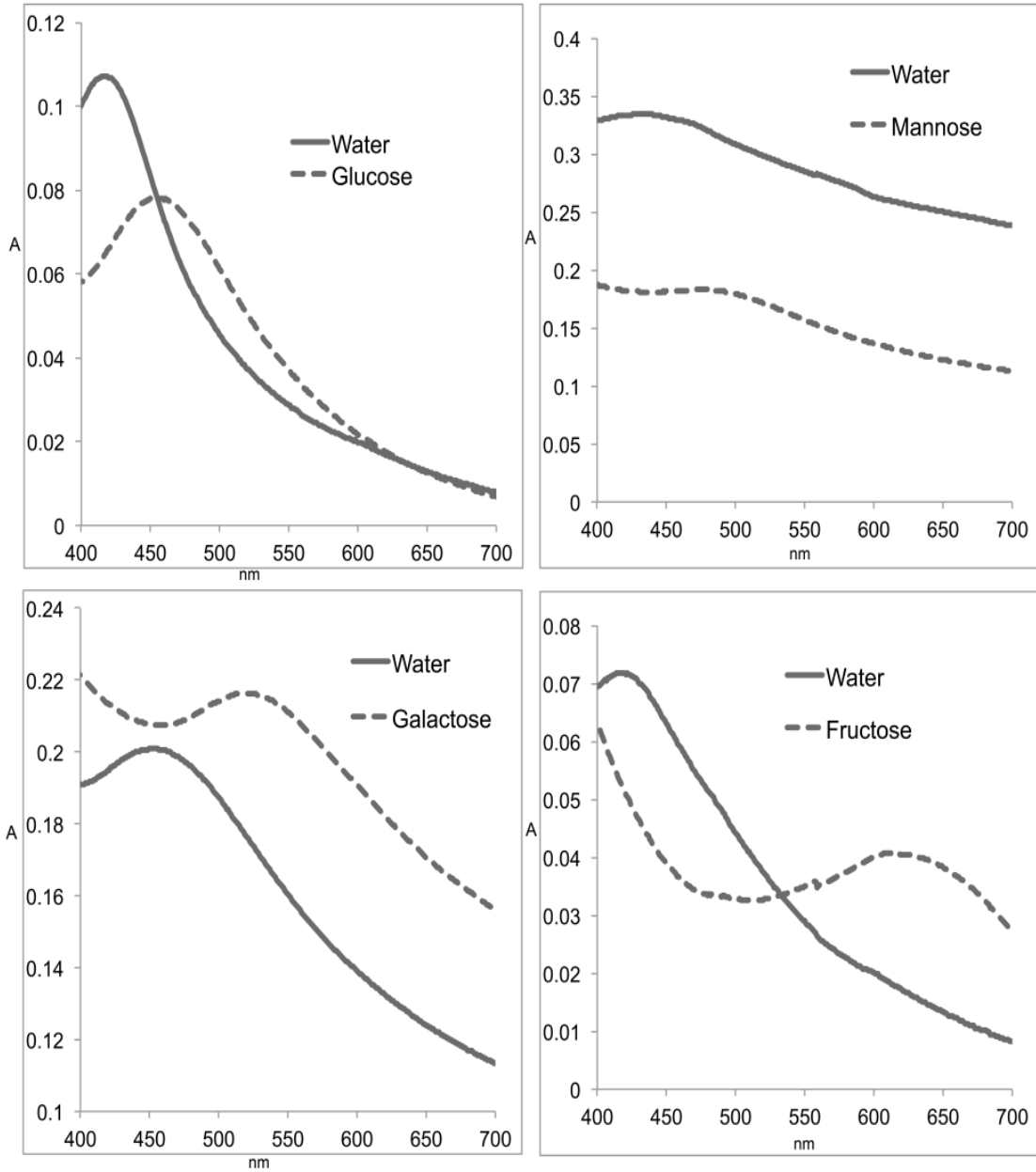
Figure 2.6 An initially tuned-blue BCP film was exposed to four different sugar solutions containing either glucose, fructose, galactose or mannose at the same concentration. The difference of the peak wavelength observed in water versus that observed in the sugar solution was calculated to obtain the shift in wavelength. As seen in the figure, fructose gave the largest response of an approximately 200nm redshift in wavelength. Galactose induced a 70nm increase in wavelength and mannose and glucose induced smaller

32

increases of approximately 40nm each. This indicates that the BCP film can differentiate between fructose, galactose, mannose and glucose for a given concentration.

As seen in Figure 2.6, the BCP film exposed to fructose gave the largest response of a 200nm redshift in wavelength. The film exposed to galactose exhibited a 70nm redshift in color. The smallest responses were from films exposed to glucose and mannose, which exhibited 44nm and 37nm decreases, respectively. Of note, in separate experiments the 50mg/ml glucose solution evoked the same shift in wavelength (compare Figure 2.5a to Figure 2.6), although in each case the original color of the BCP film in water is different. This difference in response between fructose, galactose and glucose is expected. It has been reported that fructose has the highest K_{eq} to bind to boronic acid, followed by galactose, and then glucose*(54)*. This difference in binding is due to the steric structure of each sugar. Boronic acid can bind to both 1,2 and 1,3 cis diols but preferentially binds to 1,2 cis diols. Fructose for example has a planar 1,2 cis diol. Glucose does not have a 1,2 cis diol but has a 1,3 cis diol in its dominate pyranose form. Generally glucose binds to boronic acid in its furanose form, which does contain a planar 1,2 cis diol*(52)*. This result signifies that for a given concentration, the boronic acid functionalized BCP film can differentiate between glucose, galactose and fructose.

2.5. Conclusions

Our results indicate that the PS-b-P2VP block copolymer film shows promise for detecting chemical targets. This colorimetric material system is unique in that it requires only the functionalized block copolymer to indicate an exposure to a chemical target. Once functionalized with the 2-(bromomethyl)phenylboronic acid, the PS-b-P2VP film demonstrated the ability to respond to glucose with a change in color without the use of

any supplementary enzymes such as glucose oxidase or additional equipment to assess the visible color change. The block copolymer lamellar stacks responded with a redshift in color in high concentrations of glucose and a blueshift in color for low concentrations of glucose. The BCP film also exhibited a selective response to fructose, glucose or galactose, by swelling to different degrees depending on which sugar is present. The PS-b-P2VP block copolymer can easily be processed into films, sheets or other large area coatings as needed. The color of the BCP film can be tuned to blue, green, yellow or orange as demonstrated. While similar sensors exist in porous silicon, lithography and hydrogel systems they lack the ease of fabrication and use of these block copolymer films and can require the use of a spectrometer to measure the shift in color. The results show the capabilities of photonic BCP films for chemical sensing as the functionalization can be exchanged for different sensing moieties.

3.0 Self-Assembled Block Copolymer Photonic Crystal for Selective Fructose Detection

3.1. Abstract

The use of one-dimensional photonic crystals fabricated from a self-assembled lamellar block copolymer as a sensitive and selective fructose sensor is investigated. The polystyrene-b-poly(2-vinyl pyridine) (PS-b-P2VP) films are functionalized with 2-bromomethylphenylboronic acid. The boronic acid moiety confined within the lamellar morphology can reversibly bind to sugars such as fructose imparting the photonic properties of the PS-b-P2VP film. The films exhibit a detection limit of $500\mu M$ in water and 1mM in phosphate buffered saline. Exposure to a 50mM solution of fructose invokes a highly visible color change from blue to orange. The films are also able to selectively recognize and respond to fructose in competitive studies in the presence of glucose and sucrose. It should be noted that the following chapter has been published in Biosensors and Bioelectronics, DOI: 10.1016/j.bios.2013.02.025

3.2. Introduction

The quality control and processing of food involves the analysis and detection of sugars. Diabetes, a rapidly growing healthcare problem, prompted technological strides made for the detection of glucose. For the other sugars, primarily fructose, quick and easy detection is not a readily available possibility. Fructose is an important sugar in the food industry having uses as a sweetener and being a component of table sugar or sucrose. Fructose detection has application in the food and beverage industry ranging from determining levels of high fructose corn syrup to monitoring the ripening of fruits. Additionally, quickly and accurately determining fructose levels would assist

manufacturers in the fermentation process of foods. Providing facile monitoring of fructose could ensure higher quality of food products with better economy.

Traditional methods for chemical detection include high performance liquid chromatography (HPLC) as well as gas chromatography (GC). The expensive and time consuming nature of these techniques, coupled with a requirement for in depth training, make them poor options. A variety of techniques specifically designed for fructose sensing have been described previously,*(55, 56)* the most common of which employ optical or electrochemical systems. Electrochemical systems utilize enzymes to sense fructose in a manner similar to blood glucose monitors. Fructose dehydrogenase is a frequently used enzyme in these systems.*(57, 58)* As fructose is oxidized by the enzyme a cofactor is reduced. The reduced cofactor can then liberate electrons to an electrode in contact with the reaction producing a current. While proven to be sensitive and specific, these systems tend to suffer from poor shelf life. The enzyme and its cofactor are not easily stabilized and degrade over time.

Concerns over fructose stability can be eliminated using abiotic systems. While previously mentioned optical and chromatographic techniques cover this requirement, they are laborious and expensive. To eliminate these concerns many researchers have explored the use of boronic acids to sense a variety of sugars including fructose. Boronic acids are a chemical moiety that can reversibly bind to sugars and other polyols. Their use in sugar sensors particularly for glucose and fructose has been demonstrated in large body of literature.*(52, 59–63)* Many of these described sensors employ fluorescence as a means to output a signal. While effective, this method requires extraneous equipment to measure the sensor's output. Alternatively photonic, boronic acid based sensors have

been demonstrated. The Asher group*(39, 45, 53)* in particular explored three dimensional photonic crystal sensors that utilize boronic acid to sense glucose. This type of approach produces a sensor that is simple in its operation. In this study we examined the alternative use of one dimensional photonic crystals produced from self-assembled block copolymers (BCPs) to develop a boronic acid based fructose sensor. The advantage of our approach lies in a less complex fabrication through the use of a self-assembled polymer system.

Diblock Copolymers consist of repeat units of one monomer covalently linked to repeat units of another monomer. Due to thermodynamic incompatibility between the constituent blocks, if cast into films the two sets of different repeat units or blocks will phase separate from one another at a length scale of the order of tens of nanometers, which is comparable to the size of the constituent homopolymer chains. This phenomenon, known as microphase separation, results in self-assembled periodic nanostructures including lamellar, hexagonal, cylindrical or spherical domains.*(14)* In this investigation the lamellar BCP self-assembled nanostructure was used as it can be exploited to become a one dimensional photonic crystal under the appropriate conditions. The Thomas group have previously demonstrated the use of Polystyrene-b-poly(2-vinyl pyridine) (PS-b-P2VP) for producing one dimensional photonic crystals.*(12, 47, 48)* The periodic morphology of the lamellar PS-b-P2VP films in conjunction with appropriate thickness of the P2VP block allowed for the reflection of visible light. The reflected wavelengths of light depend on the thickness of the P2VP block. In their case the P2VP block did not contain any sensing functionalities but was quaternized allowing for the

uptake of aqueous media, swelling the P2VP block to sufficient thickness to reflect visible light.

In this investigation we introduced boronic acid moieties by taking advantage of the simple chemistry that can be performed using the pyridine ring of the P2VP block. Chemically functionalizing boronic acid moieties to the photonic BCP system lead to the development of a fructose sensor. As discussed later, high affinity fructose binding events cause the BCP film to swell, changing the reflected color. This leads to a quick and easily *fabricated* sensor for fructose. The response is a highly visible color change that can immediately indicate to the user to the presence of fructose without the use of extraneous equipment. The sensors sensitivity and selectivity towards fructose was evaluated as well as its ability to detect fructose in interfering environments.

3.3. Materials and Methods

3.3.1 Materials

All materials were used as received unless otherwise specified. The block copolymer Polystyrene-b-Poly(2-vinyl pyridine) (PS-b-P2VP) of molecular weight 133kD-b-131kD was purchased from Polymer Source. 3-(aminopropyl)triethoxysilane (APTES) functionalized glass slides were purchased from Ted Pella. 2-(bromomethyl)phenylboronic acid(BMPBA), 1,4-dibromo-2-butanol, D-Fructose, D-Sucrose and D-Glucose were purchased from Sigma-Aldrich.

3.3.2 Fabrication of Unmodified Block Copolymer Films

A solution (5% wt/vol) of (PS-b-P2VP) was prepared in propylene glycol monomethyl ether acetate. The solution was filtered using a 0.2 micron Teflon filter. To produce a film the solution was spun cast onto a 1''X1'' APTES functionalized glass slide until the

casting solvent had evaporated. The films were subsequently exposed to chloroform vapor at room temperature for 24 hours.

3.3.3 BCP Functionalization with Boronic Acid

BCP Functionalization was performed using BMPBA, which acts as a sugar sensing moiety, and 1,4-dibromo-2-butanol, which acts as the cross-linker. By varying the ratio of the two chemicals, different colored films are produced. This was demonstrated in a previous study. For the purposes of this work it was found that a 0.95:0.05 ratio was optimal in order to achieve blue films. A solution containing the BMPBA and 1,4-dibromo-2-butanol in acetonitrile using this ratio was prepared. The unmodified films were exposed to this solution refluxed at 90°C for 5 hours. The resultant modified films were subsequently washed in excess deionized water for 1 hour and dried in a 50°C oven overnight.

3.3.4 Fructose Detection

Initial fructose sensitivity tests were performed in deionized water. A range of D-fructose solutions in DI water (500µM to 50mM) was prepared. BMPBA modified polymer films were washed in DI water for 10 minutes. Subsequent to washing the reflected visible spectra of the films were measured using a Perkin Elmer UV-Vis spectrometer. The peak wavelength was then recorded as the color of the film. It should be noted that for processing of the data, a background spectra taken of a swollen but colorless film was subtracted to achieve a better signal to noise ratio. After measurements in water, the films were exposed to one of the previously stated fructose concentrations (10mL) for 30 minutes. The visible spectra in the fructose solutions were then measured.

3.3.5 High Ionic Strength Fructose Detection

To demonstrate the reliability of the polymer films in a physiologically representative environment the fructose detection was again demonstrated in phosphate buffered saline (PBS) (0.1M). In this case D-fructose solutions (1-50mM) were prepared in PBS (0.1M). The polymer films were initially washed in PBS (0.1M) for 10 minutes and the visible spectra measured. The polymer films were soaked in one of the fructose solutions (10mL) for 30 minutes. The visible spectra after high ionic strength fructose exposure were then measured.

3.3.6 Selectivity Experiments

Fructose detection was quantified against glucose, mannose and sucrose to demonstrate selectivity. Initially solutions of D-glucose, D-mannose and Sucrose (100mM) were prepared in DI water. Additionally, a solution of D-fructose (10mM) and D-glucose (90mM) solution was prepared. In each study the total sugar concentration was 100mM. The polymer films were then soaked in DI water for 10 minutes and their visible spectra measured. The films were then washed with one of the sugar solutions (100mM) for 30 minutes. The visible spectra after sugar exposure were measured to compare the shifts in wavelength for each solution. Sucrose concentration studies were then preformed using a range of sucrose concentrations (35mM-500mM) following the same procedure for determine shift in wavelength. Finally to determine the interference of competing sugars for detecting D-fructose, varying sucrose concentration (1mM-100mM) were introduced to D-fructose solution (1mM). The shift in wavelength was again measured using a Perkin-Elmer UV-Vis spectrometer.

3.4. Results

3.4.1 Fructose Sensing

The initial studies verified the use of the boronic acid functionalized BCP films as sensitive fructose sensor. The response is due to the acidic nature of boronic acid. Exposure to sugars such as fructose dramatically changes the chemistry of each boronic acid moiety. Boronic acid is a Lewis acid and generates protons by abstracting a hydroxide unit from water. This produces both the proton and a negatively charged boronate anion. Diols such as fructose bind to boronic acid which causes the pKa of the acid to decrease. This decrease in pKa leads to an increase in negatively charged units on the P2VP. Higher density of negative charges causes the polymer film to swell, resulting in red shifting of its reflected color. A schematic of this chemistry can be seen in Figure 3.1.
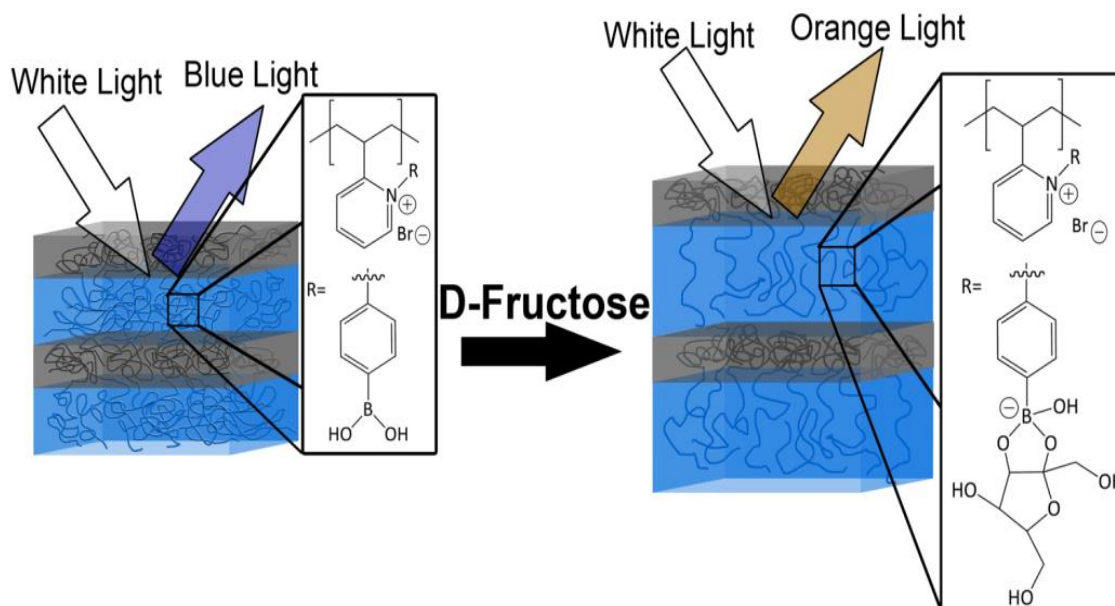
Figure 3.1 A schematic of the boronic acid moiety before and after binding fructose. Fructose binding invokes additional boronate anions to form, causing the BCP film to swell and change color from blue to orange.

The swelling of the BCP film is described by Flory's model of a swollen ionic network.*(23)* In the case of a non-ionic network the major factors influencing the swelling are the free energy of mixing, F_m, and the elastic restoring force, F_{el}. They are described by the following equations respectively:

$$\pi_m = N \left(\frac{\partial \Delta F_m}{\partial n_1}\right)_{T,P} = -RT \left(ln\left(1 - \frac{V_o}{V_m}\right) + \frac{V_o}{V_m} + \chi \left(\frac{V_o}{V_m}\right)^3\right) \tag{1.4}$$

$$\pi_{el} = N \left(\frac{\partial \Delta F_{el}}{\partial a_s}\right)_{T,P} = RT \left(V_1 \left(\frac{v_e}{V_o}\right)\left(\left(\frac{V_o}{V_m}\right)^{1/3} - \frac{2V_o}{fV_m}\right)\right) \tag{1.5}$$

where N is Avogadro's number, V_o is the volume of the BCP film when initially cross-linked, V_m is the volume of the BCP film at swelling equilibrium, V_1 is the molar volume of water, v_e is the number of cross-links, χ is the Flory-Huggins interaction parameter and f is the cross-link functionality. These two equations can then be equated to the Donnan potential seen below:

$$\pi_i = RT(C_+ + C_- - C_+^* - C_-^*) \tag{1.6}$$

where C_+ are the mobile cations in the BCP film, C_- are the mobile anions in the BCP film, C_+^* represents the mobile cations in the bulk solution and C_-^* represents the mobile anions outside the BCP film. The BCP film contains immobile charges from both the boronate ester anion and the quaternized pyridine prompting a higher concentration of mobile ions in the BCP film. This will create a Donnan potential causing an increase in osmotic pressure. When equated with the pressures developed from the free energy of mixing and the elastic restoring force, a relationship between changes in osmotic pressure and changes in volume can be developed assuming the system is at equilibrium. The change in volume, which is directly proportional to the change in thickness, can be related to shifts in reflected wavelength by Bragg's law:

$\lambda=2(n_1d_1+n_2d_2)$

(3.1)

where *d* is thickness of a given layer in this case, λ is wavelength, *n* is refractive index. The reflected wavelengths result from the Bragg stack nanostructure of the BCP film, which creates a photonic band gap, through the alternating layers of polystyrene and functionalized poly(2-vinyl pyridine). The band gap results from the swollen state of the BCP film producing periodicities of a thickness that is an integer multiple of wavelengths of visible light. Due to the periodicity, the reflected wavelengths are in phase, and therefore constructively interfere with one another creating an intense visible response. Since the reflected wavelengths are proportional to the swelling of the BCP film, wavelength shifts can be correlated to fructose concentration.
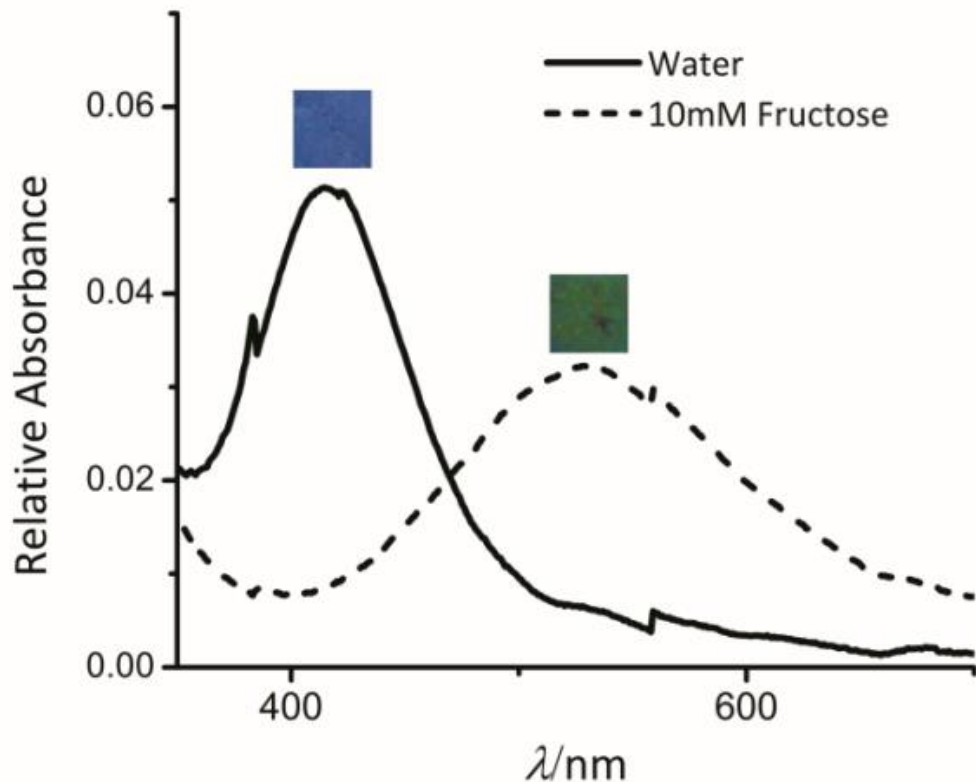
Figure 3.2 The UV-Vis spectra of a polymer film exposed to water(solid) and the same film exposed to 10mM D-fructose solution(dashed). As seen there is a red shift in peak wavelength. The inserts above each peak is a picture of the film's color.

The polymer films were exposed to solutions of D-fructose in deionized water ranging from 500μM to 50mM to demonstrate both specificity and sensitivity. As seen in Figure 3.2 the polymer films initially display a blue peak wavelength of 410nm in the absence of fructose. After exposure to a 10mM D-fructose solution the reflected wavelength red-shifted to 530nm. The insert in Figure 3.2 displays the highly visible color change of the polymer film corresponding to the spectra displayed. Exposure to varying concentrations of D-fructose would then be expected to invoke a correlated shift in wavelength due to changes in swelling. These UV-Vis spectra were utilized to determine shift in wavelength. For all future data, the shift in wavelength is displayed to represent in color change. This was determined by finding the corresponding wavelength to the peak value in the UV-Vis spectra. The difference of two peak wavelengths in then taken to determine the shift in wavelength.
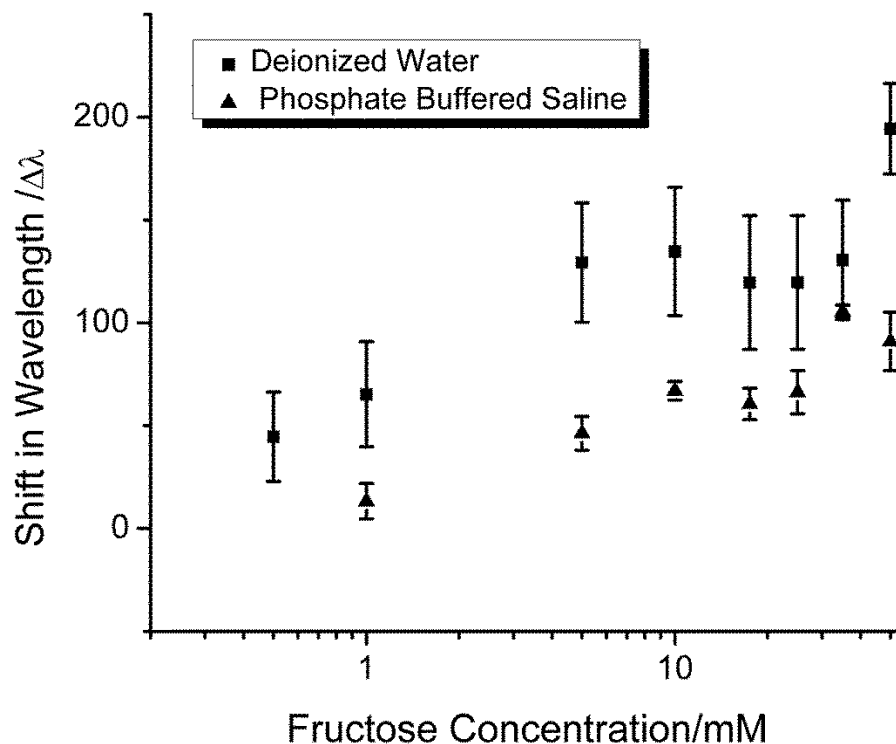
Figure 3.3 Calibration curve developed by exposing BCP films to concentration of D-fructose ranging from 500μM to 50mM. Increases in D-fructose concentration correspond with increases in wavelength shift. Detection in PBS resulted in slightly reduced sensitivity however following the same trend.

Figure 3.3 shows the shift in wavelength response resulting from each sequential concentration of D-fructose. The BCP films gave measurable responses to concentrations of fructose as low as 500μM and presented larger responses for concentrations up to 50mM. Each response gave approximately similar standard deviations and logarithmic increases in concentration gave a corresponding logarithmic response in wavelength shift. When exposed to the fructose solutions for times greater than 24 hours the BCP films

will blue shift in color. Films exposed to 50mM fructose that became orange in color will blueshift to green after 24 hours.

The initial studies performed explored fructose sensing in deionized water where the pH is not buffered and there are no ions present to disrupt the output of the sensor. Due to the sensor responding to changes in osmotic pressure brought about by increasing charge density, it is expected that ions would reduce any output produced by the BCP film. Studies performed by Kang et al*(64)* have also shown that quaternized polystyrene-b-poly(2-vinyl pyridine) films collapse in the presence of high salt concentrations. This occurs because of shielding of the immobilized charges on the quaternized P2VP. Therefore, the next phase of this study is to investigate the sensor's reliability in a more relevant environment. D-fructose solutions ranging again from 500μM to 50mM were produced in 0.01M phosphate buffered saline (PBS) at a pH of 7.4. The PBS both introduced a buffered pH as well as high salt concentration to test the BCP film's reliability. Figure 3.3 shows the shift in wavelength response to each concentration of D-fructose in 0.01M PBS. It is evident that the sensitivity of the sensor did decrease. The detection limit in the presence of the PBS was 1mM. As in the previous study, all the BCP films were originally blue in color. Application of the D-fructose solutions invoked a redshift in color. Logarithmic increases in D-fructose solution corresponded to logarithmic increases in wavelength shift. Exposure to 50mM D-fructose gave a shift from a highly visibly blue color to green. 1mM gave a shift from blue to turquoise. It is worth noting that this demonstrates the BCP film's capacity to detect fructose at a physiologic pH. The sensor also demonstrated a systematic plateau in response to concentrations ranging from 10mM to 25mM in both DI water and in PBS. This effect

could be attributed to the high molecular weight of the polymer becoming entangled or physically cross-linked. At concentrations of 35mM of higher sufficient osmotic pressure is generated to overcome this entanglement and the BCP film begins swelling again, thus redshifting in color.

Figure 3.4 displays pictures of BCP films exposed to these varying concentrations. Every BCP film was initially blue in color. Exposure to a 50mM D-fructose solution resulted in a large shift to orange. Decreases in concentration gave smaller shifts with 5mM producing green films and 500μM producing turquoise films. This not only allowed differentiation between concentrations of fructose but presented a method to qualitatively determine whether fructose is present from a simple, intense change in color.
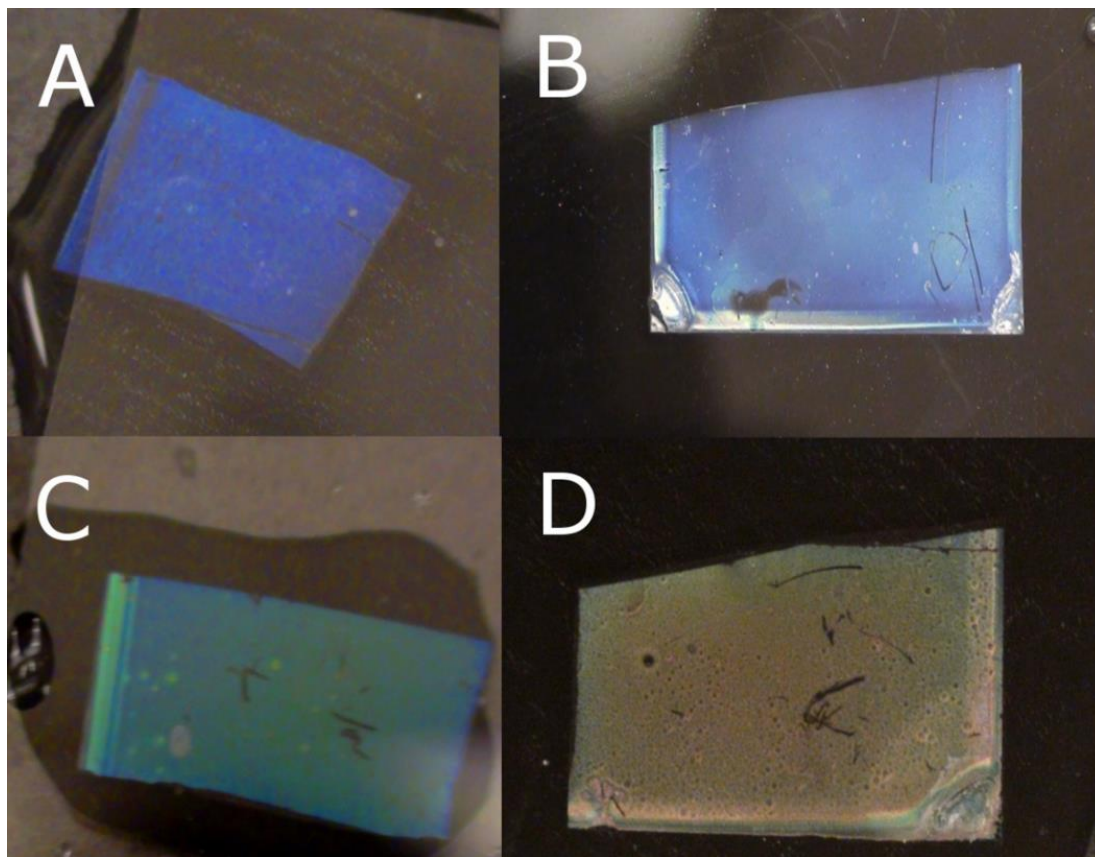
Figure 3.4 Pictures of films exposed to different concentrations of D-fructose in deionized water. As seen exposure to: (a) deionized water resulted in a blue color, (b) 500μM resulted in a turquoise color, (c) 10mM resulted in a green color and (d) 50mM resulted in an orange color.

3.4.2 Selectivity Studies

One possible applications of detecting fructose is to verify additives such as high fructose corn syrup are not present in specific foods. This would require a sensor that can selectivity respond to fructose instead of other similar sugars. Additionally, determining the selectivity of a sensor is an important benchmark in evaluating its efficacy. Selectivity was investigated by comparing the sensor's fructose response to the response invoked by glucose, mannose or sucrose. All tests performed for selectivity involved a total sugar concentration of 100mM. Sensor exposure to solutions of 100mM glucose, 100mM mannose, 100mM sucrose and a mixture of 90mM glucose with 10mM fructose were evaluated. To show there is no synergistic effect, the responses are also compared to a pure 10mM fructose solution. Sensors were then exposed to varying concentrations of sucrose in both DI water and 0.01M PBS ranging from 50mM-500mM. To determine if the sucrose would interfere with sensing fructose, the sensors were exposed to 1mM D-fructose solution with increasing concentrations of sucrose ranging from 1mM-100mM.
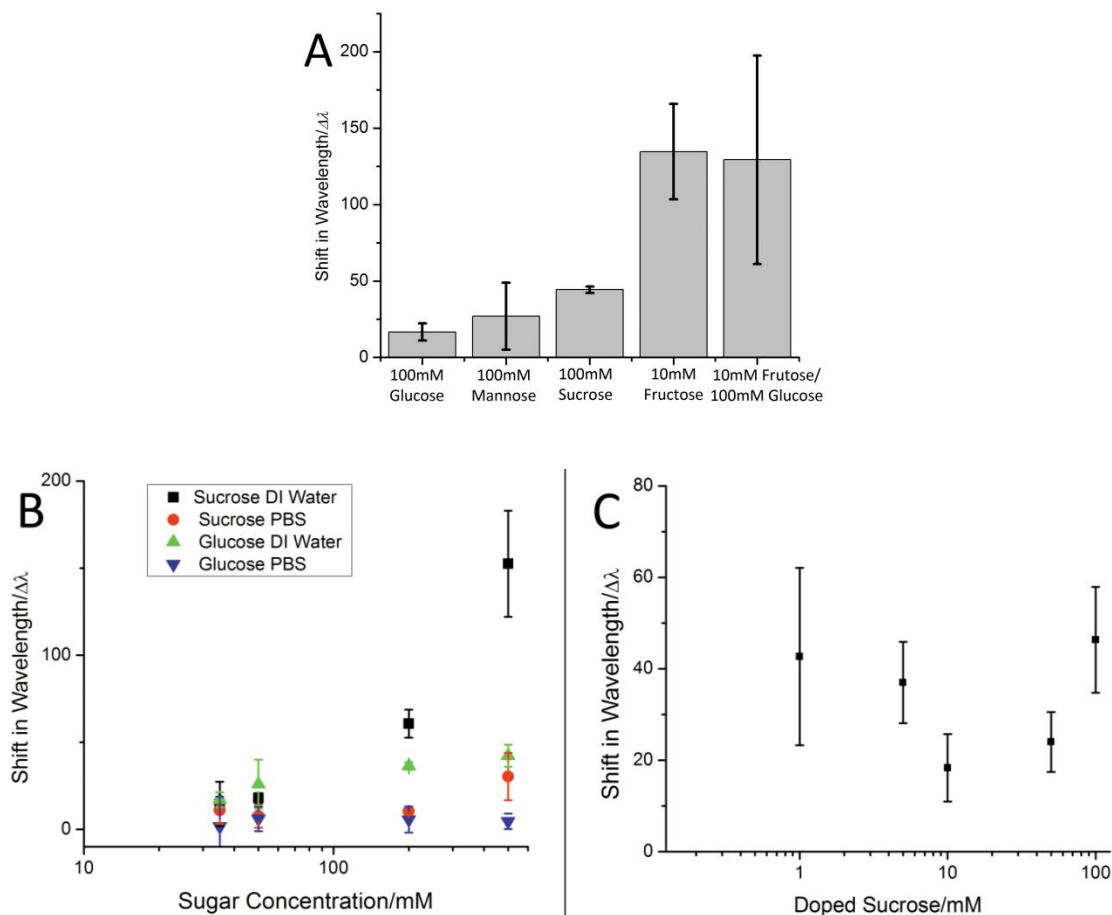
Figure 3.5(a) Selectivity of the sensor towards fructose was demonstrated by exposing BCP films to pure glucose, mannose, fructose and sucrose solutions as well as a mixture of glucose and fructose. The total sugar concentration in each case was 100mM excluding the solution containing only 10mM fructose. As seen the solutions containing 10mM fructose gave a significantly large wavelength shift or color change than the pure glucose or sucrose solutions. (b) Sensors were exposed to a range of sucrose concentrations ranging from 50mM-500mM in DI water and 0.01M PBS. (c) Sensors were exposed to solutions of 1mM D-fructose doped with sucrose concentrations ranging from 1mM-100mM. No significant interference was produced.

As seen in Figure 3.5a, wavelength shift responses to solutions containing 10mM fructose were significantly higher than either the pure glucose or sucrose solutions. Each BCP

film tested was initially blue in color. The color shifted to turquoise after exposure to the 100mM glucose, 100mM mannose or 100mM sucrose solutions. Exposure to the mixture of 90mM glucose and 10mM fructose resulted in a shift to a green color. This result not only demonstrates the selectivity of the BCP film towards fructose but furthermore agrees with previous studies,*(59)* journal articles*(46, 53)* and theory*(54)* regarding boronic acid binding sugars. As previously discussed boronic acid is a lewis acid, which once bound to a sugar or polyol, has an increase in *Ka*. The equilibrium constant of boronic acid binding to a sugar as depicted in Figure 3.1 is dependent on multiple variables based in steric effects. Boronic acid has been shown to only bind to either 1,2 or 1,3 cis diols. This makes it attractive for sugar sensing as most sugars contain these functionalities. Boronic acid does preferentially bind to 1,2 cis diols over the 1,3 cis diols.

Sugar	K_{eq}/M^{-1}
D-fructose	160
D-glucose	4.6
D-sucrose	0.67
D-maltose	2.5
D-mannose	13
D-galactose	15

Table 3.1: Equilibrium binding constant of a variety of sugars towards phenylboronic acid*(54)*. Fructose has the highest binding constant by an order magnitude, while sucrose has the lowest binding constant.

As seen in Table 3.1, this has a significant effect on the binding constant of phenylboronic acid for each of these monosaccharides. Fructose has a K_{eq} of 160M^{-1} which is an order of magnitude larger than glucose with a K_{eq} of 4.6M^{-1}. Many sugars such as glucose, mannose, or galactose contain only 1,3 cis diols. This does not explain why sucrose has less affinity for boronic acid as it contains 1,2 cis diols. Sucrose is a disaccharide which is much bulkier than fructose, a monosaccharide. Steric effects arise,

making it unfavorable for disaccharides to bind to boronic acid over monosaccharides. This effect is very pronounced. It has been demonstrated that disaccharides such as sucrose and maltose have an order of magnitude smaller binding constant for boronic acid compared to glucose and several orders of magnitude less than that of fructose.*(54)* In this case the BCP film gave larger responses to sucrose than to glucose. Published experimental binding constants were determined using a boronic compound that is free in solution while in this case the boronic acid is covalently bound to a polymer film. This could contribute to the discrepancy for sucrose binding more efficiently than glucose as compared to the opposite case reported in literature. Sucrose was examined more closely as it gave a larger response than glucose and mannose. Figure 3.5b shows the sensors color change or wavelength response to increasing concentrations of sucrose. As seen sucrose exposure invoked minimal responses until concentrations exceeded 200mM. Additionally, the sensor response to 500mM solutions of sucrose was similar to responses to 50mM solutions of fructose. This indicates that the sensor is only 10-fold more sensitive to fructose than to sucrose. This type of selectivity could produce major interference for detecting fructose if the sensor is exposed to both fructose and sucrose. To investigate this effect further the sensor was exposed to 1mM D-fructose solutions doped with a range of 1mM-100mM sucrose. As the concentration of sucrose is increased the interference should increase producing larger wavelength shifts at constant D-fructose concentrations. As seen in Figure 3.5c, no positive interference was observed. Increasing the concentration of sucrose caused small negative interference. The interference produced is additionally not statistically significant. The cause of the small negative interference most likely stems from the same signal reduction seen in measurements

51

taken in PBS. The immobile charges produced from boronic acid are shielded by the increasing concentrations of sucrose. In terms of sensing fructose in food products, this type of selectivity is relevant. Li et al, in a study examining sugar content in 70 common food products, have shown that ratio of sucrose to fructose rarely exceeds 2:1 and never exceeds 10:1*(65)*.

3.5. Conclusion

This study demonstrates the viability of photonic crystal BCP films functionalized with boronic acid for the detection of fructose. Initial results exhibit the BCP film's capability to change color in response to fructose concentrations ranging from 500μM to 50mM. The BCP film's sensitivity in a 0.01M PBS solution ranged from 1mM to 50mM. The BCP film response is highly visible with exposure to 5mM fructose invoking a change from blue to green. Additionally the BCP film could selectively bind fructose in the presence of other sugars including glucose and sucrose. These properties give the BCP film application for sensing fructose in food products, producing a quick and easy method to determine response. The system is produced from a chemically modified self-assembled BCP system allowing for simple fabrication.

4.0 Synthesis and Characterization of Microphase Separated Primary Amine Functionalized Polystyrene-b-Poly(2-vinylpyridine)

4.1. Abstract

Microphase separated block copolymers containing primary amine functionalities would have applications in sensors, templates, anti-microbial surfaces and cell scaffolds. Primary amines allow for a variety of different click chemistries that facilitate these applications. In this investigation microphase separated polystyrene-b-poly(2-vinylpyridine) films were quaternized with a primary amine functionality utilizing the less common trimethylsilyl protecting group and a substitution reaction. The glass transition of the 2-vinylpyridine block was suppressed after functionalization. The newly introduced amine functionalities are susceptible to cross-linking through the use of glutaraldehyde, demonstrating the availability of the amines for further chemical modification. We were able to perform the primary amine functionalization of a microphase separated block copolymer without disrupting the lamellar morphology.

4.2. Introduction

Block copolymers (BCPs) are macromolecules composed of sequences or blocks of chemically distinct repeat units. The covalent bond between constituent blocks allows for microphase separation into spherical, cylindrical, bi-continuous, and lamellar morphologies. The morphology and domain sizes of these self-assembled periodic nanostructures can generally be controlled by adjusting the length of each block and the total molecular mass*(14)*. Nanostructured BCPs have been developed for applications such as electronics*(66)*, templates*(67–71)*, and cell scaffolds*(72, 73)*. Many of these applications could be enriched by the introduction of block copolymers containing polar

53

or ionic blocks. BCPs of this nature could introduce interesting surface chemistries as well as allow for additional chemical modifications.

BCPs are generally synthesized using living polymerization techniques in order to achieve the low polydispersity required for microphase separation*(74)*. This makes the synthesis of BCPs consisting of polar and acidic monomers difficult as they can disrupt the polymerization process. Particularly, protic groups such as amines can induce chain transfer and termination events*(75)*. Additionally, polymers containing a high fraction of ionized units do not microphase separate due to the aggregation of the charged sites*(76)*. For these reasons it is difficult to synthesize monodisperse BCPs containing amine functionalities, while retaining the microphase separated microstructure. Amine containing BCPs permit the use of epoxide, carbodiimide, aldehyde, and N-hydroxysuccinimide chemistries, which opens the door for a variety of chemical and biological functionalizations such as free thiols, antibodies, oligonucleotides, peptides and enzymes. This would have applications in biosensors, anti-microbial surfaces and cell scaffolds. In the following study we took advantage of the nucleophilic nature of 2-vinylpyridine as a means to introduce a primary amine functionality to the block copolymer polystyrene-b-poly(2-vinylpyridine) (PS-b-P2VP) without disrupting its lamellar microphase separation.

PS-b-P2VP is a commonly studied BCP that easily microphase separates into different nanostructures, which have been exploited for applications such as antimicrobial surfaces*(77–79)*, nanoparticle templates*(80, 81)*, as well as photonic crystals*(12)*. The nucleophilic nature of P2VP has been taken advantage of in previous studies, but only in the attachment of alkyl chains for quaternization and crosslinking purposes. This

nucleophilic reaction is thought to proceed as a Sn2 reaction*(82, 83)*. Modifying nanostructured PS-b-P2VP is a delicate process to ensure the survival of the aforementioned nanostructure. The solvent utilized cannot delaminate the surface or disrupt the desired nanostructure. Covalently attaching a primary amine would require a compound containing a leaving group or electrophile and the primary amine. Reactions between the amino group and electrophile can lead to cyclization and polymerization of the reactant, necessitating the use of protected amines. Many protecting groups for amines, such as di-tert-butyl dicarbonate (Boc) can solubilize PS-b-P2VP, dewetting the surface or destroying the nanostructured morphology. Alternatively, the utilization of trimethylsilyl(TMS) protecting groups was examined in this investigation. TMS is commonly used in the protection of alcohols*(84)* but has had some use with primary amines*(85)*. The electron-poor nature of TMS groups prevents reactants from solubilizing PS-b-P2VP, while easily being removed with a proton source to yield a primary amine functionality. Utilizing this process would allow for the fabrication of primary amine containing block copolymer nanostructures.

4.3. Methods

4.3.1 Fabrication of Unmodified Microphase Separated PS-b-P2VP Films

A solution of PS-b-P2VP (133kDa-b-131kDa) was dissolved in propylene glycol monomethyl ether acetate (PGMEA) at a concentration of 5% w/v. PGMEA was chosen due to its slow rate of evaporation, allowing for the development of uniform films. 300μL solution was spun-cast onto a 1''X1'' APTES functionalized glass slide at 350 rpm for 120 s until dry. The resulting film was then solvent annealed at room temperature inside a

glass petri dish containing 2 mL of chloroform for 12 hours. This process produces an approximately 1μm thick PS-b-P2VP film with lamellae parallel to substrate.

4.3.2 Functionalizing the BCP film

To quaternize the P2VP block with a primary amine, 3-Bromo-N,N-bis(trimethylsilyl)propan-1-amine (BTMSPA) was utilized. The BTMSPA was stored under an argon environment as the trimethylsilyl protecting group is moisture sensitive. A solution of 200μL BTMSPA in 10ml of acetonitrile was prepared and blanketed with nitrogen. A PS-b-P2VP film was then immersed in this solution and allowed to reflux at $90^{o}C$ for 18 hours under a nitrogen environment. The film was then removed and rinsed with excess acetonitrile. To remove the TMS protecting group, the now modified PS-b-P2VP film was immersed in a 10% v/v solution of aqueous HCl for 7 days.

4.3.3 XPS

XPS data was collected on a Kratos Axis 165 X-ray photoelectron spectrometer operating in hybrid mode using monochromatic Kα radiation (1486.7 eV) at 260 W. Charge neutralization was required to prevent sample charging. All spectra were calibrated to the C-C/C-H peak at 284.8 eV. Quantification and peak fitting were was carried out using CASAXPS software, using relative sensitivity factors from the Kratos Vision software library after correction of a Shirley background. Peak fitting of the N 1s region was performed using peaks with a 50% Lorentzian, 50% Gaussian line shape, all peaks were fixed to have equal full-width at half-maximum.

4.3.4 Transmission Electron Microscopy

Amine functionalized (hence referred to as "modified") and unmodified films of PS-b-P2VP were etched from their glass substrates by soaking the films in a 5% v/v solution of hydrogen fluoride. The removed films were rinsed with excess NaOH and distilled water and allowed to dry at room temperature. The films were then embedded in coffins of Spurr's resin. The embedded films were then microtomed using a Leica EM UC6 and placed on nickel TEM grids. The PS-b-P2VP cross-sections were analyzed using a JEM-2100F 200 kV transmission electron microscope.

4.3.5 Fourier Transform Infrared Spectroscopy

Quaternization of PS-b-P2VP and deprotection of the newly attached amine were characterized utilizing Fourier transform infrared spectroscopy (FTIR). Unmodified, modified and ninhydrin stained PS-b-P2VP films were scraped off their glass substrates using a razor blade. Ninhydrin stained films were produced by immersing the modified PS-b-P2VP film in a 10mM solution of ninhydrin dissolved in ethanol for 5 minutes at 70°C. Once removed from the glass substrates the films were allowed to dry and room temperature. The IR spectra of each film were obtained using a Thermo Nicolet NEXUS 670 FTIR.

4.3.6 Modulated Differential Scanning Calorimetry

Modulated differential scanning calorimetry (mDSC) was performed using a TA DSC Q100 to determine the glass transition temperature of the quaternized PS-b-P2VP films. Unmodified and modified PS-b-P2VP were sealed in hermetic aluminum pans. A scan from 50 to 120°C at a rate of 3°C/min was employed. The scan was modulated +/- 0.48°C every 60 seconds.

4.3.7 Cross-linking with Glutaraldehyde

BTMSPA modified films of PS-b-P2VP were initially immersed in a solution of pH~5 solution of acetic acid. They immediately swelled and became orange in color due to the lamellar morphology acting as Bragg stack. The film was placed in a Lamda 25 UV-Vis Spectrometer and the spectrum was recorded. The film was then neutralized with 1M NaOH and rinsed with excess distilled water. Subsequently, the film was exposed to a 10% v/v solution of glutaraldehyde in distilled water for 30 minutes. The now glutaraldehyde cross-linked film was reintroduced to the acetic acid solution and the spectrum was recorded using UV-Vis.

4.4. Results and Discussion

Chemical modification of block copolymers requires the consideration of many different factors, especially when certain morphologies are desired. Modifying the polymer before casting a film can result in solubility limitations, making sample preparation impractical. Quaternizing the BCP film after obtaining the initial microphase separation or annealing can lead to disruption of the original morphology, dewetting or delamination events. One of the most common functionalizations made to PS-b-P2VP is alkylating the pyridine with compounds such as bromoethane. This reaction is generally performed in solvents such as hexane that do not interact with the polymer. Instead bromoethane causes the system to swell, allowing for the reaction between bromoethane and P2VP. This reaction is believed to be a SN2 reaction with pyridine acting as the nucleophile. In this case many reactants containing a primary amine and an electrophile can be chosen to introduce the primary amine functionality. The primary amine reactant must be protected to prevent self-cyclization reactions or polymerization from occurring. Another consideration is that

some reactants can cause the BCP to delaminate, especially if they solubilize the P2VP block, breaking its interaction with the substrate. Traditional amine protecting groups such as Boc, can solubilize the PS-b-P2VP film, destroying its morphology. In this work, a trimethylsilyl protecting group was utilized as it will not solubilize the film due to its electron poor nature. The reaction can be seen in Figure 4.1. PS-b-P2VP was immersed in a solution of BTMSPA and acetonitrile and allowed to reflux at 90°C overnight. The resulting film still contains the TMS protecting group which is removed by exposure to a 10% HCl solution for 7 days. The deprotected film is then rinsed with KOH and distilled water. No changes in the macroscopic properties of the films were evident, neither were dewetting nor delamination events.
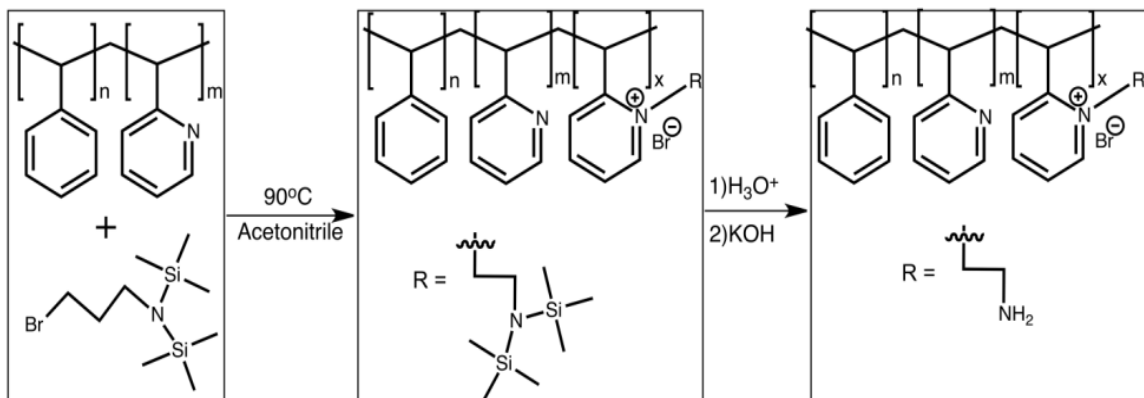
Figure 4.1 Depiction of the quaternization of PS-b-P2VP. The PS-b-P2VP film is immersed in a solution of BTMSPA in acetonitrile and refluxed at 90°C. The resulting modification contains the trimethylsilyl protecting group on the amine which is subsequently removed using HCl followed by KOH to neutralize the acid.

4.4.1 Quaternization with BTMSPA

Figure 1 shows the spectra of several different stages of the reaction as well as after staining the film with ninhydrin. The spectra of unmodified PS-b-P2VP can be seen in Figure 4.2a, demonstrating the characteristic aromatic crown of P2VP and PS at 2900 cm⁻

[1]. Initially after functionalization with BTMSPA but before deprotection of the amine, a spectrum was obtained seen in Figure 4.2b. A sharp peak appeared at 1260 cm^{-1}, which is indicative of a C-N stretch. This bond is formed after the substitution reaction between pyridine and the bromine-carbon bond on BTMSPA. It should be noted that there is a C-N peak already present due to the pyridine structure at 1140 cm^{-1}. At this stage N-H peaks were not present in the spectra as the TMS protecting group is still present. Figure 4.2c displays the spectra obtained of a film after deprotection of the amine. A double peak is present at 3300 and 3200cm^{-1} indicating both of the N-H stretches present in a primary amine. As secondary confirmation, the aminated PS-b-P2VP was exposed to a ninhydrin stain. After the stain the films has a slight pink hue. Ninhydrin is normally used as a colorimetric stain for primary and secondary amines but is also excellent as an FTIR stain as it contains carbonyl functionalities, which produce discrete, strong FTIR signals. As seen in Figure 4.2d, the presence of ninhydrin introduces the sharp peak seen at 1720cm^{-1} due to the carbonyl groups present on the stain. These FTIR spectra qualitatively demonstrate the successful modification of the P2VP block of the films with a primary amine.
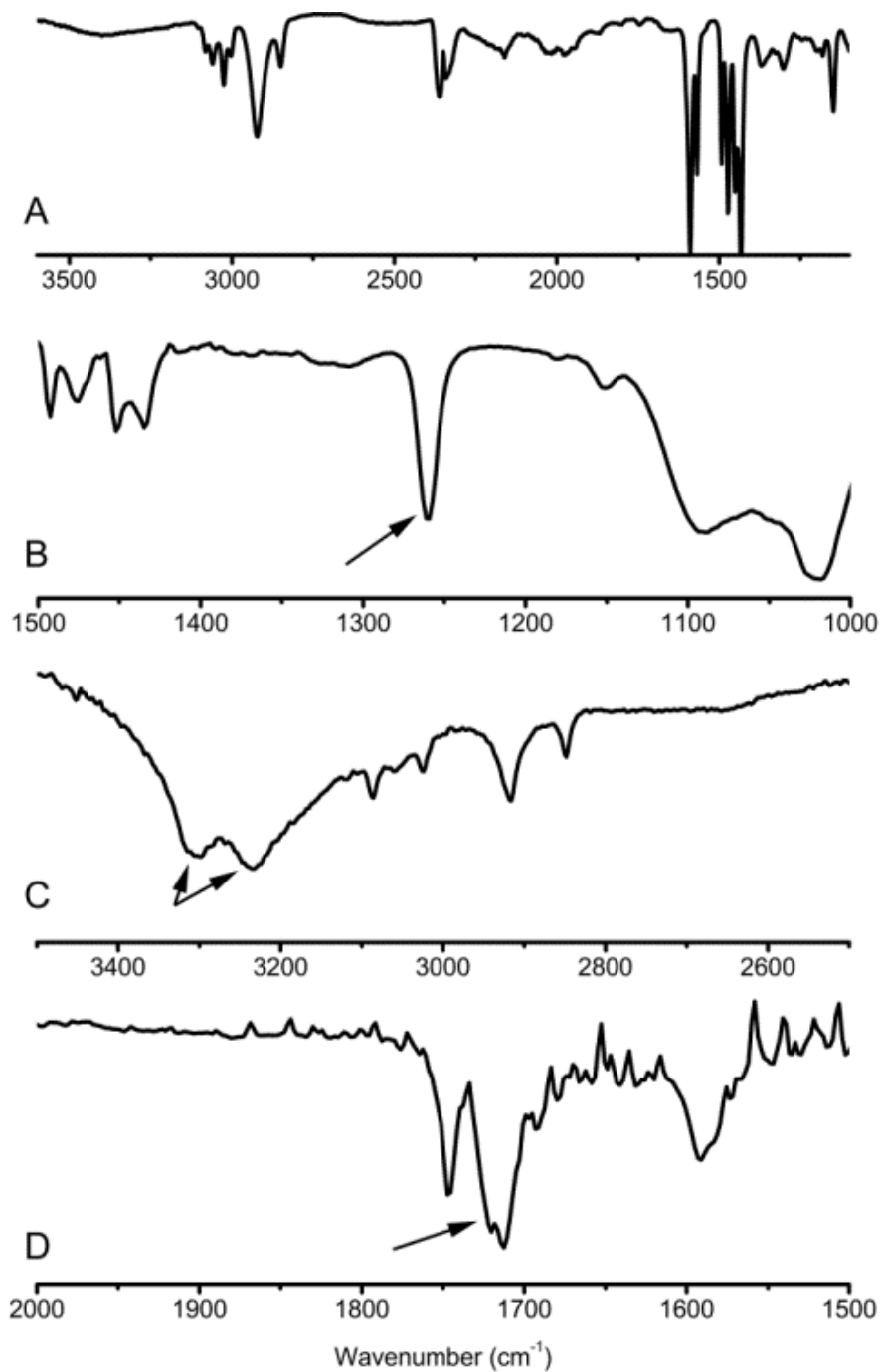
Figure 4.2 FTIR of (a) unmodified PS-b-P2VP, demonstrating the characteristic aromatic

crown at 2900 cm^{-1}. (b) Post-functionalization with BTMSPA, the C-N peak appears at

1260cm^{-1}. (c) Deprotected functionalized PS-b-P2VP, the double primary amine peak is

present at 3300 and 3200 cm^{-1}. (d) The deprotected PS-b-P2VP stained with ninhydrin. A peak appears at 1720 cm^{-1} indicative of a carbonyl, present in ninhydrin.

In order to obtain a quantitative measure of the conversion of the vinyl pyridine units of the P2VP block, X-ray photoelectron spectroscopy (XPS) was employed. The amphiphatic nature of the solid polymer post-quaternization makes it difficult to perform other analytical techniques such as nuclear magnetic resonance or gel permeation chromatography, therefore XPS was utilized. The XPS spectra for the unmodified and modified polymers can be seen in Figure 4.3. The peak at 398.4eV for N 1s is attributed to the pyridine nitrogen in P2VP. This peak is seen in both the unmodified and modified XPS data. The peak at 401.4 eV in the modified XPS data is attributed to the pyridinium, due to the SN2 reaction with BTMSPA. A shift of 3eV from pyridine to pyridinium is consistent with literature*(77, 86)*. The shift to 401.4 eV from 398.4 eV is due to relatively lower electron density around the nitrogen due to bonding with carbon versus the lone pair in the unmodified pyridine. The insert in Figure 4.3 displays the relative intensities of each source of nitrogen. As seen, pyridine comprises 88.8 % of the nitrogen while 2.5 % of the nitrogen is ascribed to pyridinium. This gives a conversion of 1:28 2VP units from the reaction of the PS-b-P2VP with BTMSPA. While the reaction efficiency is low, the effect this conversion has on different properties of the polymer is worth noting. Differential scanning calorimetry was employed to investigate this effect. The peak at 399.8 eV is attributed to amine functionalization after deprotection. The percentage of amine calculated by the peak fit of 5.42 % is approximately two times larger than the expected 1:1 ratio for amine:pyridinium this could indicate the presence some residual amine functionality from APTES. We attribute the peak at 396.5 eV that appears in both

the unmodified and modified polymer, to the artifact of differential sample charging of the surface due to the multilayered insulating nature of the material, this assertion is supported by a similarly shifted small peak to low binding energy side of the aromatic carbon peak in the C 1s region.
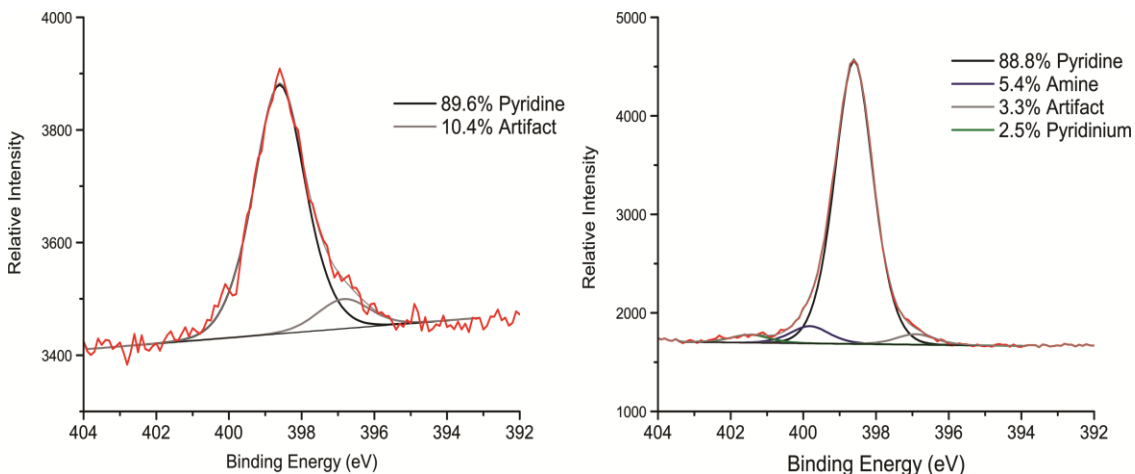
Figure 4.3 (a) N-1s XPS spectra of unmodified PS-b-P2VP. The peak at 398.3eV corresponds to the aromatic nitrogen of P2VP. (b) N-1s XPS spectra of the nitrogen present in the modified films. As seen modification with BTMSPA, causes a peak at a binding energy of 401.4eV at 2.5% of total nitrogen. This peak corresponds to pyridinium, while the peak at 398.4eV corresponds to the unmodified P2VP and comprises 88.8% of the total nitrogen.

4.4.2 Thermal Characterization

Thermal characterization was performed using modulated differential scanning calorimetry (mDSC) to determine the changes, if any, in glass transition temperature, T_g, of the modified PS-b-P2VP films. Conventional DSC failed to produce a measurable T_g of the P2VP block of the unmodified polymer. In mDSC a sinusoidal modulation is used in addition to the linear ramp in temperature. In this case a modulation of +/- 0.48 ^{o}C every 60 s was employed. mDSC was chosen as it allows for improved sensitivity of

reversing transitions such as glass transition. A heat-cool-heat cycle was initially utilized to erase the thermal history of the BCP films. As seen in Figure 4.4, the T_g for PS and P2VP was observed at 103 and 86 ^{o}C respectively, evident by the first order transition change seen in heat flow. This measurement was confirmed by the trough in the non-reversing heat flow at the same temperatures. Subsequent to modification of the PS-b-P2VP with BTMSPA, the T_g of PS remained relatively unchanged at 104 ^{o}C while the T_g of P2VP is no longer present. It is expected the T_g would increase due to potential physical crosslinks forming between the primary amines in the modified BCP film. The introduction of physical crosslinks between neutral pyridine units and hydrogens on the newly introduced primary amine would increase the T_g of P2VP. The shift in T_g can be estimated based on the molecular weight between these physical crosslinks by the following equation*(87)*:

$$T_g - T_{g0} = \frac{3.9 \times 10^4}{M_c}$$
(4.1)

where T_g and T_{g0} are the glass transition temperatures of the crosslinked and uncrosslinked polymers respectively, and M_c is the molecular weight between crosslinks. The XPS data shown previously in Figure 4.3 demonstrated that approximately 1 in 28 2VP units were modified. Using this data we can assume that M_c is approximately 2943.9g/mol^{-1}, giving an estimated ΔT_g of 13.2 degrees. A small magnitude of the T_g of the physically crosslinked polymer is also expected as crosslinked polymers have lower specific heat*(88)*. Under these assumptions the region of interest, indicated by an arrow, in the thermographs of the modified polymer could be the new T_g of the modified polymer, but due to its magnitude we cannot be confident in this assertion.
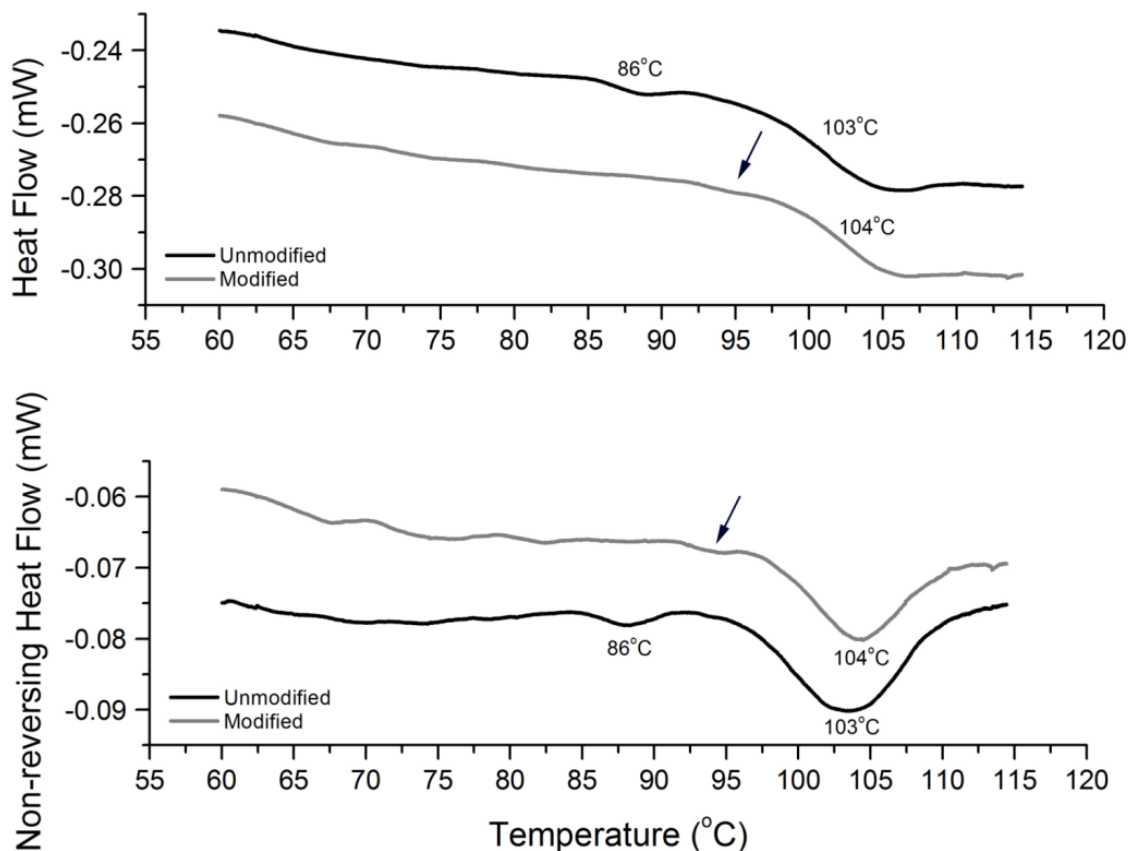
Figure 4.4 Modulated DSC of the modified and unmodified PS-b-P2VP films. Shown are both the heat flow and the non-reversing heat flow. In the unmodified film, peaks at 86 ^{o}C and 103 ^{o}C are seen corresponding to the T_g of polystyrene and poly(2-vinylpyridine) respectively. After modification the presence of the T_g of P2VP is no longer present.

4.4.3 Amine Functionality

The PS-b-P2VP used in this study contains blocks of equal molecular masses. When cast as a film, the block copolymer microphase separates into a lamellar morphology. As previously mentioned, these morphologies have a variety of applications. Therefore, maintaining the morphology after chemical modification is critical. A cross-section of the PS-b-P2VP was microtomed and placed onto a nickel TEM grid and examined under a 100kV TEM microscope. Figure 4.5 shows the resulting TEM micrograph. The parallel

to the substrate microphase separated lamellar morphology of the PS-b-P2VP film was not disrupted by the chemical modification with BTMSPA. One application of lamellar PS-b-P2VP films is the fabrication of one-dimensional Bragg stacks. By exposing the films to either acidic media or ethanol, the P2VP block swells until the spacing between PS blocks is sufficient for the system to reflect visible wavelength as light as dictated by Bragg's law.
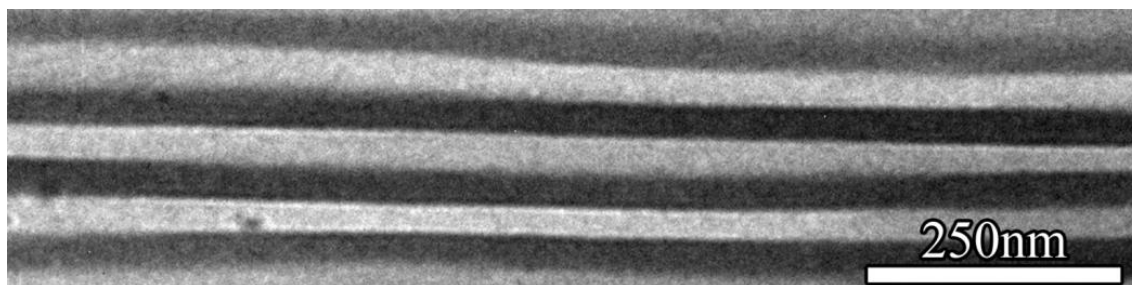
Figure 4.5 TEM of the cross section of the aminated PS-b-P2VP film following functionalization and deprotection. The lamellar morphology of the BCP is maintained after the modification.

An aminated PS-b-P2VP film was exposed to a solution of pH~5 aqueous solution of acetic acid. This protonated the P2VP block causing the film to swell dramatically and become orange in color. The UV-Visible spectrum of this swollen film is displayed in Figure 4.6, with a peak wavelength of ~590 nm. The film was exposed to an aqueous solution of glutaraldehyde, a primary amine crosslinking agent. The primary amine modification of the P2VP will allow for the formation of the crosslinks, inhibiting swelling in acidic media. Subsequent to crosslinking, the film was reintroduced to the acetic acid solution. As seen in Figure 4.6, the spectrum of the film blue-shifted to ~510 nm. This indicates an inhibition of the swelling properties of the film, due to the glutaraldehyde crosslinks. The introduction of the functional primary amine allows for

flexibility in the variety of other chemistries and biological moieties such as thiols, enzymes, antibodies or oligonucleotides that can be attached to the PS-b-P2VP nanostructures.
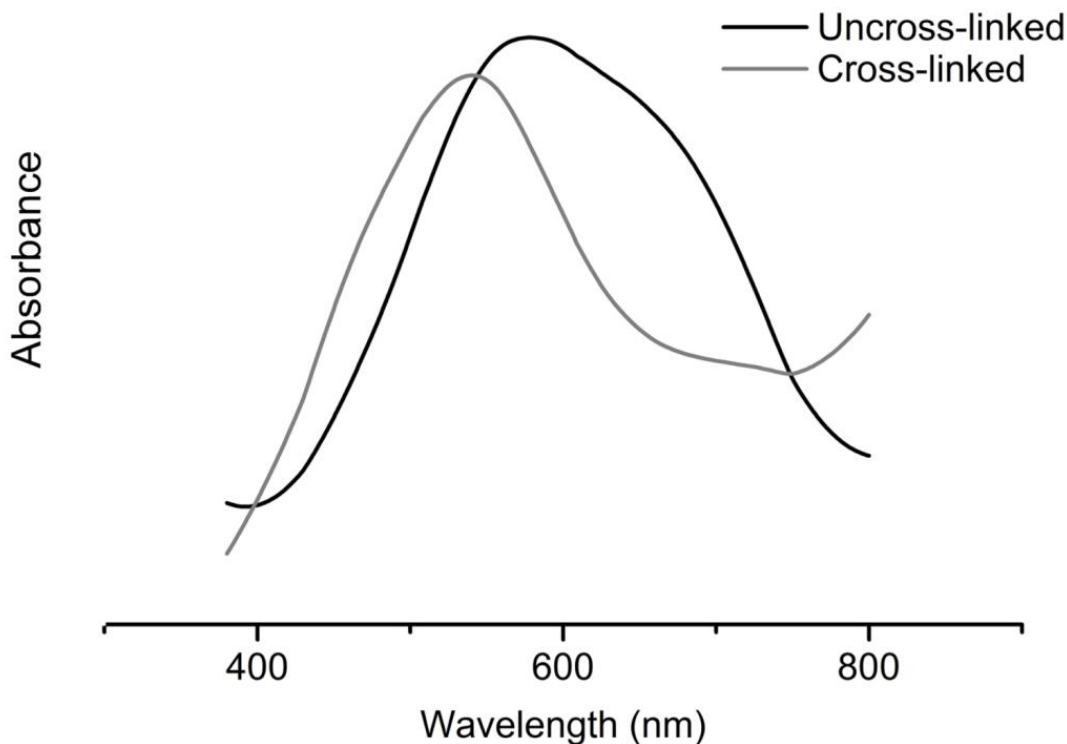
Figure 4.6 UV-Visible spectroscopy of a BTMSPA modified PS-b-P2VP film under acidic condition (pH~5). The parallel lamellar morphology of the swollen block copolymer film causes it to form a Bragg stack. The film is initially reflecting a peak wavelength of ~590nm. After cross-linking with glutaraldehyde the film collapses, causing the reflected light to blue shift to a peak value of ~550 nm.

4.5. Conclusion

Aminated block copolymers allow for further and more complex functionalization with a variety of chemical and biological moieties. Synthesizing monodispersed aminated block copolymers is difficult especially with the intended goal of producing, microphase separated morphologies. Performing a functionalization of an already microphase

separated BCP can destroy or alter the desired morphology. It is possible to perform if careful considerations are made about the reactant and solvent used. In this case the nucleophilic nature of P2VP was utilized to quaternize the BCP with a TMS protected amine. TMS protecting groups do not cause delamination events in the PS-b-P2VP film, which would normally occur with common amine protecting groups such as Boc.

5.0 Engineering a Rapid Point-of-Care Sensor for Blood Ammonia

5.1 Summary

The goal of this project is fabrication of a prototype point-of-care (POC) device for detecting ammonia in a drop of blood, obtained by pricking the finger (or heel for newborns) to be used at home, in clinics, and in hospitals, in a fashion similar to a glucometer. This POC device would assist in the diagnosis and management of hyperammonemia. The planned sensor will consist of an ammonia-specific colorimetric reaction in conjunction with an ammonia-selective filter membrane. High sensitivity allows for accurate and reliable differentiation between the colorimetric responses produced by elevated (100-500 μM) or normal (40-70 μM) levels of ammonia in blood*(89)*. The current inability to immediately measure blood ammonia places a large amount of stress on the patient and caretaker, since any sign of the patient feeling ill prompts the concern of a hyperammonemic episode and a trip to the doctor or emergency room for testing. A rapid point-of-care sensor would allow for at home and bedside testing, reducing the large burden on children with urea cycle disorders and their caretakers.

5.2 Introduction

Hyperammonemia, a life-threatening condition, is characterized by elevated blood ammonia levels and causes severe neurodevelopmental complications. The condition originates from metabolic disturbances in the urea cycle and chronic hepatic diseases such as cirrhosis. Individuals at risk for hyperammonemic episodes must consistently manage blood ammonia to prevent further complications. Currently there are no reliable point-of-care or at home blood ammonia sensors.

5.2.1 Urea Cycle Disorders

Urea cycle disorders (UCDs) are inborn errors of metabolism producing a deficiency in one or more of several enzymes including carbamoylphosphate synthetase I, ornithine transcarbamylase, argininosuccinic acid synthetase, arginiosuccinic acid lyase, arginase and N-acetylglutamate synthetase*(90)*. UCDs affect approximately 1 in 35,000 births in the United States, but due to partial defects this number is underestimated*(91)*. Following birth, affected neonates generally display no symptoms until blood ammonia rises over the course of several hours to days. Ensuing lethargy progressing to a coma is often the first sign that alerts healthcare professionals to take emergency diagnostic and treatment measures. More common maladies, such as sepsis, are frequently considered first due to over lapping symptoms and lack of experience of primary and emergency care physicians with these disorders. Improper diagnosis leads to prolonged blood ammonia elevation for the patient. These diagnostic delays increase the risk for irreversible brain damage and neurodevelopmental complications. This problem is exacerbated by the fact that current methods for blood ammonia level measurement require specific sample preparation and access to tandem mass spectroscopy or fluorometry in large central laboratories. Following a diagnosis, strict dietary measures are taken to reduce protein intake and the child is treated with ammonia scavenging molecules such as sodium benzoate*(92)*. Monitoring blood ammonia levels becomes a lifelong need to facilitate effective disease management. The effects of hyperammonemia are primarily neurological. In a developing child with a UCD, a hyperammonemic episode will cause a marked reduction in intellectual ability with an average reported IQ of 43*(93)*. The neonate will also suffer from neuropathologies such as intracerebral hemorrhage, prominent cerebral edema and

generalized neuronal loss*(94)*. Reported outcomes of children with UCDs include 79% with major intellectual disabilities, while 46% exhibited cerebral palsy and 17% presented with epilepsy*(95)*.

5.2.2 Hepatic Diseases

In addition to UCDs, Chronic hepatic diseases such as hepatic encephalopathy (HE), carcinomas, cirrhosis and hepatitis result in high ammonia levels which can lead to neurodegenerative complications. There are approximately 5 million Americans suffering from cirrhosis and 30-40% of them will develop HE, a general term that envelopes all neurological symptoms in cases of liver disease, in their lifetime*(96)*. Blood ammonia levels have been found to correlate with severity of HE in patients with cirrhosis in several studies*(97–99)*. In healthy adults, one of the many functions of the liver is the metabolism of proteins. This metabolic activity generates large quantities of ammonia which is quickly converted to both glutamine and urea. Individuals with cirrhosis have an increase in portal vein pressure causing the formation of hepatoportal venous anastomoses allowing intestinal ammonia to bypass the liver. This is compounded with the decreased number of hepatocytes reducing ammonia anabolism by as much as 80%. Ammonia levels are also elevated in cases of cirrhosis coupled with minimal HE, in which patients lack reduced verbal abilities and abnormal electroencephalograms but have impaired psychomotor ability. Individuals with HE are at risk for brain edema, herniation and Alzheimer Type II astrocytosis.

5.2.3 Pathology of Hyperammonemia

High levels of blood ammonia also increase the permeability of the blood-brain barrier which causes ammonia to diffuse freely to the brain. In the brain, ammonia is removed by

glutamine synthetase, which produces glutamine. The increase presence of glutamine causes osmotic swelling of astrocytes. This is believed to be one of the major causes of cerebral edema and the other neurological complications associated with hyperammonemia.

5.2.4 Current Detection Techniques

5.2.4.1 Conventional Detection

A full scale clinical laboratory is currently required to determine blood ammonia levels. Patient blood must be extracted at volumes excess of 200 μL and immediately placed on ice. The sample is then centrifuged to remove erythrocytes and to process the sample into plasma. The plasma is then frozen at -80$^\text{o}$C until testing. Processing of the blood is required as ammonia levels are unstable in blood due to the metabolic activity of erythrocytes. Additionally, freezing whole blood will cause many cells to burst release very high levels of ammonia. Once the blood is processed, tandem mass spectroscopy or fluorometry are employed to quantify the ammonia. Before testing the plasma, it must be treated with trichloroacetic acid in order to remove the plasma proteins that could interfere with the sensing events.

These conventional techniques, while accurate, are only available in large hospitals, and central or private laboratories. If a patient at risk for hyperammonemia feels ill they must travel to the hospital to have blood drawn which is either tested on site or shipped to a nearby laboratory. The turnaround time in these cases can be 9-14 days. Logistically this is inadequate for proper management of blood ammonia levels. It is difficult to determine what is causing hyperammonemic episodes and the effectiveness of the treatment. Additionally, these repeated trips to the hospital pose a risk for secondary infections on

the child. In similar metabolic disorders, such as phenylketonuria, it has been found that trips to the hospital for metabolite testing will eat up 260 hours per year of the patient and caregivers time, increasing the burden of the illness*(100)*.

5.2.4.2 Point-of-Care Detection

5.2.4.2.1 Separation of Ammonia from Blood

A majority of point-of-care (PoC) techniques for ammonia detection revolve around first separating the ammonia from blood. A common approach is to take advantage of ammonia's volatility in alkaline conditions. In solutions with a pH higher than 10, ammonia primarily exists in its gaseous form NH_3 instead of NH_4^+. The alkalization of ammonia solutions gave way to distillation as a separation mechanism. Distillation techniques were mostly consolidated into what is known as microdiffusion techniques*(101, 102)*. The ammonia containing sample is taken up into a reservoir containing an alkaline tablet. The ammonia volatilizes from the solution and passes through a membrane into another reservoir containing a second solution with a colorimetric pH indicator. These methods generally suffer from hydrolysis of proteins and amino acids such as glutamine in alkaline conditions which produces ammonia*(103)*. Another approach, investigated primarily in the 1960's, employed ion-exchange resins*(104, 105)*. Cation exchange resins would be mixed with the ammonia containing blood. The resin is then removed and washed with an alkali such as a sodium salt to extract the ammonia. The process described in these publications is laborious, involving multiple washing steps, constraining its use in a PoC sensor.

5.2.4.2.2 Quantifying Blood Ammonia

Once separated from blood, the ammonia must be measured using a quantitative, analytical technique. Titration, a simplistic approach, is a commonly investigated method. The separated alkaline ammonia is added to an acidic solution and the resulting pH change is then monitored by a colorimetric indicator such as bromocresol green or by the use of an electrode. The commercial product Blood Ammonia Checker II by Arkray utilized this technology*(106)*. The titration method relies on the presence of only ammonia and thus primarily used in conjunction with distillation separation techniques. Gas sensing electrodes have also been used in combination with alkaline based distillation techniques. In this case ammonia gas will diffuse to a gas sensing electrode or pH meter which quantifies the ammonia through impedance measurements. Due to small amounts of ammonia present these methods are hindered by changes in temperature or humidity. They also suffer from the same issues as the previously mentioned distillation techniques as electrode-based sensing relies on distillation as a separation mechanism.

Enzymatic and chemical reactions have also been investigated as a means to measure ammonia, offering specificity as a means to avoid the issues present in pH or distillation based technologies. Most enzymatic methods described in literature utilize the enzyme glutamate dehydrogenase which reductively aminates α-ketoglutarate in the presence of ammonia and the reduced form of nicotinamide adenine dinucleotide (NADH)*(107)*. The system can be probed either optically or electrochemically for the decreasing concentration of NADH. This enzymatic technique is very sensitive but measuring a loss in signal can be difficult, especially in consideration of the poor stability of NADH*(108)*. A variety of different colorimetric reactions are specific to primary amines such as ammonia including ninhydrin and Nessler's reagent. Ninhydrin is a very sensitive

chemical which turns a brilliant purple color in the presence of primary and secondary amines. It will react with any and all primary and secondary amines, however, making its use for a specific and selective ammonia sensor ineffective. Nessler's reagent or potassium tetraiodomercurate(II), is fairly selective and can be found in ammonia test kits for aquariums and waste water. This reaction generates different products depending on the concentration of ammonia present. The primary product is an opaque red-brown precipitate indicating ammonia presence. The processing of this precipitate in the context of optical quantitation can be difficult.
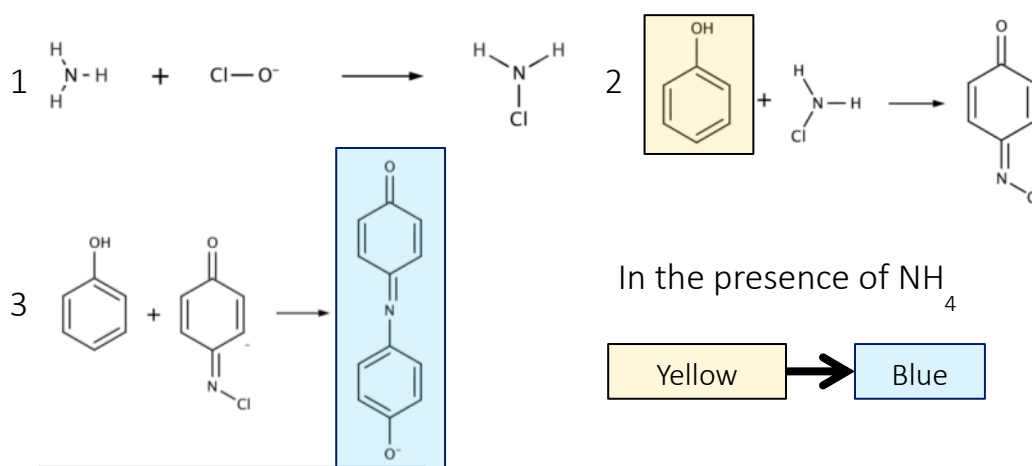
Figure 5.1 Mechanism for the indophenol reaction. Hypochlorite reacts with ammonia forming chloramine. Chloramine then reacts with two phenol units producing the blue indophenol compound.

One of the first chemical methods ever described for ammonia detection was in 1859 by the French chemist Berthelot*(109)*. He discovered a reaction between ammonia, hypochlorite and phenol which produces a deep blue, water soluble product. The mechanism of this reaction can be seen in Figure 5.1. In the proposed mechanism ammonia reacts with hypochlorite to form chloramine which in turn reacts with phenol

forming a quinone intermediate. The intermediate covalently bonds to another phenol producing the final indophenol product. This reaction occurs at any pH but the indophenol compound is only blue in alkaline conditions. This reaction will occur with other primary amines but at a reduced rate. Previous studies have also demonstrated that utilization of 2-phenylphenol will introduce steric hindrance reducing the reactions effectiveness with bulkier primary amines, improving ammonia selectivity*(110)*.

5.2.4.2.3 Investigated Approach

The presented work demonstrates how the systematic investigation of previously known technologies yielded the fabrication of an effective blood ammonia sensor. The indophenol reaction, in tandem with a polyelectrolyte membrane, was explored as a means to quantify ammonia concentrations in whole blood.

5.3 Methods

5.3.1 Ammonia-Indophenol Standard Curve

The ammonia-indophenol standard curve was produced using a range of ammonium chloride concentrations in 1X phosphate buffered saline (PBS) of 0 to 750 μM. These concentrations were utilized in the indophenol reaction adapted from Berthelot*(109)*. Specific concentrations of hypochlorite, 2-phenylphenol, sodium nitroprusside, and sodium hydroxide were mixed with the ammonium solution and allowed to react at room temperature for 10 minutes. The absorbance of the resulting solution was measured at a wavelength of 635nm.

5.3.2 Stability Studies

The reagents utilized in the indophenol reaction were investigated for long term stability. Aqueous solutions of hypochlorite, sodium nitroprusside, sodium hydroxide and a solution of 2-phenylphenol in ethanol were stored in separate 50mL falcon tubes, with limited exposure to light. At intervals of 3, 5, 7, 15, 21, 28, 35, 50, 75 and 100 days the hypochlorite, sodium nitroprusside, sodium hydroxide and 2-phenylphenol were utilized to develop a standard curve using ammonia concentrations ranging from 0-750μM. Significant deviations from the original standard curve indicated the degradation of the stored reagents. It should be noted that fresh ammonia samples were utilized at each test interval.

5.3.3 Response to Amino Acids

Primary amines can also undergo the indophenol reaction. Total amino acid concentrations in blood can be as high as 2.5mM, therefore the selectivity of 2-phenylphenol was determined in the indophenol reaction. 1mM solutions of each of the 21 amino acids was prepared in 1X PBS. The same protocol utilized with the indophenol reagents for the ammonia standard curve was utilized with each amino acid solution. 10 minutes after the indophenol reagents and amino acid solution was mixed, its absorbance at 635nm was measured using a plate reader. The response was directly compared to the response seen from a 1mM solution of ammonium chloride and expressed as a percentage of the ammonium response.

5.3.4 Sensor Design

A bisected well containing blood in one section and a concentrated alkali solution in the other would provide a means for cation exchange of the whole blood to occur, yielding a strong recovery of the ammonium. A computer-aided design of the well that is both

reusable and modular was 3D printed. As seen in Figure 5.2, two modular pieces were 3D printed from acrylonitrile-butadiene-styrene thermoplastic. The pieces will snap together with the membrane in the middle, forming a Nafion bisected well. This design was chosen to provide a uniform platform for all future experiments involving this sensing mechanism. Silicone gasketing material, at a 1/64'' thickness, was glued to the inner face of each well-half to ensure a water tight seal. The wells were then back-filled with polydimethylsiloxane to improve their mechanical properties.
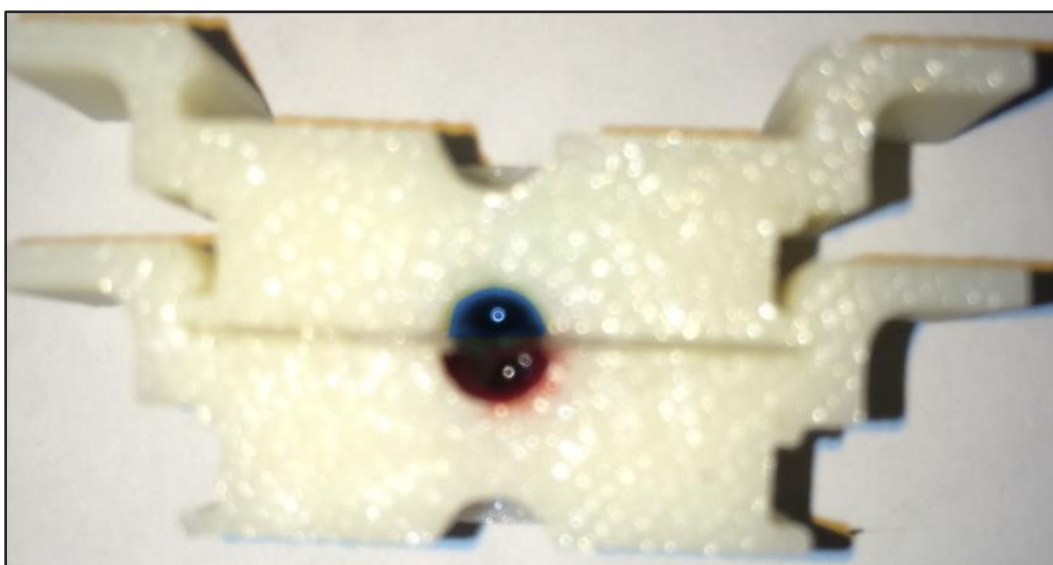
Figure 5.2 Photograph of the 3D printed modular pieces snapped together around Nafion to form the bisected well utilized for the sensing experiments.

5.3.5 Sensor Response to Ammonia in Phosphate Buffered Saline and Whole Blood

The 3D printed wells were constructed with $1cm^2$ pieces of Nafion membrane. In one bisection of the well a range of 0-500 μM concentrations of ammonium chloride in 1X PBS was added. In the opposing bisection a 1M alkali solution was added. Ion-exchange of ammonium was allowed to occur for 20 minutes. The alkali solution, now containing ammonia, was then extracted and utilized in the indophenol reaction. The absorbance of

the resulting indophenol reaction was measured at 635nm after 10 minutes using a microplate reader.

Whole human blood was spiked using ammonium chloride to generate concentrations of ammonia of 25, 50, 75, 100, 150, 200, 250, 300, 400 and 500 μM. This method of producing ammonia-spiked blood was verified utilizing a Siemens RXL to determine the true ammonia concentrations of the resulting whole blood. The ammonia-spiked whole blood was pipetted into the sensor in a protocol identical to the one used in the case of the ammonium in 1X PBS. In one section of the well the ammonia-spiked blood was added. In the other section was the concentrated alkali solution. After 20 minutes the ion-exchange has taken placed and the ammonia is extracted into the alkali solution. The ammonia-containing alkali solution was then mixed with the hypochlorite, sodium hydroxide, sodium nitroprusside, and 2-phenylphenol. The resulting indophenol reaction's absorbance was measured at 635nm after 10 minutes.

5.3.6 Fouling of Nafion with Blood Cells and Proteins

100 μL of whole sheep's blood was drop cast onto $1cm^2$ pieces of Nafion for 20 minutes. The Nafion was then washed in deionized water to remove any unbound cells or proteins. The resulting layer of cells and proteins were then dehydrated using sequentially concentrated solutions of ethanol in water. The now fixed cells on the Nafion were carbon coated and examined using a scanning electron microscope.

To eliminate fouling of the Nafion surface, the membrane was exposed to 5% bovine serum albumin(BSA) blocking buffer for 2 hours. After blocking any unbound protein was removed by washing the Nafion with excess DI water three times. The now blocked Nafion was again exposed to a 100 μL drop cast of whole sheep's blood for 20 minutes.

The membrane was washed in excess deionized water to remove any unbound cells or proteins.

5.3.7 Hypochlorite Concentrations Effect on Indophenol Response to Blood Ammonia

To reduce interference from reducing species in blood, higher concentrations of hypochlorite than conventionally utilized were employed in the indophenol reaction with ammonia extracted from whole sheep's blood. 1, 2, 3, 5, and 10X concentrations of hypochlorite were utilized and the resulting absorbance at 635nm was recorded.

5.4 Results and Discussion

5.4.1 Ammonia-Indophenol Standard Curve
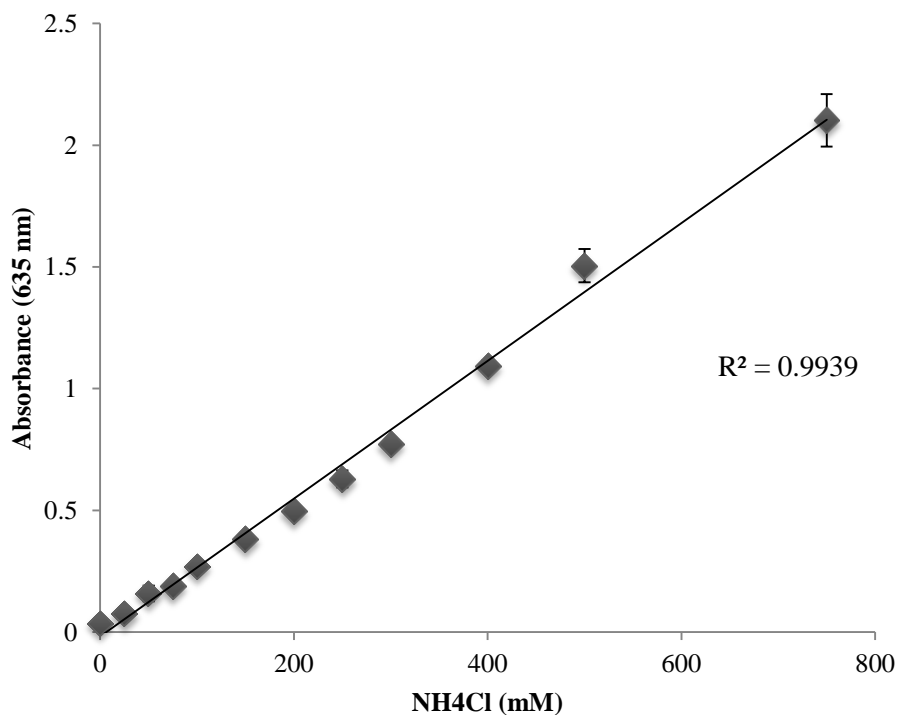
Figure 5.3 The indophenol reaction produces a linear curve with concentrations of ammonium chloride ranging from 0-750 μ M with a COD of 0.9939.

The efficacy of the indophenol reaction was initially evaluated for its lower limit of quantification (LLoQ), resolution, range and, response time. The utilized reagents were optimized to produce a response from 25-1000 μM ammonium chloride demonstrated in Figure 5.3. An LLoQ of 25 μM was recorded with an average error of ~15%, therefore the sensor's resolution in terms of concentration is higher at lower ammonium concentrations.

5.4.2 Stability Studies

One major advantage of using the indophenol reaction for determining ammonia concentrations is that it does not require any biological components such as enzymes, which are prone to stability issues. The shelf-life of the solutions used for the indophenol reaction was examined over the course of 100 days. The components of the indophenol reaction are not stable when mixed together, potentially due to the hypochlorite and the coupling agent's, sodium nitroprusside, reactivity. The response to the range of ammonium chloride concentrations was stable for up to 50 days. As seen in Figure 5.4, the response to 25, 150 and 500 μM ammonium chloride does not change significantly until day 75.
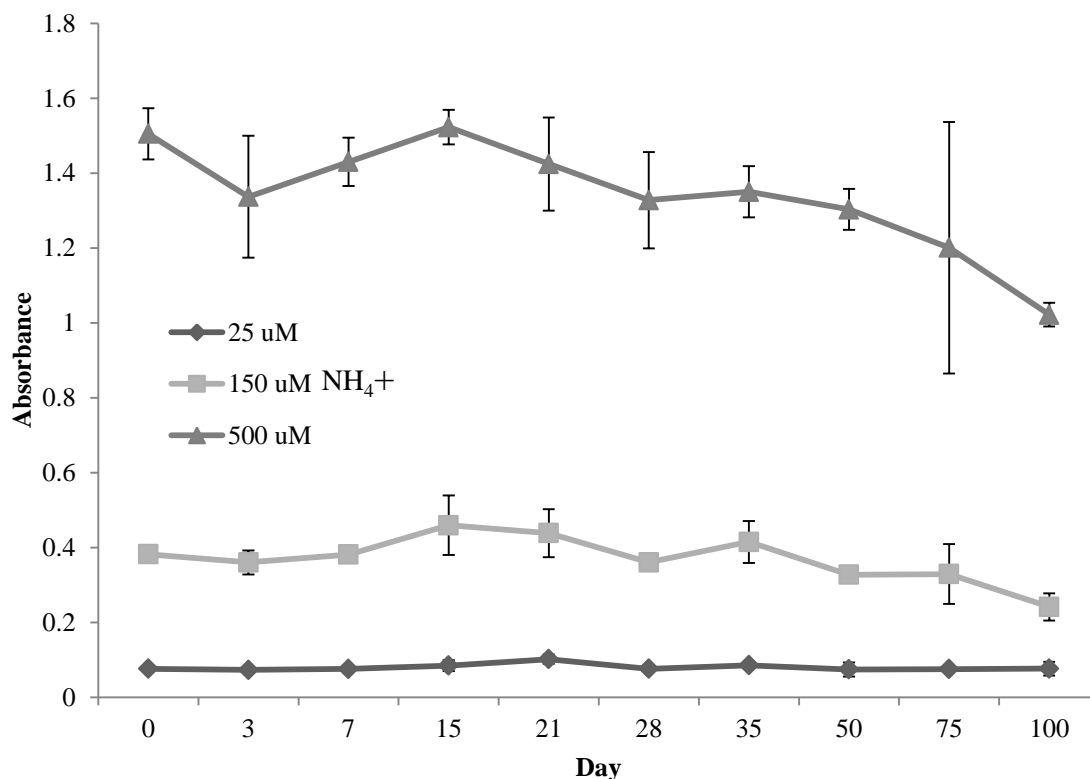
Figure 5.4 The reagents for the indophenol reaction were stored at room temperature and used to generate an ammonia standard curve at regular intervals for 100 days. The response to 500μM ammonia began to degrade at day 75. The reagents of the indophenol reaction are stable at room temperature for up to 50 days before its response to different concentrations of ammonia begins to deteriorate.

5.4.3 Response to Amino Acids

The mechanism for the indophenol reaction is also applicable to other primary amine containing compounds. For whole blood applications this is problematic due to the presence of small amine containing molecules such as amino acids which would cause interference when measuring blood ammonia. The phenol compound utilized in the indophenol reaction, 2-phenylphenol, is thought to introduce some form of selectivity due the large phenyl group adding a degree of steric hindrance to the reaction. The selectivity

of the reaction was tested with a large array of different amino acids. Since the response to the amino acids was so low, a concentration of 500 µM was utilized for ammonia and 1mM for the amino acids. The absorbance values recorded for the amino acids were normalized with the ammonia acting as 100%. The radar graph in Figure 5.5 shows the response of each amino acid, the highest of which was threonine that was just 7% of the ammonia response.
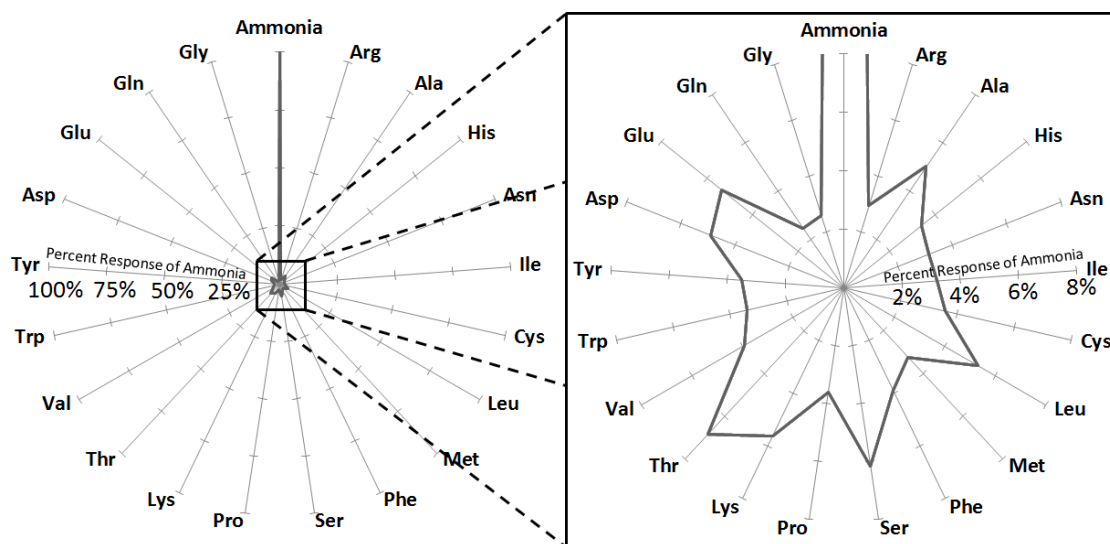
Figure 5.5 1mM concentrations of each of the 21 amino were tested using the indophenol reaction. The absorbance measured at 635nm for each amino acid after the indophenol reaction was calculated as percentage of the response from indophenol reaction with 1mM ammonium chlroide. The radar graph displays the percent response as compared to 1mM ammonium chloride. The highest response was threonine which produced an absorbance value that was just 7% of ammonia's response.

5.4.4 Cation Exchange of Whole Blood

The other major source of interference for the indophenol reaction is proteins. Small quantities of proteins can completely disable the reaction from proceeding. In order to

rapidly separate ammonium from whole blood while excluding any proteins, Nafion, a cation exchange membrane, was utilized. Nafion has had previous application in biosensors but almost entirely for protection of electrodes in electrochemical sensors. In this case Nafion is being operated as a cation exchange membrane rather than a nanoporous form of Teflon, as used in electrochemical sensors. Nafion is a fluorinated ionomer block copolymer. When cast into films, usually from solution in a hot press, the ionomeric block aggregate into long-range pores of the sulfones surrounded by a matrix of the fluoropolymer. The pores are highly negatively charged due to the sulfonic acids groups and are generally 1-4nm in size. These pores allow for the rapid diffusion of hydroxyl containing molecules and cations through the Nafion while inhibiting anions and completely preventing macromolecules. This would allow for the rapid diffusion of ammonia while reducing amino acid diffusion and completely eliminating proteins from passing and disabling the indophenol reaction.

The ion-exchange of ammonium through the use of the Nafion is the main mechanism of recovery of the analyte. Ammonium will diffuse across the membrane passively as well, but at a rate that is not sufficient for a beneficial point-of-care sensor. Alkali solutions of different ionic strength were tested for their effectiveness in exchanging with the ammonium from a PBS solution. It was expected that higher concentrations of salt would yield larger recoveries of ammonium. Bisected wells were prepared with Nafion membranes. A 500mM solution of ammonium chloride in PBS was placed on the 'analyte' side of the bisected well and solutions of a concentrated aqueous alkali in the opposing bisection. Distilled water resulted in a 10% recovery, in the control case, while the concentrated aqueous alkali resulted in a 75% recovery of the ammonium. The larger

concentration of ammonium in the alkali solution versus the analyte is indicative of the ion exchange mechanism occurring, as the concentration would be equal if the mechanism was simply passive diffusion.

5.4.5 Sensor Response to Ammonia in PBS

The sensor was initially challenged with ammonium chloride solution in PBS, before introducing an environment as complex as whole blood. Concentrations ranging from 0-500 µM were analyzed. In healthy adults ammonia levels are generally 50-80 µM whereas concentrations greater than 100 µM are suspect. These numbers are higher in neonates in which case less than 110 µM is normal, up to 180 µM could be attributed to other illnesses and greater than 200 µM is cause for concern. In severe cases ammonia levels can be as high as 500 µM*(89)*.
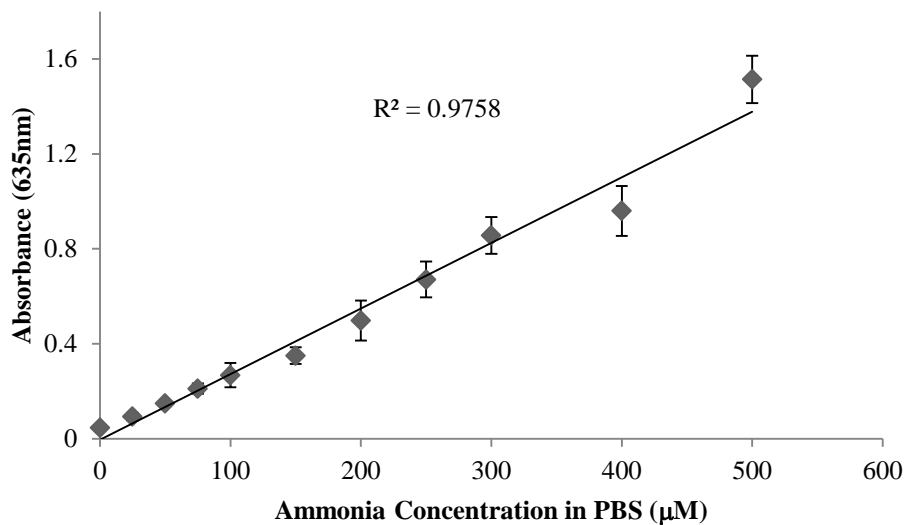
Figure 5.6 The constructed sensor's response to a range of ammonia concentrations in 1X PBS. The COD is 0.9758 with n=5 samples.

The sensor reliably extracted the ammonia in 20 minutes time. The extracted solution was then tested using the indophenol reaction and the developed color analyzed using a plate reader measuring absorbance at 635nm. This process produced the standard curve seen in Figure 5.6. The COD for detection in PBS was 0.97, with an error of 5-15%. In the range of 0-100mM, there was a resolution of ~30 µM ammonium. The sensor was efficacious over the entire clinically relevant range of ammonia levels in PBS.

5.4.6 Initial Sensor Response to Ammonia in Whole Blood
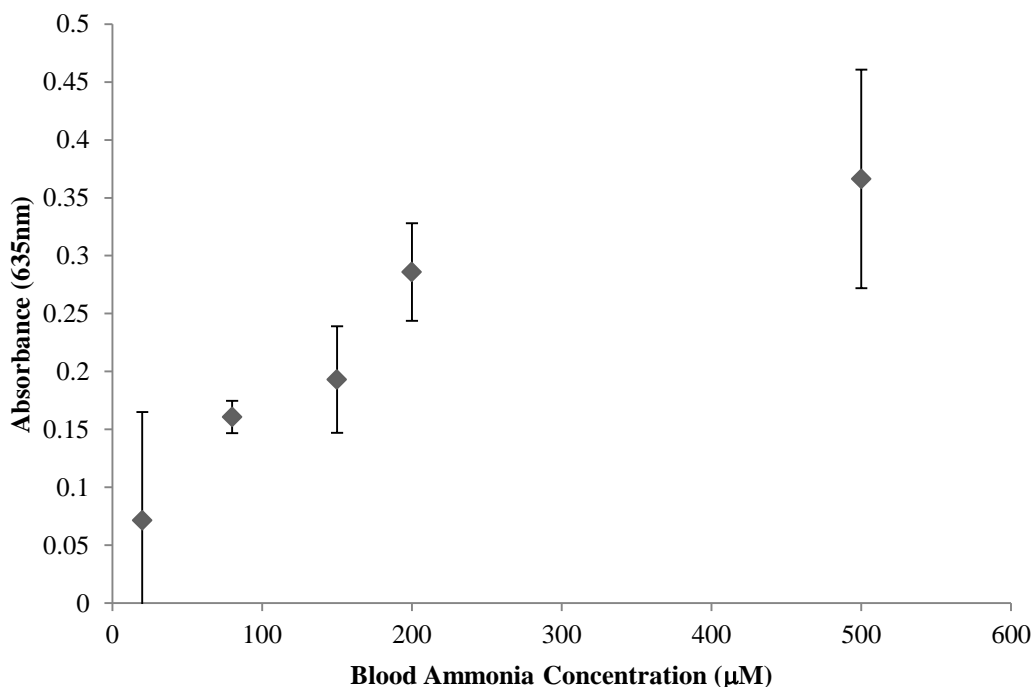
Figure 5.7 Initial experiments of determining blood ammonia concentration demonstrated a limited response. Responses were hindered and would not exceed an absorbance of 0.35 indicating some degree of interference.

Initial studies in blood produced a non-linear relationship between ammonia concentration and absorbance. The response was limited at an absorbance of 0.35 at a blood ammonia concentration of 500 µM. These responses are markedly reduced from

the same concentrations of ammonia in PBS. This suggests that the ammonia is either

inhibited from diffusing across the Nafion membrane or small molecules from blood are

interfering with the indophenol reaction.
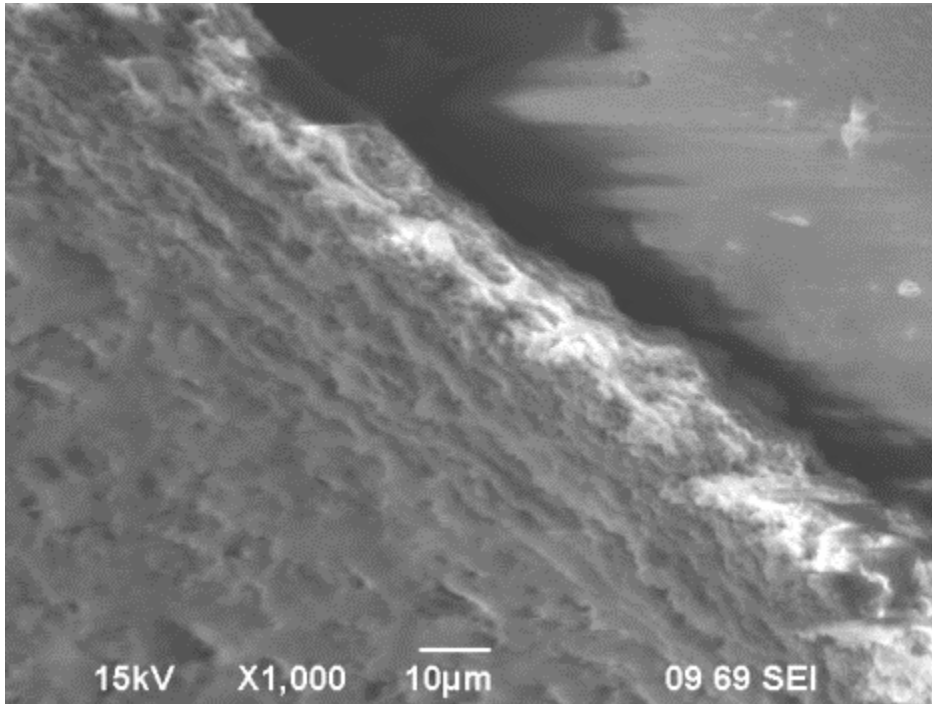
Figure 5.8 Electron micrograph of Nafion after exposure to whole sheep's blood for 20

minutes. A dense, adsorbed, layer of proteins and cell were formed on the hydrophobic

surface of the Nafion. This large degree of biofouling could prevent free ammonia

diffusion through the membrane.

A potential mechanism of interference is fouling of the Nafion membrane, rescinding its

permeability to ammonia. Nafion was exposed to whole sheep's blood for 20 minutes to

examine the effects on the membrane. After 20 minutes a visible layer of red proteins and

cells formed on the Nafion surface. The adsorbed cells were fixed and imaged using

SEM. The electron micrograph displayed in Figure 5.8 demonstrates the thick layer of

blood proteins and cells adsorbed to the surface of Nafion. To determine if this fouling

event was the source of the interference, Nafion was exposed to a blocking buffer of 5% bovine serum albumin. Blocking buffers contains either a single type of protein or a surfactant. In the case with BSA, the protein denatures while adsorbing to the surface of the hydrophobic Nafion, exposing its hydrophobic core to the surface and its hydrophilic residues to the aqueous media. This process forms a hydrophilic monolayer of BSA which prevents any further cell or protein based fouling events from occurring. BSA blocked Nafion was subsequently exposed to whole sheep's blood for 20 minutes. In this case no visible fouling occurred of the membrane indicating the hydrophilic treatment prevented fouling by blood proteins and cells. The effectiveness of the BSA blocked Nafion in separating ammonia was investigated in both blood and PBS. As seen in Figure 5.9 the BSA blocking layer does not prevent ammonia diffusion across the Nafion membrane. When this experiment was repeated in whole blood, however, it was determined that the blocking did not improve ammonia detection.
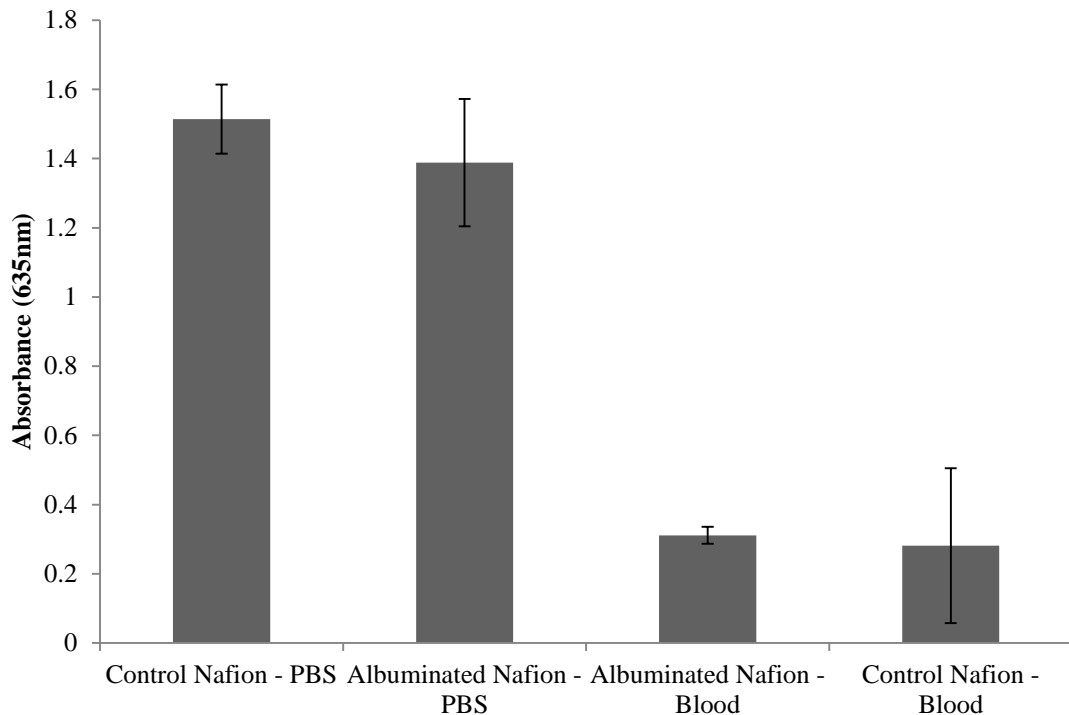
Figure 5.9 The bisected well sensor was constructed using either untreated Nafion or Nafion that had been blocked with 5% BSA solution. Both constructions were exposed to 500mM ammonia in 1X PBS and whole sheep's blood. The BSA blocking did not reduce the sensing of ammonia in the PBS. It, however, did not improve the responses in whole blood.

Negative interference of the indophenol reaction can also occur from the presence of certain small molecules. It has been previously reported that high concentrations of amines, thiols and reducing agents will disrupt the indophenol reaction, all of which are present in blood(111). Reducing agents will readily react with hypochlorite, an oxidizing agent, effectively disabling the indophenol reaction. To determine if this was the case, ammonia extract from whole sheep blood was exposed to a modified indophenol reaction using 2, 3, 5 and 10X more concentrated hypochlorite than conventionally utilized. As seen in Figure 5.10, increasing the hypochlorite concentration up to 3X improved the reaction's response to the ammonia extracted from the whole blood. At 5 and 10X concentrated hypochlorite, the reactions response to ammonia began to degrade, indicating that 3X hypochlorite is optimal for reducing the interference introduced by reducing agents found in blood.
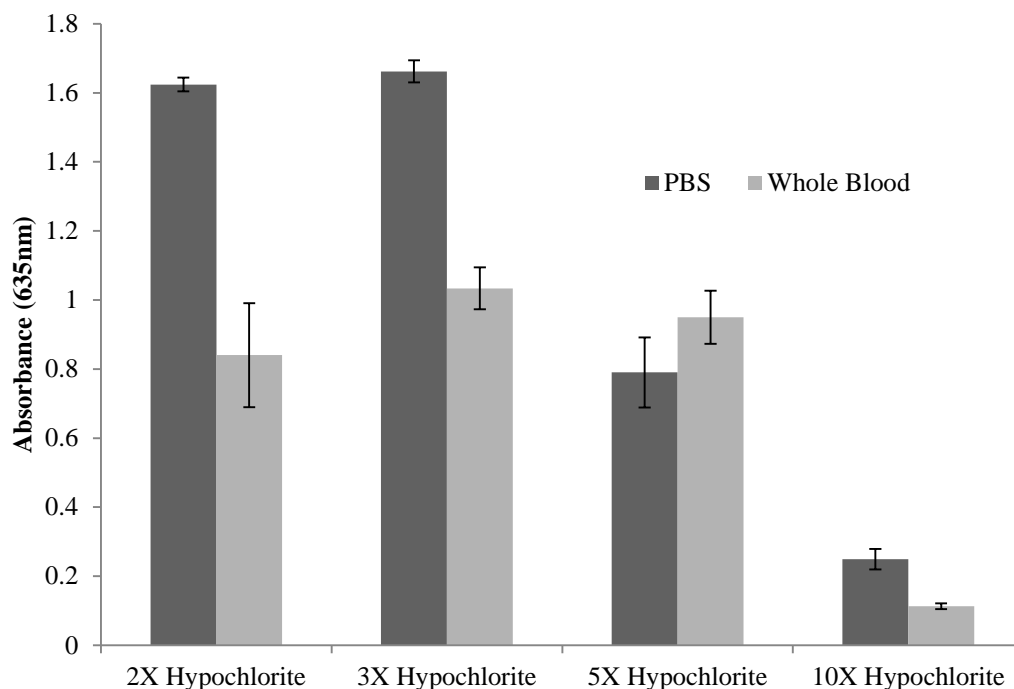
Figure 5.10 Concentrations of 2-10X hypochlorite were utilized in the analysis of 500mM ammonia in 1X PBS and whole sheep's blood. Increasing the concentration of hypochlorite utilized in the indophenol reaction reduced the negative interference small blood molecules had on the indophenol reaction. At concentrations higher than 3X, reaction itself began to degrade. A 3-fold increase in hypochlorite concentration was optimal.

5.4.7 Modified Sensor Response to Ammonia in Whole Blood

The 3X hypochlorite-modified indophenol reaction was examined in conjunction with the Nafion based separation technique for its effectiveness in distinguishing blood ammonia concentrations ranging from 25 to 500 μM, representing healthy to diseased levels. The resulting standard curve, in Figure 5.11, demonstrated the response in this range. There was a significant correlation, with a COD of 0.9573, between blood ammonia concentrations and the resulting absorbance at 635nm after the indophenol reaction.
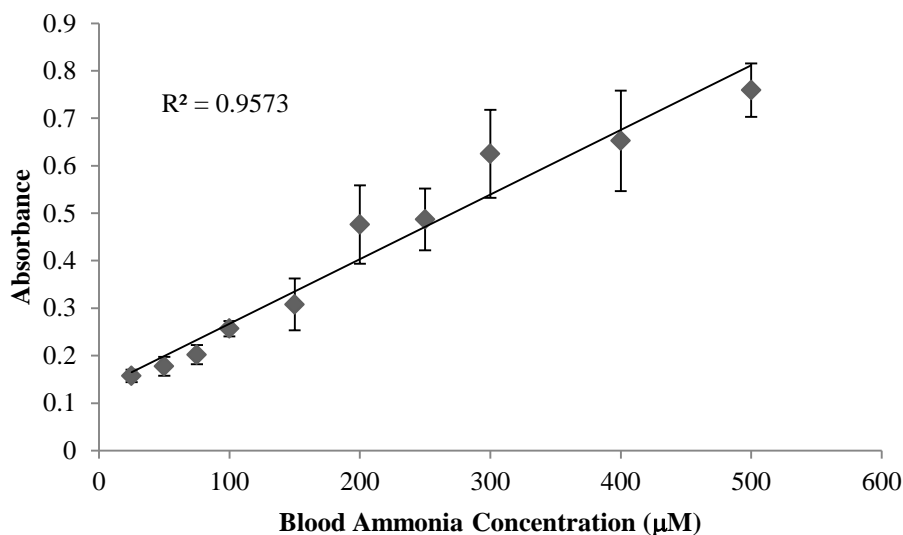
Figure 5.11 The bisected well sensor was again used to extract ammonia in whole human blood. The extracted ammonia solutions were tested with the 3X hypochlorite-modifed indophenol reaction and the absorbance measured at 635nm. In the range of 0-500 μM the COD was 0.9573 with n=5 samples.

In the range of 25-150 μM, where high resolution measurements are critical for examining treatment effectiveness, the COD was 0.9777, seen in Figure 5.12. The error in this range was ~10%, giving a preliminary resolution of 15 μM. The relative standard deviation of 10% percent falls within the FDA guide for validation of a bioanalytical method which requires an relative standard deviation of 15% at n=5 samples. The LLoQ, 25μM, is at least 3σ above the mean background reading of 0.04483+/-0.00117 absorbance. Additionally, the sensor can reliably differentiate between 50 and 100μM blood ammonia with a p=0.0001.
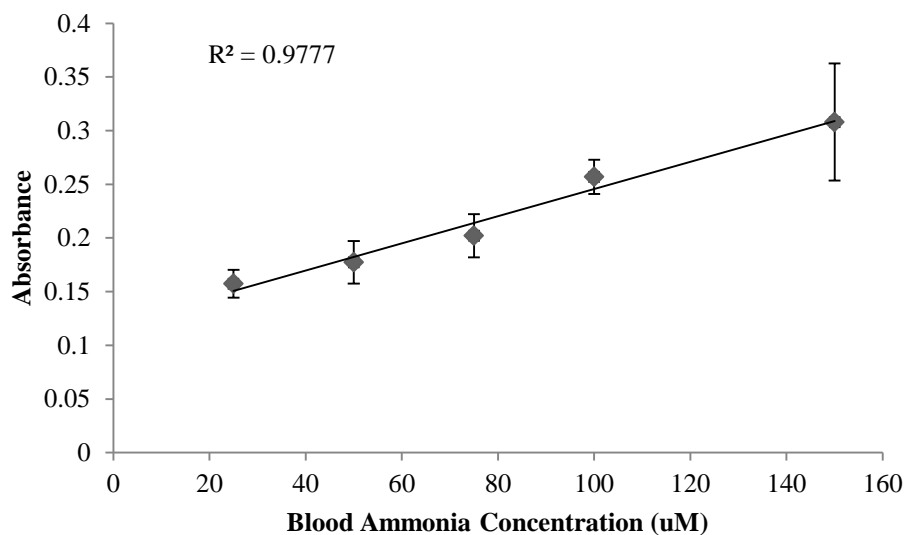
Figure 5.12 The sensor's response to blood ammonia concentrations ranging from 0-150 μM. The relative standard deviation is ~10% with a COD of 0.9777 with n=5 samples.

5.5 Conclusion

The investigated bioanalytical method for evaluating blood ammonia levels demonstrated a high degree of correlation between blood ammonia and sensor response. In the range of 25-150mM, which is the most critical concentrations, the relative standard deviation was just 10%. The sensor has a 20 minute response time, and the interference from other small molecules was greatly reduced. The components used are stable at room temperature for up 50 days and inexpensive.

6.0 Conclusions

6.1 Polystyrene-b-poly(2-vinylpryidine) Photonic Crystals

6.1.1 Summary of Results

PS-b-P2VP films were investigated as 1D photonic crystal sensors that could reflect visible wavelengths of light. By quaternized the P2VP block, it can swell in aqueous media, actuating the spacing to the correct distance for the system to reflect visible wavelengths of light. Boronic acid was covalently attached to the P2VP block to impart fructose sensing abilities. Boronic acid modified PS-b-P2VP could detect fructose in a range of 500μM to 50mM. The photonic crystal would change from blue to orange in the presence of 50mM fructose in a 30 minute time frame. This demonstrated the ability of PS-b-P2VP, self-assembled photonic crystal to behave as specific chemical sensors, which has not been previously reported.

The introduction of primary amine functionalities to PS-b-P2VP was subsequently investigated. Primary amines open the door for a variety of click chemistries for the attachment of enzymes, antibodies, pepties, oligonucleotides and aptamers, which would allow different sensing events. The use of trimethylsilyl protecting groups was investigated for the attachment of bromominated primary amine containing compounds to the P2VP block of PS-b-P2VP. Traditional protecting groups such as Boc can degrade the nanostructure of microphase separated PS-b-P2VP. Alternatively, the trimethylsilyl protecting group allowed for the attachment of a primary amine, without disrupting the nanostructure. The reaction efficiency was shown to be 3.5%, but still allowed the PS-b-P2VP to be cross-linked by glutaraldehyde.

6.1.2 Contributions

The work presented in chapters 2, 3 and 4 demonstrated the use of PS-b-P2VP lamellar films as sensitive, color changing photonic crystal sensors. While this particular system has been shown to behave as a visible photonic crystal, very little work has been demonstrating is capacity as a chemical sensor. This work demonstrated that the nucleophilic nature of 2VP can be exploited as a means to introduce different chemical functionalities to this photonic crystal BCP system. The protocol reviewed has allowed for the attachment of both boronic acids for the sensing of sugars, and the attachment of primary amines. Primary amines open the door for a variety of different click chemistries such as reactions with aldehydes and carboxylic acids, or the conversion into thiols through the use of Traut's reagent. These now available click chemistries would allow for the attachment of different biological capture moieties to P2VP block such as enzymes, antibodies and oligonucleotides.

6.1.3 Future Work

The primary amine functionalization of PS-b-P2VP should be further optimized to improve the reaction efficiency. Once improved, peptide based cross-links can be introduced to the P2VP block of the photonic crystal through the use of amine based click chemistry. The peptide cross-links would prevent the swelling of the P2VP block. When exposed to a target protease, the peptide cross-links would be cleaved allowing the system to swell, redshifting the reflected wavelength of the photonic crystal, indicating the presence of the target protease. A similar system can be achieved through the use of oligonucleotides. In this case the P2VP block could be cross-linked with hybridized oligonucleotides. When a target oligonucleotide is introduced that complementary for the

94

one of the attached oligonucleotide, the cross-link will break so that one of the oligonucleotides can bind the target. The breaking of the cross-links would allow the system to swell, redshifting the reflected color, indicating the presence of the target oligonucleotide.

6.2 Point-of-Care Blood Ammonia Sensor

6.2.1 Summary of Results

There are currently no reliable options for measuring blood ammonia without the aid of a clinical laboratory. Patients with urea cycle disorders and hepatic encephalopathy must travel to a hospital for blood ammonia tests. In emergency medicine, hyperammonemia is often not diagnosed due to overlapping symptoms with sepsis. A point-of-care sensor would allow for more effective disease management and more accurate diagnosis of hyperammonemia. The fabricated point-of-care blood ammonia sensor utilized the indophenol reaction in tandem with Nafion. The indophenol reaction is a sensitive and specific colorimetric reaction, which turns blue in the presence of ammonia. To reduce macromolecular interference with the reaction, Nafion, a cation exchange membrane was utilized to first extract the ammonia from whole blood. Nafion essentially acts as an ammonia selective membrane. The constructed sensor could detect blood ammonia levels ranging from 25-500μM with a 15% error and COD of 0.9573. In the range of 25-150μM, the COD was 0.9777 and the error was just 10% with n=5 samples. The sensor could reliably differentiate between 50 and 100μM blood ammonia with a p=0.0001. The indophenol reagents used for the colorimetric determination of ammonia are shelf-stable at room temperature for up to 50 days.

6.2.2 Contributions

The work described in Chapter 5, provided the means for reliable extraction of ammonia from blood and its subsequent detection using the colorimetric indophenol reaction. This work demonstrated the capacity of Nafion, normally utilized in fuel cells, as an effective membrane for the rapid extraction of ammonium cations from whole blood. The use of the indophenol reaction as a means for reliable detection of ammonia in blood had not been previously described in a compact sensor. The work also demonstrated the value in optimizing the indophenol reagents by increasing the concentration of hypochlorite to counteract any reducing agents in blood such as uric acid, from inhibiting the sensing event. This has led to an interesting platform for the rapid detection of ammonia in whole blood which has not been previously described.

6.2.3 Future Work

In its current state the blood ammonia sensor requires the extracted ammonia solution to be pipetted along with each reagent of the indophenol reaction into a 384 well-plate, mixed, and the probed for absorbance at 635nm using a microplate reader. The future work for the sensor would involve incorporating the extraction and indophenol reaction steps into fluidic device. The device would still contain the bisected well, which would extract the ammonia. The extracted ammonia could be pumped into another microcontainer within the fluidic along with the reagents for the indophenol reaction. The microcontainer would be probed optically utilizing a 635nm light-emitting diode and a photodiode to determine the absorbance of the resulting solution. This would provide a compact test cartridge that could be used in conjunction with a handheld device to determine blood ammonia concentrations.

7.0 References

1. E. Yablonovitch, Inhibited Spontaneous Emission in Solid-State Physics and Electronics, *Phys. Rev. Lett.* **58**, 2059–2062 (1987).

2. C. Fenzl, T. Hirsch, O. S. Wolfbeis, Photonic crystals for chemical sensing and biosensing., *Angew. Chem. Int. Ed. Engl.* **53**, 3318–35 (2014).

3. M. J. Bloemer, M. Scalora, Transmissive properties of Ag/MgF[sub 2] photonic band gaps, *Appl. Phys. Lett.* **72**, 1676 (1998).

4. K. M. Chen, A. W. Sparks, H.-C. Luan, D. R. Lim, K. Wada, L. C. Kimerling, SiO[sub 2]/TiO[sub 2] omnidirectional reflector and microcavity resonator via the sol-gel method, *Appl. Phys. Lett.* **75**, 3805 (1999).

5. J. Bellessa, S. Rabaste, J. C. Plenet, J. Dumas, J. Mugnier, O. Marty, Eu[sup 3+]-doped microcavities fabricated by sol–gel process, *Appl. Phys. Lett.* **79**, 2142 (2001).

6. H.-Y. Lee, H. Makino, T. Yao, A. Tanaka, Si-based omnidirectional reflector and transmission filter optimized at a wavelength of 1.55 μm, *Appl. Phys. Lett.* **81**, 4502 (2002).

7. M. Patrini, M. Galli, M. Belotti, L. C. Andreani, G. Guizzetti, G. Pucker, a. Lui, P. Bellutti, L. Pavesi, Optical response of one-dimensional (Si/SiO[sub 2])[sub m] photonic crystals, *J. Appl. Phys.* **92**, 1816 (2002).

8. S. Noda, a Chutinan, M. Imada, Trapping and emission of photons by a single defect in a photonic bandgap structure, *Nature* **407**, 608–10 (2000).

9. J. R. Wendt, G. A. Vawter, P. L. Gourley, T. M. Brennan, B. E. Hammons, Nanofabrication of photonic lattice structures in GaAs/AlGaAs, *J. Vac. Sci. Technol. B* **11** (1993).

10. a. Rosenberg, R. J. Tonucci, E. a. Bolden, Photonic band-structure effects in the visible and near ultraviolet observed in solid-state dielectric arrays, *Appl. Phys. Lett.* **69**, 2638 (1996).

11. S. W. Leonard, H. M. van Driel, K. Busch, S. John, a. Birner, a.-P. Li, F. Müller, U. Gösele, V. Lehmann, Attenuation of optical transmission within the band gap of thin two-dimensional macroporous silicon photonic crystals, *Appl. Phys. Lett.* **75**, 3063 (1999).

12. Y. Kang, J. J. Walish, T. Gorishnyy, E. L. Thomas, Broad-wavelength-range chemically tunable block-copolymer photonic gels., *Nat. Mater.* **6**, 957–60 (2007).

13. J. J. Walish, Y. Kang, R. A. Mickiewicz, E. L. Thomas, Bioinspired Electrochemically Tunable Block Copolymer Full Color Pixels, *Adv. Mater.* **21**, 3078–3081 (2009).

14. F. S. Bates, G. H. Fredrickson, Block copolymer thermodynamics: theory and experiment., *Annu. Rev. Phys. Chem.* **41**, 525–57 (1990).

15. Glossary of Nanotechnology and Related Terms (available at http://eng.thesaurus.rusnano.com/wiki/article1191).

16. G. M. Miyake, V. A. Piunova, R. A. Weitekamp, R. H. Grubbs, Precisely Tunable Photonic Crystals From Rapidly Self-Assembling Brush Block Copolymer Blends, *Angew. Chemie Int. Ed.* **51**, 11246–11248 (2012).

17. J. H. Holtz, S. A. Asher, Polymerized colloidal crystal hydrogel films as intelligent chemical sensing materials, *Nature* **389**, 829–832 (1997).

18. M. M. W. Muscatello, L. E. Stunja, S. a Asher, Polymerized crystalline colloidal array sensing of high glucose concentrations., *Anal. Chem.* **81**, 4978–86 (2009).

19. T. Kanai, D. Lee, H. C. Shum, D. a Weitz, Fabrication of tunable spherical colloidal crystals immobilized in soft hydrogels., *Small* **6**, 807–10 (2010).

20. T. Kanai, D. Lee, H. C. Shum, R. K. Shah, D. a Weitz, Gel-immobilized colloidal crystal shell with enhanced thermal sensitivity at photonic wavelengths., *Adv. Mater.* **22**, 4998–5002 (2010).

21. J.-G. Park, S.-H. Kim, S. Magkiriadou, T. M. Choi, Y.-S. Kim, V. N. Manoharan, Full-spectrum photonic pigments with non-iridescent structural colors through colloidal assembly., *Angew. Chem. Int. Ed. Engl.* **53**, 2899–903 (2014).

22. W. Shen, M. Li, C. Ye, L. Jiang, Y. Song, Direct-writing colloidal photonic crystal microfluidic chips by inkjet printing for label-free protein detection., *Lab Chip* **12**, 3089–95 (2012).

23. P. J. Flory, *Principles of Polymer Chemistry* (Cornell University Press, 1953; http://books.google.com/books?id=CQ0EbEkT5R0C).

24. Y. Y. Li, F. Cunin, J. R. Link, T. Gao, R. E. Betts, S. H. Reiver, V. Chin, S. N. Bhatia, M. J. Sailor, Polymer replicas of photonic porous silicon for sensing and drug delivery applications., *Science* **299**, 2045–7 (2003).

25. T. Endo, S. Ozawa, N. Okuda, Y. Yanagida, S. Tanaka, T. Hatsuzawa, Reflectometric detection of influenza virus in human saliva using nanoimprint lithography-based flexible two-dimensional photonic crystal biosensor, *Sensors Actuators B Chem.* **148**, 269–276 (2010).

26. M. R. Lee, P. M. Fauchet, Two-dimensional silicon photonic crystal based biosensing platform for protein detection, *Opt. Express* **15**, 4530–4535 (2007).

27. M. M. Orosco, C. Pacholski, G. M. Miskelly, M. J. Sailor, Protein-Coated Porous-Silicon Photonic Crystals for Amplified Optical Detection of Protease Activity, *Adv. Mater.* **18**, 1393–1396 (2006).

28. K. A. Kilian, T. Böcking, K. Gaus, M. Gal, J. J. Gooding, Peptide-Modified Optical Activity, **1**, 355–361 (2007).

29. M. M. Orosco, C. Pacholski, M. J. Sailor, Real-time monitoring of enzyme activity in a mesoporous silicon double layer, **4**, 255–258 (2009).

30. K. a Kilian, L. M. H. Lai, A. Magenau, S. Cartland, T. Böcking, N. Di Girolamo, M. Gal, K. Gaus, J. J. Gooding, Smart tissue culture: in situ monitoring of the activity of protease enzymes secreted from live cells using nanostructured photonic crystals., *Nano Lett.* **9**, 2021–5 (2009).

31. E. Kim, C. Kang, H. Baek, K. Hwang, D. Kwak, E. Lee, Y. Kang, E. L. Thomas, Control of Optical Hysteresis in Block Copolymer Photonic Gels: A Step Towards Wet Photonic Memory Films, *Adv. Funct. Mater.* **20**, 1728–1732 (2010).

32. C. E. Reese, S. a Asher, Photonic crystal optrode sensor for detection of Pb2+ in high ionic strength environments., *Anal. Chem.* **75**, 3915–8 (2003).

33. K. Lee, S. A. Asher, R. V June, Photonic Crystal Chemical Sensors : pH and Ionic Strength, **15260**, 9534–9537 (2000).

34. J. Shin, P. V. Braun, W. Lee, Fast response photonic crystal pH sensor based on templated photo-polymerized hydrogel inverse opal, *Sensors Actuators B Chem.* **150**, 183–190 (2010).

35. E. Tian, J. Wang, Y. Zheng, Y. Song, L. Jiang, D. Zhu, Colorful humidity sensitive photonic crystal hydrogel, *J. Mater. Chem.* **18**, 1116 (2008).

36. V. L. Alexeev, A. C. Sharma, A. V Goponenko, S. Das, I. K. Lednev, C. S. Wilcox, D. N. Finegold, S. a Asher, High ionic strength glucose-sensing photonic crystal., *Anal. Chem.* **75**, 2316–23 (2003).

37. V. L. Alexeev, S. Das, D. N. Finegold, S. a Asher, Photonic crystal glucose-sensing material for noninvasive monitoring of glucose in tear fluid., *Clin. Chem.* **50**, 2353–60 (2004).

38. M. Ben-Moshe, V. L. Alexeev, S. a Asher, Fast responsive crystalline colloidal array photonic crystal glucose sensors., *Anal. Chem.* **78**, 5149–57 (2006).

39. Q. Cui, M. M. Ward Muscatello, S. a Asher, Photonic crystal borax competitive binding carbohydrate sensing motif., *Analyst* **134**, 875–80 (2009).

40. J. P. Walker, S. A. Asher, Nerve Agent Sensing Photonic Crystal (PCCA) photonic crystal sensing material that senses the, **77**, 1596–1600 (2005).

41. J. P. Walker, K. W. Kimble, S. a Asher, Photonic crystal sensor for organophosphate nerve agents utilizing the organophosphorus hydrolase enzyme., *Anal. Bioanal. Chem.* **389**, 2115–24 (2007).

42. B.-F. Ye, Y.-J. Zhao, Y. Cheng, T.-T. Li, Z.-Y. Xie, X.-W. Zhao, Z.-Z. Gu, Colorimetric photonic hydrogel aptasensor for the screening of heavy metal ions, *Nanoscale* **4**, 5998–6003 (2012).

43. X. Hu, G. Li, M. Li, J. Huang, Y. Li, Y. Gao, Y. Zhang, Ultrasensitive Specific Stimulant Assay Based on Molecularly Imprinted Photonic Hydrogels, *Adv. Funct. Mater.* **18**, 575–583 (2008).

44. Y.-X. Zhang, P.-Y. Zhao, L.-P. Yu, Highly-sensitive and selective colorimetric sensor for amino acids chiral recognition based on molecularly imprinted photonic polymers, *Sensors Actuators B Chem.* **181**, 850–857 (2013).

45. K. Lee, S. A. Asher, Photonic crystal chemical sensors: pH and ionic strength, *J. Am. Chem. Soc.* **122**, 9534–9537 (2000).

46. Q. Cui, M. M. Ward Muscatello, S. A. Asher, Photonic crystal borax competitive binding carbohydrate sensing motif, *Analyst* **134**, 875–880 (2009).

47. A. C. Edrington, A. M. Urbas, P. DeRege, C. X. Chen, T. M. Swager, N. Hadjichristidis, M. Xenidou, L. J. Fetters, J. D. Joannopoulos, Y. Fink, E. L. Thomas, Polymer-based photonic crystals, *Adv. Mater.* **13**, 421–425 (2001).

48. A. Urbas, R. Sharp, Y. Fink, E. L. Thomas, M. Xenidou, L. J. Fetters, Tunable block copolymer/homopolymer photonic crystals, *Adv. Mater.* **12**, 812–814 (2000).

49. L. I. Bosch, T. M. Fyles, T. D. James, Binary and ternary phenylboronic acid complexes with saccharides and Lewis bases, *Tetrahedron* **60**, 11175–11190 (2004).

50. W. Chen, V. Leung, H. Kroener, R. Pelton, Polyvinylamine-Phenylboronic Acid Adhesion to Cellulose Hydrogel, *Langmuir* **25**, 6863–6868 (2009).

51. Y. Kim, S. A. Hilderbrand, R. Weissleder, C. H. Tung, Sugar sensing based on induced pH changes, *Chem. Commun.* , 2299–2301 (2007).

52. M. Bielecki, H. Eggert, J. C. Norrild, A fluorescent glucose sensor binding covalently to all five hydroxy groups of alpha-D-glucofuranose. A reinvestigation, *J. Chem. Soc. Trans. 2* , 449–455 (1999).

53. S. a Asher, V. L. Alexeev, A. V Goponenko, A. C. Sharma, I. K. Lednev, C. S. Wilcox, D. N. Finegold, Photonic crystal carbohydrate sensors: low ionic strength sugar sensing., *J. Am. Chem. Soc.* **125**, 3322–9 (2003).

54. G. Springsteen, B. H. Wang, A detailed examination of boronic acid-diol complexation, *Tetrahedron* **58**, 5291–5300 (2002).

55. M. Tominaga, S. Nomura, I. Taniguchi, D-Fructose detection based on the direct heterogeneous electron transfer reaction of fructose dehydrogenase adsorbed onto multi-walled carbon nanotubes synthesized on platinum electrode, *Biosens. Bioelectron.* **24**, 1184–1188 (2009).

56. S. G. Bhand, S. Soundararajan, I. Surugiu-Warnmark, J. S. Milea, E. S. Dey, M. Yakovleva, B. Danielsson, Fructose-selective calorimetric biosensor in flow injection analysis, *Anal. Chim. Acta* **668**, 13–18 (2010).

57. G. F. Khan, H. Shinohara, Y. Ikariyama, M. Aizawa, An Amperometric Biosensor for Fructose Using a Pqq Enzyme, *Sensors and Actuators B-Chemical* **14**, 673–674 (1993).

58. U. B. Trivedi, D. Lakshminarayana, I. L. Kothari, P. B. Patel, C. J. Panchal, Amperometric fructose biosensor based on fructose dehydrogenase enzyme, *Sensors and Actuators B-Chemical* **136**, 45–51 (2009).

59. O. B. Ayyub, J. W. Sekowski, T. I. Yang, X. Zhang, R. M. Briber, P. Kofinas, Color changing block copolymer films for chemical sensing of simple sugars, *Biosens Bioelectron* **28**, 349–354 (2011).

60. N. DiCesare, M. R. Pinto, K. S. Schanze, J. R. Lakowicz, Saccharide detection based on the amplified fluorescence quenching of a water-soluble poly(phenylene ethynylene) by a boronic acid functionalized benzyl viologen derivative, *Langmuir* **18**, 7785–7787 (2002).

61. J. J. Li, Z. Wang, P. Li, N. Zong, F. Li, A sensitive non-enzyme sensing platform for glucose based on boronic acid-diol binding, *Sensors and Actuators B-Chemical* **161**, 832–837 (2012).

62. W. K. Oh, Y. S. Jeong, K. J. Lee, J. Jang, Fluorescent boronic acid-modified polymer nanoparticles for enantioselective monosaccharide detection, *Anal. Methods* **4**, 913–918 (2012).

63. Y. J. Zhang, Z. F. He, G. W. Li, A novel fluorescent vesicular sensor for saccharides based on boronic acid-diol interaction, *Talanta* **81**, 591–596 (2010).

64. Y. Kang, Effect of Salts on the Tunability of Photonic Gels, *Bull. Korean Chem. Soc.* **29** (2008).

65. B. W. Li, K. W. Andrews, P. R. Pehrsson, Individual sugars, soluble, and insoluble dietary fiber contents of 70 high consumption foods, *J. Food Compos. Anal.* **15**, 715–723 (2002).

66. H.-C. Kim, S.-M. Park, W. D. Hinsberg, Block copolymer based nanostructures: materials, processes, and applications to electronics., *Chem. Rev.* **110**, 146–77 (2010).

67. M. Aizawa, J. M. Buriak, C. Tg, R. V May, V. Re, M. Recei, V. July, Block Copolymer Templated Chemistry for the Formation of Metallic Nanoparticle Arrays on Semiconductor Surfaces, , 5090–5101 (2007).

68. J. J. Chiu, B. J. Kim, G.-R. Yi, J. Bang, E. J. Kramer, D. J. Pine, Distribution of Nanoparticles in Lamellar Domains of Block Copolymers, *Macromolecules* **40**, 3361–3365 (2007).

69. Q. Li, J. He, E. Glogowski, X. Li, J. Wang, T. Emrick, T. P. Russell, Responsive Assemblies: Gold Nanoparticles with Mixed Ligands in Microphase Separated Block Copolymers, *Adv. Mater.* **20**, 1462–1466 (2008).

70. T. Thurn-Albrecht, Ultrahigh-Density Nanowire Arrays Grown in Self-Assembled Diblock Copolymer Templates, *Science (80-.).* **290**, 2126–2129 (2000).

71. E. J. W. Crossland, S. Ludwigs, M. a. Hillmyer, U. Steiner, Freestanding nanowire arrays from soft-etch block copolymer templates, *Soft Matter* **3**, 94 (2007).

72. D. Beattie, K. H. Wong, C. Williams, L. a Poole-Warren, T. P. Davis, C. Barner-Kowollik, M. H. Stenzel, Honeycomb-structured porous films from polypyrrole-containing block copolymers prepared via RAFT polymerization as a scaffold for cell growth., *Biomacromolecules* **7**, 1072–82 (2006).

73. H. L. Khor, Y. Kuan, H. Kukula, K. Tamada, W. Knoll, M. Moeller, D. W. Hutmacher, Response of cells on surface-induced nanopatterns: fibroblasts and mesenchymal progenitor cells., *Biomacromolecules* **8**, 1530–40 (2007).

74. C. Burger, W. Ruland, a. N. Semenov, Polydispersity effects on the microphase-separation transition in block copolymers, *Macromolecules* **23**, 3339–3346 (1990).

75. P. Rempp, E. Merrill, *Polymer Synthesis* (New York, ed. 2nd, 1991).

76. R. A. Register, S. L. Cooper, P. Thiyagarajan, S. Chakrapani, R. Jerome, Effect of ionic aggregation on ionomer chain dimensions. 1. Telechelic polystyrenes, *Macromolecules* **23**, 2978–2983 (1990).

77. S. Krishnan, R. J. Ward, A. Hexemer, K. E. Sohn, K. L. Lee, E. R. Angert, D. a Fischer, E. J. Kramer, C. K. Ober, Surfaces of fluorinated pyridinium block copolymers with enhanced antibacterial activity., *Langmuir* **22**, 11255–66 (2006).

78. J. Huang, R. R. Koepsel, H. Murata, W. Wu, S. B. Lee, T. Kowalewski, A. J. Russell, K. Matyjaszewski, Nonleaching antibacterial glass surfaces via "Grafting Onto": the effect of the number of quaternary ammonium groups on biocidal activity., *Langmuir* **24**, 6785–95 (2008).

79. C. M. Grozea, N. Gunari, J. A. Finlay, D. Grozea, M. E. Callow, J. A. Callow, Z. Lu, G. C. Walker, and Diblock Polystyrene- block -poly (methyl methacrylate) Cylindrical Patterned Surfaces Inhibit Settlement of Zoospores of the Green Alga Ulva, , 1004–1012 (2009).

80. A. Haryono, W. H. Binder, Controlled arrangement of nanoparticle arrays in block-copolymer domains., *Small* **2**, 600–11 (2006).

81. S. G. Jang, E. J. Kramer, C. J. Hawker, Controlled supramolecular assembly of micelle-like gold nanoparticles in PS-b-P2VP diblock copolymers via hydrogen bonding., *J. Am. Chem. Soc.* **133**, 16986–96 (2011).

82. I. Tokarev, M. Orlov, S. Minko, Responsive Polyelectrolyte Gel Membranes, *Adv. Mater.* **18**, 2458–2460 (2006).

83. A. B. Rudine, M. G. Walter, C. C. Wamser, Reaction of dichloromethane with pyridine derivatives under ambient conditions., *J. Org. Chem.* **75**, 4292–5 (2010).

84. T. D. Nelson, R. D. Crouch, Selective Deprotection of Silyl Ethers, *Synthesis (Stuttg).* **1996**, 1031–1069 (1996).

85. B. Goeller, A. Dicko, M. Baboulene, NEW SYNTHESIS OF 1,2-AZABOROLIDINES BY METHANOLYSIS OF SILYLATED AMINOPROPYLBORANES: INVOLVEMENT OF THE N->B BOND*Main Gr. Met. Chem.* **20**, 795 (1997).

86. J. Lahaye, G. Nans, P. Fioux, A. Bagreev, A. Broshnik, V. Strelko, I. De Chimie, S. Mulhouse, C. France, X . P . S . ANALYSIS FOR THE THERMAL C O N V E R S I O N OF A V I N Y L P Y R I D I N E RESIN INTO ACTIVE CARBON, , 490–491.

87. L. E. Nielsen, Cross-Linking–Effect on Physical Properties of Polymers, *J. Macromol. Sci. Part C* **3**, 69–103 (1969).

88. X. Jin, T. S. Ellis, F. E. Karasz, The effect of crystallinity and crosslinking on the depression of the glass transition temperature in nylon 6 by water.pdf, *J. Polym. Sci. Polym. Phys. Ed.* **22**, 1701–1717 (1984).

89. J. Zschocke, G. F. Hoffmann, *Vademecum Metabolicum* (Milupa Metabolics, Friedrichsdorf, Germany, ed. 3rd, 2011).

90. B. C. Lanpher, A. L. Gropman, K. A. Chapman, U. Lichter-Konecki, M. L. Summar, *Urea Cycle Disorders Overview* (NCBI Bookshelf, 2003).

91. M. L. Summar, S. Koelker, D. Freedenberg, C. Le Mons, J. Haberle, H.-S. Lee, B. Kirmse, The incidence of urea cycle disorders., *Mol. Genet. Metab.* **110**, 179–80 (2013).

92. R. H. Singh, Nutritional management of patients with urea cycle disorders., *J. Inherit. Metab. Dis.* **30**, 880–7 (2007).

93. M. Msall, Neurological Outcome in Children with Inborn Errors of Urea Synthesis.pdf, *N. Engl. J. Med.* **310**, 1500–1505 (1984).

94. A. L. Gropman, M. L. Batshaw, Cognitive outcome in urea cycle disorders., *Mol. Genet. Metab.* **81 Suppl 1**, S58–62 (2004).

95. M. L. Batshaw, S. Brusilow, L. Waber, W. Blom, A. M. Brubakk, B. K. Burton, H. M. Cann, D. Kerr, P. Mamunes, R. Matalon, D. Myerberg, I. A. Schafer, Treatment of Inborn Errors of Urea Synthesis, *N. Engl. J. Med.* **306**, 1387–1392 (1982).

96. F. F. Poordad, Review article: the burden of hepatic encephalopathy., *Aliment. Pharmacol. Ther.* **25 Suppl 1**, 3–9 (2007).

97. R. F. Butterworth, J. F. Giguere, J. Michaud, J. Lavoie, G. P. Layrargues, Ammonia: key factor in the pathogenesis of hepatic encephalopathy, *Neurochem Pathol* **6**, 1–12 (1987).

98. R. F. Butterworth, Pathophysiology of hepatic encephalopathy: a new look at ammonia., *Metab. Brain Dis.* **17**, 221–7 (2002).

99. J. Stahl, Studies of the Blood Ammonia in Liver Disease, *Ann. Intern. Med.* **58** (1963).

100. I. Eijgelshoven, S. Demirdas, T. A. Smith, J. M. T. van Loon, S. Latour, A. M. Bosch, The time consuming nature of phenylketonuria: A cross-sectional study investigating time burden and costs of phenylketonuria in the Netherlands, *Mol. Genet. Metab.* **109**, 237–242 (2013).

101. P. V. D. Burg, H. W. Mook, A simple and rapid method for the determination of ammonia in blood, *Clin. Chim. Acta* **8**, 162–164 (1962).

102. Y. Murawaki, K. Tanimoto, C. Hirayama, Y. Ikuta, N. Watabe, A simple and rapid microdiffusion method for blood ammonia using a reflectance meter and a reagent plate, and its clinical evaluation for liver diseases., *Clin. Chim. Acta1* **144** (1984).

103. R. J. Barsotti, Measurement of ammonia in blood, *J. Pediatr.* **138**, S11–S20 (2001).

104. J. Buttery, R. Ratnaike, B. Chamberlain, The measurement of erythro-cyte ammonia using the Hyland ammonia kit, *J Clin Chem Clin Biochem* **20** (1982).

105. S. Dienst, An ion exchange method for plasma ammonia concentration, *J. Lab. Clin. Med.* **58** (1961).

106. J. Huizenga, C. Gips, Determination of blood ammonia using the Ammonia Checker, *Ann Clin Biochem* **20** (1983).

107. H. van Anken, M. Schiphorst, A kinetic determination of ammonia in plasma, *Clin Chim Acta* **56** (1974).

108. L. Rover Júnior, J. C. Fernandes, G. de Oliveira Neto, L. T. Kubota, E. Katekawa, S. H. Serrano, Study of NADH stability using ultraviolet-visible spectrophotometric analysis and factorial design., *Anal. Biochem.* **260**, 50–5 (1998).

109. M. Berthelot, B, *Repert. Chim. Appl.* , 254 (1859).

110. E. D. Rhine, G. K. Sims, R. L. Mulvaney, E. J. Pratt, Improving the Berthelot Reaction for Determining Ammonium in Soil Extracts and Water, *Soil Sci. Soc. Am. J.* **62** (1998).

111. T. T. Ngo, A. P. H. Phan, C. F. Yam, H. M. Lenhoff, Interference in Determination of Ammonia with the Hypoehlorite-Alkaline Phenol Method of Berthelot, , 46–49 (1981).